Surface defect engineering of metal oxides photocatalyst for energy application and water treatment

Raizada, Pankaj; Soni, Vatika; Kumar, Abhinandan; Singh, Pardeep; Parwaz Khan, Aftab Aslam; Asiri, Abdullah M.; Thakur, Vijay Kumar; Nguyen, Van-Huy

Published in:
Journal of Materiomics

DOI:
10.1016/j.jmat.2020.10.009

Print publication: 01/03/2021

Document Version
Version created as part of publication process; publisher's layout; not normally made publicly available

Journal Pre-proof

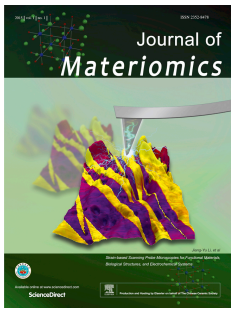

Surface defect engineering of metal oxides photocatalyst for energy application and water treatment

Pankaj Raizada, Vatika Soni, Abhinandan Kumar, Pardeep Singh, Aftab Aslam Parwaz Khan, Abdullah M. Asiri, Vijay Kumar Thakur, Van-Huy Nguyen

PII: S2352-8478(20)30502-5

DOI: https://doi.org/10.1016/j.jmat.2020.10.009

Reference: JMAT 362

To appear in: *Journal of Materiomics*

Received Date: 2 August 2020

Revised Date: 14 September 2020

Accepted Date: 23 October 2020

Please cite this article as: Raizada P, Soni V, Kumar A, Singh P, Parwaz Khan AA, Asiri AM, Thakur VK, Nguyen V-H, Surface defect engineering of metal oxides photocatalyst for energy application and water treatment, *Journal of Materiomics*, https://doi.org/10.1016/j.jmat.2020.10.009.

Surface defect engineering of metal oxides photocatalyst for energy application and water treatment

Pankaj Raizada[a,b,*], Vatika Soni[a], Abhinandan Kumar[a], Pardeep Singh[a,b], Aftab Aslam Parwaz Khan[c,d], Abdullah M Asiri[c,d], Vijay Kumar Thakur[e], Van-Huy Nguyen[f,**]

[a]School of Chemistry, Faculty of Basic Sciences, Shoolini University, Solan (HP)-173229, India

[b]Himalayan Centre for Excellence in Nanotechnology, Shoolini University, Solan (HP) 173229, India

[c]Center of Excellence for Advanced Materials Research, King Abdulaziz University, P. O. Box 80203, Jeddah 21589, Saudi Arabia

[d]Chemistry Department, Faculty of Science, King Abdulaziz University, P. O. Box 80203, Jeddah 21589, Saudi Arabia

[e]Department of Engineering, Science and Technology Scotland Rural College(SRUC), Edinburgh, United Kingdom

[f]Institute of Research and Development, Duy Tan University, Da Nang, 550000, Vietnam

Corresponding Authors

* Pankaj Raizada: pankajchem1@gmail.com

** Van-Huy Nguyen: nguyenvanhuy20@duytan.edu.vn

Biography

Name	Photo	Biography
Pankaj Raizada		**Pankaj Raizada** is an Assistant Professor of the School of Chemistry, Shoolini University of Biotechnology and Management Sciences Solan (H.P.), India. She received her PhD from Vikram University, Ujjain (M.P.), India in 2010. She was awarded the DST Young Scientist Award in 2015. Her research interest involves designing of new advanced photocatalytic materials (metal free carbonaceous materials) for environmental and energy applications. Her research group published around 67 papers, 22 patents, and 6 book chapters in the area of photocatalysis. Email: pankajchem1@gmail.com
Vatika Soni		**Vatika Soni** received her M.Sc. degree from D.A.V University, Jalandhar (Pb.), India in 2018. Presently, she is a research scholar in the School of Chemistry, under the supervision of Dr. Pankaj Raizada at Shoolini University of Biotechnology and Management Sciences Solan (H.P.), India. Her current research interests include synthesis and modification of semiconductor photocatalysts for environmental and energy applications.
Abhinandan Kumar		**Abhinandan Kumar** obtained his master's degree (M.Sc. Chemistry) from Punjabi University, Patiala, India. Currently, he is a doctoral student under the supervision of Dr. Pankaj Raizada in the School of Chemistry, Shoolini University of Biotechnology and Management Sciences Solan (H.P.), India. His research interest focus on the design and tailoring of new advanced semiconductor photocatalytic materials and their environmental and energy applications. Email: abhinandank1313@gmail.com
Pardeep Singh		**Pardeep Singh** is an Associate professor of School of Chemistry, Shoolini University of Biotechnology and Management Sciences Solan (H.P.), India. He received his PhD from Vikram University, Ujjain (M.P.), India in 2010. He has been awarded with DST Young Scientist Award and VC Young Academician Award. His research interest interests cover the interdisciplinary areas of Water Purification, Fenton Process and Advanced Oxidation Process. Dr. Singh is reviewers of 56 international journals. His research group published around 110 research papers, 22 patents, and 8 book chapters in the area of photocatalytic water treatment and energy applications. Email: pardeepchem@gmail.com

Aftab Aslam Parwaz Khan		**Dr. Aftab Aslam Parwaz Khan** is currently working as an Assistant Professor in the Center of Excellence for Advanced Materials Research, King Abdulaziz University, Jeddah, Kingdom of Saudi Arabia. He obtained his PhD. in Chemistry from Aligarh Muslim University, Aligarh, India. He has secured 4 Books, 15 Chapters, and more than 130 research papers. He is a potential reviewer of several reputed international journals, including Nature, ACS, RSC, WILEY, Elsevier, Springer's, Bentham, IOP, and Frontiers publishers, etc. He has been serving as an Editorial Board Member of many reputed international journals since 2013. More than 20 international conférences/ workshop and 20 research Project has been completed. His research encompasses all aspects of polymer nanomaterials and catalyst synthesis, properties as well as application in photocatalyst, chemical sensing, biosensing, environmental remediation of pollution, drug delivery system for mechanistic and interaction studies using a wide range of spectroscopic techniques with thermodynamic parameters.
Abdullah M. Asiri		**Abdullah M. Asiri** received PhD from the University of Wales, College of Cardiff, UK in 1995. He is the Head of the Chemistry Department at King Abdulaziz University since October 2009, and he is the founder and the Director of the Center of Excellence for Advanced Materials Research. He is a Professor of Organic Photochemistry. His research interest covers color chemistry, synthesis of novel photochromic, thermochromic systems, synthesis of novel coloring matters and dyeing of textiles, Materials Chemistry, Nanochemistry and Nanotechnology Polymers, Energy materials and composite materials. He is the Editor-in-Chief of King Abdulaziz University Journal of Science. He is also a member of the Editorial Board of Pigments and Resin Technology (UK), Designed Monomers & Polymers. He holds 12 granted USA patents, more than 1500 Publications in international Journals (WoS) Journals with more than 51,030 citations and an h-index of 98, 41 book Chapters, and 60 Books. Prof. Asiri Won many awards, including The custodian of the two holy mosques awards (2017), Khalifa Prize for educations (Best researchers Field) (2018), Shoman Prize (2018). He won the best researcher award in KAU for many successive years. www.aasiri2.kau.edu.sa

Vijay Kumar Thakur		**Vijay Kumar Thakur** is currently a Professor and Head of the Biorefining and Advanced Materials Research Centre at SRUC, Edinburgh, U.K., and also holds an Adjunct Professor position in the Research School of Polymeric Materials, Jiangsu University, China and is a Visiting Professor at Shiv Nadar University, India, and Visitor at Cranfield University, the U.K. He has previously held faculty positions at Cranfield University, U.K., Washington State University, U.S.A., and Nanyang Technological University, Singapore. His research activities span the disciplines of Biorefining, Chemistry, Chemical Engineering, Manufacturing, Materials Science, and Nanotechnology, as well as all aspects of Sustainable and Advanced Materials. He has been a PI/Co-I on several projects sponsored by BAE Systems, EPSRC (EP/T024607/1), Royal Academy of Engineering (IAPP-33-24/01/2017; IAPP18-19\295), UKIERI (DST/INT/UK/P-164/2017), Innovate UK, and others. He has published over 200 SCI journal articles, 2 patents, 50 books, and 37 book chapters in areas concerning polymers, nanotechnology, and materials science (Hi 67, citations >13000). He sits on the editorial board of several SCI journals (e.g., *Nature Scientific Reports*, *Industrial Crops & Products*, *Journal of Renewable Materials*, *Advances in Polymer Technology*, *International Journal of Polymer Analysis and Characterization*, *Polymers for Advanced Technologies*, *Biomolecules*, *Nanomaterials*, *Surfaces and Interfaces*, *Sustainable Chemistry and Pharmacy*, *Current Opinion in Green and Sustainable Chemistry*, and *Nano-Structures & Nano-Objects*) as an Editor or Editorial Advisory Board member.
Van-Huy Nguyen		**Van-Huy Nguyen** received the B.S. degree (2008) in Environmental Engineering from the Ho Chi Minh City University of Technology and M.S. degree (2010) in Chemical Engineering from National Taiwan University (NTU). He obtained his Ph.D. degree in Chemical Engineering from the National Taiwan University of Science and Technology in 2015. Dr. Nguyen was previously a Post-doctoral Fellow at NTU. He has gained the knowledge and experiences of working in both academia and industry. Prior to joining Key Laboratory of Advanced Materials for Energy and Environmental Applications (AMEEA, Lac Hong University) as Principal Researcher, he has worked for Nan Pao (Vietnam), and Ton Duc Thang University,

		Duy Tan University as a Principal Investigator and Research Fellow, respectively. Dr. Nguyen has published over 90 peer-reviewed journal articles, 3 book chapters, and has presented at many international conferences. Currently, he is the Associate Editor of Applied Nanoscience (Springer Nature), Editorial Board Member of PLOS One. He is also the Managing Guest-Editor, Guest-Editor of eight Special Issues in respected journals such as the Journal of Chemical Technology & Biotechnology (Wiley), Arabian Journal of Chemistry (Elsevier), Topics in Catalysis (Springer), Chemical Engineering Science (Elsevier), Biomass Conversion and Biorefinery (Springer), Materials Letters (Elsevier), Journal of Environmental Chemical Engineering (Elsevier), and Sustainable Chemistry and Pharmacy (Elsevier). He is an Editor for edited book under production in Elsevier about photocatalysis. Dr. Nguyen is an active reviewer for many high-impact journals published by Elsevier, ACS, Wiley, Springer Nature, RSC, MDPI and PLOS Publishers. His research works have gained wide interest through his highly-cited research publications, book chapters, conference presentations, and workshop lectures. His research focuses on chemical and materials aspects of (photo)catalytic processes and a basic understanding of (photo)catalysts, with emphasis on applied to environmental problems and production of clean energy, value-added chemicals.

Surface defect engineering of metal oxides photocatalyst for energy application and water treatment

Pankaj Raizada[a,b,*], Vatika Soni[a], Abhinandan Kumar[a], Pardeep Singh[a,b], Aftab Aslam Parwaz Khan[c,d], Abdullah M Asiri[c,d], Vijay Kumar Thakur[e], Van-Huy Nguyen[f,**]

[a]School of Chemistry, Faculty of Basic Sciences, Shoolini University, Solan (HP)-173229, India

[b]Himalayan Centre for Excellence in Nanotechnology, Shoolini University, Solan (HP) 173229, India

[c]Center of Excellence for Advanced Materials Research, King Abdulaziz University, P. O. Box 80203, Jeddah 21589, Saudi Arabia

[d]Chemistry Department, Faculty of Science, King Abdulaziz University, P. O. Box 80203, Jeddah 21589, Saudi Arabia

[e]Department of Engineering, Science and Technology Scotland Rural College(SRUC), Edinburgh, United Kingdom

[f]Institute of Research and Development, Duy Tan University, Da Nang, 550000, Vietnam

Corresponding Authors

* Pankaj Raizada: pankajchem1@gmail.com

** Van-Huy Nguyen: nguyenvanhuy20@duytan.edu.vn

Abstract

Despite metal oxides offer excellent characteristics in the field of photocatalysis, they often suffer from charge carrier recombination as well as limited visible response, which indeed reduce the charge kinetics process and ultimately reduce the photocatalytic output. Defect engineering is a sophisticated technique to manufacture defects and alter the geometric structure and chemical environment of the host. The present study provides an all-inclusive outline of recent developments on the classification of metal oxide defects based on the dimensions of a host crystal lattice. Precisely, surface modification of metal oxides through 0D (point), 1D (line), 2D (planar), and 3D (volume) defects with their subsequent mechanism and impact on photocatalytic performance are presented. By wisely amending the morphology (cores along with the shells) and electronic structure of metal oxide photocatalysts (TiO_2, ZnO, Bi_2O_3, Fe_2O_4 etc.) through different attuned and veritable approaches, their photocatalytic activity can be substantially improved. Optimal studies on defect engineering not only expose the altered physicochemical features but also modulate the electron-hole pair dynamics, stability, and active radical production for various photoredox reactions. Altered atomic, as well as electronic configuration, facilitated a photocatalyst material to have different optical features, adsorption properties along with improved carrier transfer as well as isolation rate. Thus, the systematic exploration of photocatalytic rudiments of defect rich metal oxide for various applications such as H_2 evolution, CO_2 reduction, pollutant degradation, and bacterial disinfection could bring significant research advancement in this field.

Keywords:

Defect engineering; Nanostructured metal oxides; Photocatalysis; Surface reactions; Point defects; Dislocations; Boundaries; Voids.

Contents:

Abbreviations

ϕ, Apparent quantum efficiency; AOP's, Advanced oxidation processes; AFM, Atomic force spectroscopy; CVD, Chemical vapour deposition; CB, Conduction band; DOS, Density of states; e^-, Electron; EPR, Electronic paramagnetic resonance; EDS, Energy dispersive X-ray spectroscopy; E.coli, Escherichia coli; FTIR, Fourier transform infrared spectroscopy; h^+, Hole; •OH, Hydroxyl radical; ξ, Intrinsic quantum efficiency; LNs, Long nanowires; MOs, Metal oxides; MB, Methylene blue; MO, Methylene orange; NIR, Near infrared radiations; NC-AFM, Non-contact atomic force microscopy;1D, One dimensional; V_o, Oxygen vacancy; RhB, Rhodamine blue; STEM, Scanning transmission electron microscopy; SNs, Short nanowires; $\bullet O_2^-$, Superoxide radical; SPR, Surface plasmon resonance; 3D, Three dimensional; TEM, Transmission electron microscope; 2D, Two dimensional; UV, Ultraviolet radiations; VB, Valance band; λ, Wavelength; XRD, X-ray diffraction; XPS, X-ray photo electron spectroscopy; XAS, X-ray absorption spectroscopy.

1. Introduction

Escalating environmental and energy problems are becoming one of the biggest challenges in this contemporary world, which demands substantial attention from researchers to develop advanced and sustainable routes to overcome them. Shortage of energy resources, increasing environmental pollution due to green-house gases, organic and inorganic pollutants, rapidly growing industrialization and urbanization are the severe human facing tribulations [1-3]. Solar energy conversion into chemical energy has been deliberated as the most effective way to improve the gradually deteriorating environmental apprehensions and energy catastrophe [4-6]. Precipitation, filtration, adsorption, and centrifugation techniques are utilized traditionally to remove toxic environmental contaminants, but they are not considered as efficient methods due to certain limitations like a generation of toxic by-products, partial organic pollutants removal etc. Sustainable development of new nanomaterials due to the fast advancement in the field of material chemistry has led to a noteworthy improvement in various technologies [7, 8]. Advanced oxidation processes (AOPs) are the designed set of chemical treatment in order to eradicate various organic as well as inorganic contaminants from the water *via* the generation of highly active oxidants like hydroxyl radicals (•OH) and other active oxygen species [9, 10]. These active species are formed from ozone, hydrogen peroxide, oxygen (primary oxidants), ultraviolet (UV) light (energy sources), and photocatalysts (like ZnO, TiO_2) etc. [11-15].

A promising photocatalyst is one with captivating potentials of absorbing maximum sun rays, producing electron (e^-) - hole (h^+) pairs that ultimately cause various surface reactions and will regenerate itself after each photocatalytic cycle [16]. These materials are either triggered by UV, visible or near-infrared (NIR) rays, which generate e^- - h^+ pair in conduction and valance band, respectively, for various redox reactions [17]. However, low light absorption ability, high cost,

rapid e^- - h^+ pair reassembly, poor stability, and sluggish surface reactions of a photocatalyst resulted in deprived photocatalytic yield [18]. Therefore, various stratagems like surface moderations, facet control, defect (surface as well as interface) engineering and morphology control etc. have been developed to improve the photocatalytic performance by amending band potentials, light absorption, chemical and surface properties [19-21].

Recently, defect engineering of semiconductor photocatalyst is considered as one of the most enlightened and extensive means to overcome the limitations of semiconductor materials. Thus, defect engineering is a practical approach to understand the electronic, geometric as well as chemical properties and their synergistic relationships in order to amend the photocatalytic activity of semiconductor photocatalysts [22-24]. Various applications of defect rich photocatalysts (like metal oxides, metal chalcogenide, graphene, graphene oxide, and carbon nitride etc.) include photocatalysis, energy storage devices, organic synthesis, and electrocatalysis [25, 26]. Photocatalytic materials can be shaped by either top-down chemical exfoliation or bottom-up self-assembly technique. In contrast, defects in these semiconductor photocatalysts were created with different methods like high temperature, chemical reduction, vacuum activation, rapid heating, ball milling, plasma etching, and lithium-induced conversion etc. Basically, defects are of three types: surface, bulk as well as interface defects which are of great significance in photocatalysis [27, 28]. Surface defects include modulation in surface area, energy, and the exposed lattice atoms, whereas bulk defects include a change in bond length, energy, electron affinity, the density of states (DOS) as well as trapping potential etc. and interface include both surface as well bulk defects [29-32]. Defects in a semiconductor can be categorized into four types (Fig. 1):

1. 0D point defects- Point defects are the defects that occur only at or around a single lattice point and are not extended in space in any dimension (e.g. TiO_2, ZnO, Bi_2O_3, V_2O_5, Ga_2O_3 etc.). 0D defects are either generated by doping or by removing a lattice atom (vacancy).
2. 1D line defects - Line defects are the defects that arise due to the misalignment of atoms in a crystal lattice (e.g.TiO_2 and ZnO), and these are of two types: (i) Edge dislocation and (ii) Screw dislocation.
3. 2D planer defects - Planar defects include the formation of planes or boundaries that separate the structure into regions with the same crystal structure but different orientations (e.g., WO_3, TiO_2, Cu_2O etc.). These are of three types (i) Stacking faults. (ii) Grain boundaries (iii) Twin boundaries.
4. 3D volume defects - Volume defects include the deviation in crystal structure from ideality by inducing two or more chemical species in one or more crystal sites, which give rise to voids or various disorders in the crystal lattice (Fe_3O_4, TiO_2 etc.).

< Please insert Fig. 1 here >

These defects, as mentioned above, are not usually quarantined as they are coexisted (native and induced) within a semiconductor photocatalyst [33, 34]. The photocatalytic output of Metal oxides (MOs) strongly depends upon the type of defects generated in the host lattice. Noting that MOs are considered as potential photocatalytic material owing to their apt physicochemical properties, cost-effectiveness, stable nature, and thermodynamically favorable band edge potentials for various photocatalytic applications. Bare metal oxides with broad bandgap energy generally exhibit photocatalytic performance by utilizing only 5% (UV range) of the total solar energy spectrum [30]. Therefore, various strategies were developed mainly to improve MOs absorption competence, enhance e^- - h^+ pair isolation, improve electronic as well as surface

properties and activate the absorbed moiety on the photocatalyst [35-38]. In a semiconductor, defected sites usually act as effective active centers, which mainly accelerate the surface reactions and substantially expand (visible or NIR) their spectral responses.

Via the DFT (Density functional theory) calculations of defect rich metal oxide (O deficient), it could predict the increased density of states (DOS) and active facilitation of various gaseous (O_2, CO_2, N_2) moieties to amplify the photocatalytic output of metal oxides involving TiO_2, In_2O_3, WO_3 etc. The amount of energy required to remove the host atom or ion (cation or anion) from its surface can be used to rationalize and envisage catalytic output in the photocatalytic process [39]. For instance, Pan *et al*. introduced oxygen vacancies at a higher temperature (<300□) and a lower O_2 environment in wide bandgap semiconductor TiO_2 [40]. Oxygen ion (O^+) ejection from the host TiO_2 surface indeed stimulated desorption with strong coupling between surface oxygen defective TiO_2 and O_2. Shifted band potentials due to defect rich TiO_2 thus, accelerated its structural, optical, reductive, and adsorption properties. The valance states of oxygen (2s, 2p), as well as metal (3p, 3d, 4s, 4p say for Ti), are overtly treated in DFT calculations to compare calculated values with experimental data. DFT studies are usually made at 0K for the defect rich MOs surface and at high temperature for their certain thermodynamic as well as transport experiments [39].

A certain amount of defects or imperfections is always present in MOs nanomaterials. MOs usually exhibit oxygen vacancies, metal ion defect (M^{n+}), a defect due to dopant insertion etc. which can modulate their donor densities along with optical and electronic properties resulted in improved photocatalytic activity [39]. They are useful for avoiding the glass fogging process, split H_2O into O_2 and H_2 and competently removal of a wide variety of different organic/ inorganic pollutants and toxic dyes thereby, mineralizing them into nontoxic, stable moieties like

CO_2 and H_2O. Photocatalysis produces various reactive oxygen species (ROS), for instance; •OH, •O_2^-, $^1O_2$, H_2O_2 and h^+ by reacting with O_2 or H_2O/OH^- which can smooth the pollutants degradation progress under suitable conditions [14].

Herein,

2. Basics of photocatalysis

Photocatalysis on the surface of semiconductor photocatalyst has grown enormously due to its analogous behavior with photosynthesis (natural chemical) process. Photochemical e^--h^+ pairs generation, charge confinement, migration of interfacial e^- are the necessary imperative steps involved in heterogeneous photocatalysis [41-43]. Photogenerated charge carriers are trapped at the surface of a photocatalyst where they perform specific interfacial redox reactions (oxidation and reduction) with the target moiety. The primary products are reactive (short-lived) radicals, which at last transformed to secondary stable products by the formation of selective chemical bonds (Fig. 2 a) [44]. All the photocatalyst semiconductors possess a filled valance band (VB) and an empty conduction band (CB) with suitable bandgap energy. Photocatalytic redox reactions and light assimilation range of a photocatalyst are totally reliant on its apt VB and CB band potentials and bandgap energy, respectively. Thus, the above-mentioned factors are known to be a very decisive one to select a suitable semiconductor photocatalytic material for water splitting and pollutant degradation applications [45-47]. According to energy band theory, the VB with e^- possesses lower energy, whereas CB occupies a higher energy state at absolute Zero. The e^- from the VB gets excited to the empty CB only on the absorption of photons (light source) with higher energy as compared to its bandgap, as shown in Eq. 1.

$$Photocatayst + hv \rightarrow \; e^-_{CB} \; + \; h^+_{VB} \qquad (1)$$

Thereby, VB is left out with empty holes while CB is occupied with e^- which participates in oxidation and reduction reactions, respectively [48-50]. From a thermodynamics perspective, there are different routes of calculating the efficacy of a photocatalytic process due to various energy interactions. For instance: Intrinsic quantum efficiency (ϕ) as well as apparent quantum efficiency (ξ), which are classified on the basis of number and energy, respectively [51]. ϕ is the number of products shaped by total absorbed photons, whereas ξ is the ratio of the rate of the photocatalytic reaction to the incident light intensity [52]. Both these photocatalytic efficiencies, therefore, depended on the intensity and λ-value of absorbed solar radiations. Similarly, according to reaction kinetics (Eq. 2) the photodegradation rate of a photocatalyst is depended on the number of reactive species formed by redox reactions on its surface (•OH and $•O_2^-$) [53,54].

$$R = -d\frac{[Red]}{dt} = -d\frac{[Oxi]}{dt} \tag{2}$$

The basic principle of photocatalytic water splitting operation along with potentials depicts the excellent redox nature of empty holes and excited e^- which facilitates the photocatalytic proficiency owing to surface generated active radical species Fig. 2 b. Precisely, the bottom of CB should be more –ve than the reduction potential of H^+ to H_2 (0 V), whereas the top of VB should be more +ve than the oxidation potential of H_2O to O_2 (1.23 V) for achieving efficient overall water splitting [49]. The overall water splitting is an uphill reaction and mainly include two half-reactions, as shown in Eq.3-5

$$H_2O + 2h^+ \rightarrow \frac{1}{2}O_2 + 2H^+ \; [HER] \tag{3}$$

$$2H^+ + 2\,e^- \rightarrow H_2 \; [OER] \tag{4}$$

$$H_2O \rightarrow \frac{1}{2}O_2 + H_2 \; [Over\ all\ splitting] \tag{5}$$

Similarly, CO_2 is a linear, highly thermodynamic stable moiety exhibiting higher C=O bond energy of 750 kJmol^{-1}. Owing to the stable and inert nature, photocatalytic CO_2 conversion requires a high amount of energy input [50]. Photoexcited e^- with apt reduction potential is the main driving force for CO_2 reduction. Multistep and multielectronic (2, 6, 8 or 12) reaction pathway leads to the generation of different reduced products as depicted by Eq. 6-11;

$$CO_2 + e^- \rightarrow CO_2^{\bullet -}\ [E^\circ = -1.85\ V] \tag{6}$$

$$CO_2 + 2H^+ + 2e^- \rightarrow HCOOH\ [E^\circ = -0.61\ V] \tag{7}$$

$$CO_2 + 4H^+ + 4e^- \rightarrow HCHO + H_2O\ \ [E^\circ = -0.48\ V] \tag{8}$$

$$CO_2 + 6H^+ + 6e^- \rightarrow CH_3OH + H_2O\ \ [E^\circ = -0.38\ V] \tag{9}$$

$$CO_2 + 8H^+ + 8e^- \rightarrow CH_4 + 2H_2O\ \ [E^\circ = -0.24\ V] \tag{10}$$

$$2CO_2 + 12H^+ + 12e^- \rightarrow C_2H_5OH + 3H_2O\ \ [E^\circ = -0.329\ V] \tag{11}$$

Merely a diminutive amount of photocarriers are migrated to the surface of a photocatalytic material, whereas others endure reassembly attributable to rapid relaxation of excited e^- from CB to VB (10 ~100 ns) [55-57]. Consequently, the most significant issue is to suppress the reassembly rate of photogenerated carriers in single component photocatalyst for better photocatalytic productivity, as pristine semiconductor materials with a single component could not accomplish all the necessary conditions for diverse surface redox reactions. Thereby, the coupling of two semiconductors having surface intersection (heterojunction), inducing various dimensional defects (active sites) and loading of cocatalyst etc. are considered as effectual schemes to overcome the drawbacks of the bare photocatalyst. Among these strategies, the present review mainly focused on defect engineering strategy owing to various advantages like

defective states below CB or above VB (Fig. 2c), reduced band potentials, generated active centers which reduce the carriers reassembly rate, and indeed boost up their migration [58].

< Please insert Fig. 2 here >

After an exhaustive literature review on defect engineered photocatalysts, the present study mainly focused on metal oxide semiconductor photocatalysts owing to their stupendous properties. Defect induced MOs are promising candidates exhibiting high potential for various photocatalytic applications. Also, data from the "Scopus" database have been retrieved in order to have an idea of entire research reports available on defect rich MOs for multiple photocatalytic applications. "Metal oxide + Defect engineering," "Metal oxide + Point defects," "Metal oxide + Dislocation," "Metal oxide + Boundaries," and "Metal oxide + Voids" are the keywords used to explore the research work on defect engineered MOs from 2011 to 2020. As illustrated by the bar graph and pie chart (Fig. 3a and b), defect engineered MOs are emerging as potential photocatalyst for pollutant degradation, water splitting, and CO_2 reduction. Based on the above-mentioned literature survey, it was found that a comprehensive article reviewing the potential of distinct dimensionality induced defect engineered MOs is still missing. Therefore, herein, an overview and in-depth knowledge of the importance of distinct defects involving point defects (vacancy and doping), dislocations (edge and screw dislocations), grain boundary, and voids in metal oxide photocatalysts have been summarized. Furthermore, various surface modifications through the above-mentioned dimensionality driven defects in the metal oxide host lattice have been highlighted. The effect of surface modulation in MOs *via* controlled creation of different defects and their identification techniques useful to improve the photocatalytic water treatment, H_2 generation, and CO_2 reduction efficacy is systematically reviewed. It will also exemplify how defects on the surface of metal oxides played an exclusive role in amending their

morphological as well as chemical features beneficial in photocatalysis. With an up to date, inclusive study and cumulative efforts from researchers, more efficient defect modified MOs semiconductor materials with broad applicability can be designed since defect engineering is a fundamental strategy which brings about enhanced physicochemical properties desired in photocatalytic nanomaterials along with new useful functionalities that are not present in the pristine samples.

< Please insert Fig. 3 here >

3. Potential and Limitations of metal oxides as photocatalyst

MOs possess exceptional thickness (thin layers) with weak interlayer interaction as well as binding energy, which ultimately results in a blue shift (in the visible range) [59]. Various MOs nanomaterials for instance: ZnO, TiO_2, WO_3, Cu_2O, ZrO_2, CeO_2, SnO_2, In_2O_3 etc. have been used as semiconductor photocatalyst in the field of material chemistry owing to their outstanding properties (anisotropic, optical as well as electronic) [60-62] as:

1. The majority of metal oxide photocatalytic materials (TiO_2, ZnO, SnO_2, CeO_2 etc.) are abundant in nature with crystalline lattice. Sharp, as well as more intense MOs diffraction facets depicted the refined crystalline nature of MOs lattice.
2. Metal oxide nanomaterials are generally with higher surface area, several surface-exposed atoms, and active sites, which helps in dropping the charge shift distance, thus accelerates diverse photoreactions.

3. The weak interlayer interactions in 2D MOs would result in swinging chemical bonds in between their lattice atoms. This result might cause polarized surface rendering surface instability.
4. The enhanced surface morphology of MOs leads to the maximum utilization of light in shorter duration under stumpy photon flux density.
5. The fascinating features involving suitable band potentials, chemical, and thermal stability, biocompatibility as well as reusability promotes the applicability of MOs in photocatalytic reactions.
6. The absorption of solar light (UV, visible, or both) by MOs accelerates the charge isolation process with the generation of $(VB)_{h+}$ that are capable of oxidizing various harmful organic/inorganic pollutants and $(CB)_{e-}$ which could reduce absorbed species on the surface of photocatalysts.

The favorable combination of electronic structure, light absorption, charge transport properties, and a lifetime of exciton in MOs has made it possible for their use as photocatalyst [63, 59]. Hence, a tremendous devoted effort in research has been made for the formation and characterization of MOs to apply in the broad fields of photocatalysis. Apart from various useful properties of MOs mentioned above, there are certain disadvantages of bare MOs photocatalyst, which obstruct their wide-scale applicability in photocatalysis [64, 65].

1. Applications of earth-abundant, stable, nontoxic broadband semiconductor photocatalyst (ZnO, TiO_2 etc.) are hindered mainly owing to its low quantum efficiency, low utilization of solar light (UV(4%) light active), and enormous bandgap potentials (3.2 - 3.4 eV) which indeed lessened the photocatalytic output.

2. Instead of having the potential to absorb maximum solar light (visible range), narrow (2.6 – 3.0 eV) bandgap MOs (CuO, Fe_2O_3, WO_3, MoO_3, V_2O_5 and In_2O_3 etc.) photocatalyst showed hasty recombination of excited charge carriers, which reduce their efficiency for photocatalytic reactions.

To overcome these above-listed drawbacks, there is a necessity to design and utilize more efficient MOs photocatalytic materials with superior efficacy. The utilization of appropriate designing strategies along with characterization techniques could help to attain better photocatalytic output with large scale applicability.

4. Surface defects in metal oxides

Several useful techniques like doping and sensitization (to modify bandgap), charge transfer complex formation, coupling with other suitable semiconductors (to accelerate carriers separation), the addition of noble metal nanoparticles (for effective utilization of exciting e^-), defect engineering (to modify the surface, chemical, electronic, light absorption properties) etc. are vastly employed strategies to improve the photocatalytic performance of MOs [66-68]. Among these strategies, defect engineering is a potential strategy to overcome the above-mentioned drawbacks of bare MOs and indeed to develop a potential (broadband as well as narrow bandgap) metal oxide photosystem [69,66]. Defects are generally the disrupted periodic arrangement of host atoms or molecules; hence, they should be controllably generated and accurately characterized in crystalline MOs. Defects in Crystalline MOs are widespread as they are with perfect alignment of lattice atoms. MOs can be simply modified by altering the surface organization by creating point defects (charge traps), including oxygen vacancies, doping

(impurities), and metal interstitials, as well as their vacancies [70-71]. Basically, two main types of defects exist in MOs as described below:

4.1 Oxygen vacancy defects

Oxygen atoms in bulk or on the surface, subsurface in MOs are with higher electronegativity as compared to the other metal atom in the lattice [72]. Oxygen removal ($V_{o,}$ distorted crystal structure) from the lattice of MOs photocatalyst resulting in the generation of uneven (sub or nonstoichiometric) charge states, which leads to the effective isolation of excited charge carriers [73]. Positively charged oxygen vacancies are generally created in MOs by activating the oxygen via annealing under inert or reductive atmospheric conditions, bombardment with high energy moiety, under H_2 atmosphere, chemical vapor deposition (CVD), reducing agents etc. [74]. For instance, Pei *et al.* revealed the effect of generated V_o in TiO_2 (reduced) via hydrothermal action of Ti (II) O in HCl. The nature and location of V_o in reduced TiO_2 played a vital role in reducing the bandgap energy and extending its response towards visible range [75]. To a certain extent, V_o (known as effective active sites) defects are useful in optimizing photogenerated charge migration as well as isolation and accelerating visible light absorption range. But too much distortion (V_o) in the host lattice will generate recombination centers, which would inhibit the rapid transfer of excitons to the surface for redox reactions. Furthermore, it is also observed that a specific concentration of V_o defects is different from the distinct fabrication approach along with MOs structure [67].

4.2 M^{n+} defects

Other than V_o defects in MOs, M^{n+} defects were also created by the addition of aliovalent metal cation dopant (transition metal cation) via mainly self-doping [76]. Self-doped defects (amount less than parent cation) chiefly act as surface or bulk trappers for effective isolation of charge carriers and also to inhibit photocorrosion rate. For instance, Lira and co-workers demonstrated the enabled O_2 absorption on reduced rutile TiO_2 through effective charge removal from Ti^{3+} (deeper layers). Bulk Ti^{3+} defects in a crystal that served as e^-/h^+ pair trapper leads to the inhibition of excited carriers reassembly and causing upward band bending [77]. Similarly, Pie and his team fabricated Ti^{3+} defect rich TiO_2 through high-temperature treatment. The shifting of g value from 1.975 to 2.02 in Electronic Spin Resonance (ESR) spectra indicated the formation of Ti^{3+} defects, as shown in Fig 4 a and b. They further demonstrated that proper location, distribution of Ti^{3+} (subsurface/bulk) defects were responsible for improving charge carrier isolation rate, and visible light absorption response. It was observed that as-fabricated TiO_2 showed 30-fold improvement in decomposing methylene blue (MB) as compared to pristine TiO_2 [78]. Surface/bulk $V_{o,}$ along with M^{n+} defects, sometimes occur simultaneously in single MOs photocatalyst resulting in enhanced photocatalytic output by overcoming the particular limitations of wide and narrow bandgap MOs.

< Please insert Fig. 4 here >

5. Fabrication and photocatalytic applications of defect engineered metal oxides

Surface modification is a phenomenon of amending the surface properties (solid) of photocatalyst nanomaterials by bringing physical, electronic, magnetic, biological, or chemical characteristics different from the ones originally found on the surface of a semiconductor

nanomaterial [79, 80]. These surface amendment processes not only provide stability to the nanoparticles but also useful for enhancing the efficacy of photocatalyst towards various applications. Modifications on the surface can be done by using different methods with a view to increment a broad range of characteristics of the surface involving surface energy, and reactivity as well charge kinetics, active sites, biocompatibility, and hydrophilicity [81-84] etc. Effectual strategies for controlling the development of various defects in metal oxide photocatalyst along with their inherent mechanism were summarized as:

(1) High-temperature treatment under reducing or inert atmosphere – This is the best treatment to generate V_o (surface) defects, whereas reducing atmosphere leads to the change in color and the conversion of M^{n+} to $M^{(n-1)+}$ in MOs. For instance, Yan *et al*. reported the successful fabrication of WO_3 nanosheets through two steps post-treatment, *i.e*. alcohothermal strategy under reducing (hydrogen) atmosphere (573K) [85]. WO_3 nanosheets were facilely synthesized first, followed by the treatment under vacuum (WO_{3-x} -VT) or hydrogen (WO_{3-x} -HT) atmosphere to generate V_o defects. The olive color of WO_3 nanosheets indicated the generation of V_o in the lattice. The shift in UV- vis- NIR spectra (Fig. 4c) from 480 to 490-700 nm range depicted the generation of discrete fermi levels (below CB) due to the generation of V_o (Fig. 4d). As-fabricated WO_3 nanosheets exhibit surface plasmon resonance effect owes to the presence of V_o defects, which definitely showed enhanced charge carrier isolation and light-harvesting in UV as well as the visible region.

(2) Chemical reduction – Various reducing reagents, for instance: $NaBH_4$, CaH_2, N_2H_4, ethylene glycol, glycerol etc. react with the lattice ($K_4Nb_6O_{17}$, BiOCl etc.) oxygen atoms to generate V_o on the surface of MOs without altering the host structure as well as crystallinity. For instance, Ren *et al*. fabricated reduced TiO_2 nanoparticles (dark grey) using $NaBH_4$, a reducing agent *via*

hydrothermal route [86]. The light yellow color of TiO_2 changes to light grey on increasing the concentration of $NaBH_4$, indicating the generation of V_o defects as analyzed with the help of Scanning electron microscope (SEM) images. Consistent lattice spacing (0.351nm) value in Electrospray ionization (ESI) depicted the successful creation of Ti^{3+} defects devoid of altering TiO_2 dimensions. Generated Ti^{3+} defects, as well as Vo in bare TiO_2, indeed improved the bandgap (narrow), visible light assimilation, and absorption rate for the organic dye to 438.2 nm thus, showed higher photocatalytic output.

(3) Low temperature based vacuum activation – One of the cheapest, simple strategies for only MOs activation and known to promote their photocatalytic performance. With the increase in temperature as well as time, surface oxygen tends to get away from the host (ZnO, WO_3, MoO_3) lattice due to lack of outside pressure resulting in V_o and M^{n+} defects. For instance, Xing and his group fabricated defect (Ti^{3+} and V_o) rich TiO_2 through a cheap low temperature based vacuum activation route, without altering the host crystal lattice [87]. Broad EPR peak intensity with higher g value (2.004, 1.99) demonstrated the existence of V_o and Ti^{3+}, respectively, owing to the trapping of charge carriers. Generated defects in TiO_2promoted the light absorption, H_2 generation as well as photodegradation rate by creating defective states. It is observed that controlled vacuum time and temperature conditions are essential to regulate the concentration of V_o and Ti^{3+} defects.

(4) Phase transformation – Nanosheets of MOs like CeO_2, In_2O_3, WO_3, Co_3O_4 etc. under high temperature undergoes phase transformation resulting in a porous structure with V_o defects [88-90]. For instance, Sun *et al.* fabricated pitted ultrathin CeO_2 (Ce, IV) photocatalyst through a high-temperature technique [91]. As-constructed thin CeO_2 sheets (three-atom-layer) with numerous surface pits were analyzed with the help of a Transmission electron microscope

(TEM) as well as atomic force microscopy (AFM) images. Unsaturated pit-surrounding Ce sites (2.302Å) in CeO_2 with low activation energy (61.7 $kJmol^{-1}$) and increased carrier density (near the Fermi level) ensured fast CO catalytic activity as well as activation of O_2 moiety. Superior photocatalytic activity (about 50 times more) was observed for as-fabricated CeO_2 sheets (pits rich) than bulk CeO_2 (0.89%).

(5) Lithium induced conversion – Novel strategy to create defects, boundaries as well as dislocations like active sites in crystal structure owing to the formation of ultra-small size (2-5nm) exhibiting large surface area MOs nanoparticles [92-94]. Berger *et al*. fabricated defect rich MgO *via*. Lithium ions (Li^+) doping through the thermal annealing route [95]. Results were monitored with the help of IR and EPR spectrum, which showed the formation of relevant active absorption sites on the surface of MgO lattice. It was observed that improved ion mobility was achieved due to the proper localization of Li^+ ions in MgO surface or near-surface region. High-temperature conditions (above 1170 K) were accountable for the generation of surface V_o defects, which indeed altered the surface spectroscopic features of the host MgO nanocrystals.

(6) UV irradiation - UV irradiation is a possible means to create V_o only in MOs with low bond energy and weak (long) M-O bond length. For example, Magdalane *et al.* tailored binary CeO_2/Y_2O_3 (Ce_1/Y_1, Ce_2/Y_1) nanohybrids by varying the amount of precursors materials through chemical precipitation supported hydrothermal route. Raman spectra at 560 cm^{-1} depicted the generation of extrinsic V_o defects in as-synthesized Ce_2/Y_1 nanohybrid, as illustrated in Fig. 4e, and f [96]. Defect rich CeO_2/Ye_2O_3 showed an absorption shift in blue region 435nm- 460nm from 350 nm (UV, bare CeO_2). It was observed that as-fabricated CeO_2/Ye_2O_3 binary photocatalyst with improved surface morphology (active sites as well as surface area), visible

light activity, charge isolation revealed enhanced RhB decomposition rate (98%) under UV and visible light.

As discussed above, constructing defects in MOs seem as an effective approach to shifting their absorbance range (UV to visible or NIR) as well as to improve the segregation of excited e^--h^+ pairs. Similar to rational synthesis techniques, characterization of several induced MOs defects is also very imperative to specify a location, density, and the type (surface and bulk) of induced defects [97]. Thereby, it is necessary to effectively characterize defect rich MOs in order to evaluate their structure-photoactivity relationship. Characterization is useful for designing high-performance defect rich MOs photocatalytic material. Numerous characterization techniques are categorized under two main categories which have been proposed to identify MOs defects: (a) Microscopic characterization: Atomic-level microscopic characterization is an effective tactic to observe as well as distinguish defect rich MOs directly which include: TEM a powerful, effective characterization technique to evaluate both surfaces as well as bulk defects in MOs [98], High-resolution noncontact atomic force microscopy (NC-AFM) as well as SEM (a useful technique to characterize surface MOs defects only [99,100], light element sensitive annular bright-field (ABF)-STEM as well as high-angle annular dark-field (HAADF)-STEM [101], Scanning tunneling microscopy (STM): Low temperature based technique to observe the dissociated absorbed moiety on MOs surface [102]. (b) Spectroscopic characterization: To characterize detailed defect rich MOs lattice structure, the spectroscopic characterization techniques plays a critical role in providing their in-depth understanding of various photocatalytic applications. Spectroscopic techniques like X-ray photoelectron spectroscopy (XPS) is widely utilized to characterize chemical and surface elemental properties of defect rich MOs. Peak shifting, peak intensity variation, new peak formation in the XPS spectrum are the

basic indication for defect induced MOs (vacancy, dislocations etc.) [103]. ESR shows the presence of unpaired e^- present either on the surface or in the bulk of MOs [104]. Similarly, X-ray absorption spectroscopy (XAS), X-Ray absorption near edge structure (XANES) as well as X-Ray absorption fine structure (EXAFS) spectroscopic techniques are used to detect the chemical as well as coordination environment in defective MOs. Positron annihilation spectroscopy (PAS) is very powerful in distinguishing the induced intrinsic defects in MOs. Photoluminescence spectroscopy: PL is known as an ingenious and non-destructive characterization technique to probe discrete energy levels as well as the structural composition of defect rich MOs [105].

Thereby, location, type, concentration, along with the characterization of defects, is mainly responsible for understanding MOs unique outstanding function. Surface modulations can be done through (i) point defects, which mainly induced by either vacancy generation or by adding impurity in the host lattice [106]; (ii) line and planer defects, which are induced by dislocations as well as by boundaries [107,108]; (iii) volume defects induced by creating void or disorder [109]. Defects can be introduced either before (where defect formation is not dependent on growth kinetics of nanoparticles) or during (where it is totally dependent) the fabrication of MOs semiconductor photocatalyst. Generally, it was observed that 0D, as well as 3D defects, are mainly independent of the growth kinetics of MOs nanomaterial, whereas 1D, as well as 2D defects, are unswerving on the MOs growth kinetics [59]. Thereby diverse types of surface defects with their positive results on photocatalytic activity of MOs for different applications involving biotic and abiotic pollutant degradation, H_2 generation and CO_2 reduction are discussed as below:

5.1 Defect engineering through point defects

Point defects are known to alter the composition of semiconductor material through inducing smaller or similar size dopant (impurity) into the crystal lattice. Impurity ions can be placed either by replacing lattice ions/atoms or at empty interstitials sites of a crystal lattice. Dopants can be introduced through a process known as diffusion doping, and its doping degree in a semiconductor is totally based on the adopted strategies as well as the structure of the host nanomaterial. Similarly, surface-level vacancies in the host are often established through the reduction or thermal action of target nanocrystal [110-113]. V_o or doped photocatalyst semiconductor showed improved activity towards various photocatalytic applications like CO_2 reduction, pollutant degradation, H_2 reduction etc. In MOs, generally, anion vacancies (lattice V_o) are easily engendered as compared to cationic vacancies (M^{n+} defects) due to high formation energy as well as lower stability. Point defects (both) mainly results in the generation of unbalanced charge states, electric field (non-stoichiometry) that indeed mainly reduces the reassembly rate of excited carriers. Point defects can efficiently regulate the electronic properties, band potentials reduce the host lattice coordination number, and act as effective active centers to improve MOs photocatalytic efficiency. Anion vacancies generally create midgap states in order to narrow the bandgap and to promote MOs light absorption rate (i.e., UV to Visible or even NIR). Similarly, cationic vacancies act as shallow acceptor, which induces p-type conductivity and hence encourage h^+ migration rate [111].

< Please insert Fig. 5 here >

Among various MOs, ZnO is a wide gap (3.8eV), nature-rich, nontoxic semiconductor photocatalytic material that utilizes ultraviolet radiations only (λ<380nm). Many researchers found that under high temperature, vacuum treatment, H_2 reduction like techniques, various V_o

related defects were created in ZnO lattice due to change in color of the host lattice. Therefore, a lot of research work has been done to study the correlation between the generated V_o defects as well as their photocatalytic response [114-116]. For instance, Heo and his team reported facile self-assembled e^- rich interface in defected ZnO: rGO-Cu: Cu_2O nanohybrid with the help of various starting materials using the solvothermal method [117]. Defect induced ZnO and other rGO-def-ZnO, rGO-Cu, def-ZnO@Cu_2O as well as rGO/Cu_2O nanomaterial photocatalysts were synthesized using their respective starting materials in alcohol followed by heat treatment (200℃, N_2). Different peaks from Raman at 214, 296, and 625cm^{-1} in def-ZnO: rGO-Cu: Cu_2O suggested successive loading of Cu_2O nanoparticles on the ZnO surface. Crystalline nature, as well as disorders or defects in as-synthesized samples, were characterized using X-Ray diffraction (XRD) and Raman spectroscopy. Besides, XPS results showed that the peak spectrum of O1s for Zn-O as well as Zn-OH was at 530.2 and 531.0 eV, respectively, suggested the presence of oxygen vacancies in def-ZnO: rGO-Cu: Cu_2O heterostructure (Fig. 5a). Bandgap was reduced from 3.20 eV (bare) to 2.70 eV due to the generation of V_o defects. From above these two strategies, i.e., the formation of e^- rich interface in between def-ZnO as well as Cu_2O and the induction of V_o (via. TEM) (Fig. 5b), it was observed that there is a transformation of absorbance edge from UV to visible region which accelerated the photoreduction rate (41.0 μmol/g) of CO_2. In another report, Al-Sabahi and co-workers used a simple microwave-assisted hydrothermal process to introduce V_o in the framework of ZnO nanorods. ZnO with surface defects were characterized with the help of PL and XRD spectra. Due to the existence of surface Zn^{2+} states and V_o defects, ZnO nanorods exhibited prolonged light absorbance from UV (388 nm) to the visible (418 nm) region and superior phenol photodegradation activity (50%) than ZnO with lower surface defects [111].

Improvement in various photocatalyst involving their enhanced photocatalytic output, solar light assimilation power, recyclability is mainly known as important factors in order to achieve multi photocatalytic applications. Li and his peer group studied the impact of defect engineered ZnO samples to reduce CO_2 into other valuable products *via* forming its porous nanoplates using simple precursors (Zinc, sulfur powder, and ethylenediamine) [118]. As-obtained $ZnS(en)_{0.5}$ were consequently annealed in the presence of air under varying temperatures to achieve defect rich (porous) ZnO-600, ZnO-650, ZnO-700℃ nanoplates. Specifically decreased surface morphology i.e., 17.96 m^2/g at 600 ℃, 10.89 m^2/gat 650 ℃ and 9.55 m^2/g at 700℃, as well as CO_2 adsorption rate, was depicted by porosity and surface detector. FT-IR (Fourier-transform infrared spectroscopy), as well as XRD (Fig. 5c) analysis, showed no impurity peaks indicating the complete conversion of ZnS (en) $_{0.5}$ to ZnO. VB and CB potentials of porous ZnO-600, ZnO-650, ZnO-700℃ were (2.87eV, -0.32V), (2.87eV, -0.35V) and (2.87eV, -0.36V), respectively depicted the increased bandgap potentials (3.21, 3.24, 3.25eV) with increasing temperature range. Fig. 5d exhibited different Raman peaks at 99, 437 (bare), and 590 cm^{-1} (V_o) thus, confirmed the presence of V_o defects in the host lattice. Hence, with above-observed characteristics, it was confirmed that as-synthesized different defect rich ZnO nanoplates were well efficient photocatalyst to reduce the absorbed CO_2 to CO with 3.8 (600℃), 3.1 (650℃) as well as 2.5 μmol/g (700℃), respectively. Therefore, photocatalytic results of ZnO (II-IV) semiconductor photocatalyst can be boosted by creating V_o, $M^{n+,}$ like point defects. It was observed that concentrations of V_o in the host lattice at different temperature leads to unequal light assimilation capacity. The more the number of V_o in the host, the stronger will be the light absorption towards the visible region owing to the different alignment of energy levels. Similarly, TiO_2 is another wide bandgap semiconductor photocatalyst whose photocatalytic

activity was reduced due to various limitations (charge carriers recombination, corrosion, UV light absorption etc.). Defect rich TiO_2 exhibited improved photoactivity, polished surface structure, colored, extended light absorption range due to the raised local states under CB, and tailored (decreased) bandgap potential [119].

For instance, Yu *et al*. designed hydroxyl-group-rich mesoporous TiO_2 photocatalyst through the hydrothermal route (450-550 ℃) for better photocatalytic CO_2 reduction [119]. Results from the EPR spectrum (Fig. 6a) at 3340 G and negative Ti shift attributed to the presence of V_o along with the formation of Ti^{3+}in the host TiO_2. It was observed that V_o in the host lattice could encourage the formation of Ti^{3+} from Ti^{4+} by accepting e^- (from F^- during calcination) to maintain the neutrality of TiO_2 lattice. After calcination, XPS along PL peak spectra were still at 684 eV and 385 nm, respectively indicated the unsuccessful replacement of host lattice sites with F^-(Fig. 6b-e) (no peak shifting). The effective photoactivity of an as-prepared visible, active mesoporous TiO_2 sample was appraised by photoconversion of CO_2 into CH_4 owing to the narrowed bandgap and functional -OH groups. It was observed that with an increase in the surface area (9.43 m^2/g) the rate of CO_2 absorption (67.75 μmol/g) increases due to more exposed V_o as well as functional -OH groups. These defects in the TiO_2 (host) can serve as the isolation centers or trappers to trap charge carriers and to boost the photo-absorption efficiency.

< Please insert Fig. 6 here >

Dopants (metal or non-metal) usually replace the original metal or oxygen atoms or are either placed at the vacant interstitial sites in MOs depending on their size as well as electronic nature. Therefore, in order to study the effect of both anionic and cationic dopants on TiO_2, Mandari and his team designed a convenient technique to synthesize visible active codoped (N and Gd) TiO_2 using the sol-gel route [120]. N and Gd (4f) showed strong lattice distortion owing to the

formation of new O-Ti-N as well as Gd-O-Ti bonds. Dopants with large ionic radii, i.e., N^{3-}(1.71 Å), as well as Gd3+ (0.94Å), usually placed the bare lattice Ti^{4+} (0.61Å) and O^{2-} (1.32Å) ions, resulting in the formation of V_o. Obtained N/Gd doped defect rich TiO_2 nanohybrid showed a redshift owing to the generation of more e^- and h^+ (less recombination rate) in the presence of solar light. Trapping sites in defect rich TiO_2along with e^-/h^+ pairs transfer and migration rate during photoexcitation were illustrated with the help of the PL technique. NTi, as well as GdNTi nanostructures, showed broad range wavelength spectrum (350 to 550nm), where peak at 470nm contributed to the formation of surface V_o(Ti^{4+} replaced by Gd^{3+}) and metal defects in the host lattice (Fig. 7a). Similarly, EPR analysis report of NTi (g = 1.919, 2.001 and 2.079) and GdNTi (g = 4.11, 3.07, 2.51 and 2.063) displayed the trapping of e^- in V_o, presence of Gd^{3+} and V_o-Gd^{3+} ions interaction, respectively (Fig. 7b). Owing to the formation of V_o and Gd^{3+} defects in the host, the energy for photoexcitation decreased and accelerated the visible, active redox reactions with water or methanol. The bandgap of as-fabricated nanostructure was reduced as a consequence of the new Fermi level below CB (Gd 4f) and above VB (N 2p), as depicted in Fig. 7c. Mechanistic studies revealed that CB e^-(surface) reacted with H^+ ions to generate H_2, and it was observed that Gd/ N-TiO_2 showed 10764 μmol/g photocatalytic H_2 generation, which is approximately 26 times higher than the bare (N-TiO_2 and Gd-TiO_2) sample.

< Please insert Fig. 7 here >

Similarly, Zhu *et al*. synthesized Au, and CoO loaded hollow TiO_2 sphere through a solvothermal route (Fig. 8a) for the superior photocatalytic CO_2 reduction than bare TiO_2 [121]. XPS spectrum of oxygen (1s) revealed the generation of V_o (at 530.91eV) defects on the surface of hollow TiO_2. They generated an internal electric field along with e^- (CB_{Au}), as well as h+ (VB CoO) trappers in the as-synthesized Au 2.0@TiO2@CoO heterostructure, facilitated the isolation

of photogenerated e^--h^+ pairs (Fig. 8b). It was demonstrated with the help of the EPR (Fig. 8c) spectrum under dark (g = 2.003, N_2) and light conditions that surface V_o defects created in $Au_{2.0}$@TiO_2@CoO assisted the absorption (7.6 cm^3/g) as well as activation of CO_2 moiety. Along with the EPR spectrum, the chemical absorption of CO_2 moiety on V_o was also demonstrated with the help of FTIR spectra. Different FTIR peaks of as-synthesized nanohybrid with absorbed CO_2, H_2O, and various active intermediates were illustrated in Fig. 8d. Thereby, above mentioned results confirmed that the homogenous deposition of the cocatalyst (Au, CoO) and V_o defects on the surface of TiO_2 enhanced CO_2 reduction rate (13.3μmol/h/g) approximately 60 times higher than the bare TiO_2 sample.

< Please insert Fig. 8 here >

Thus, the above discussion demonstrates that the increase in photoactivity of as-synthesized nanohybrid OH rich-TiO_2, Gd/N-TiO_2 and$Au_{2.0}$@TiO_2@CoO photocatalyst is attributed to the presence of V_o and M^{n+} defects, induced surface junction internal electric field, respectively. OH groups have an excellent affinity for CO_2 moiety activation, and hence they are formed by the decomposition of water (OH^- and H^+) followed by oxidation (h^+). Here, V_o defects in TiO_2 are induced either by replacing host TiO_2 lattice oxygen atom by F atoms or by removing O itself. Similarly, another approach by using dopant (Gd/N) demonstrates that metal or non-metal doping indeed delays the charge carriers recombination rate by creating intermediate energy levels in the TiO_2 lattice. From dopant studies, it is scrutinized that non-metal dopant (N) slightly shifted the VB position (uplifted) as compared to CB for improved e^- and h^+ generation by reducing energy requirement for photoexcitation. Dopant atomic radii are mainly responsible for various different MOs photocatalytic mechanisms. Similar to the dopant effect on MOs photoactivity, cocatalysts (Au and CoO) incorporation also plays a vital role owing to their

unique architecture as well as a strong synergistic effect. Cocatalyst usually acts as e^- sink (CoO) as well as h^+ acceptor (Au). As a result, induced internal electric field by successful interaction of CoO, Au, and the host, TiO_2 significantly imparts a higher segregation rate of charge carriers and also provides less transmission distance for the photoinduced e^-. Therefore, we conclude that momentous exploration of the photocatalytic mechanism behind various defects rich MOs becomes more significant than that.

In another report, Lin *et al*. reported the successful formation (in-situ) of Pt/V_o mediated defective TiO_2 photocatalyst using a diffusion flame aerosol reactor [122]. Defect rich Pt/TiO_2-V_o nanoparticles were achieved under the H_2 (hydrogenation) atmosphere at a very high temperature (~700°C). Surface V_o defects and loading of Pt on the semiconductor photocatalyst helped to trap the photoexcited e^- (isolated them from h^+) and hence reduced their (e^- and h^+) recombination rate. Here, Pt^0 as well its oxidized counterparts, act as effective charge carriers separators owing to its higher e^- trapping nature, as illustrated in Fig. 9a. The binding energy of Ti $2p_{3/2}$ at 457.4 eV for both the sample (TiO_2-V_o and Pt/TiO_2-Vo) and band energy (O1s) at 528.2 eV and 530.6 eV demonstrating the existence of suitable concentration of V_o in the nonstoichiometric Pt/TiO_2-V_o semiconductor (Fig. 9b and c). The amended morphological properties indeed accelerated the rate of photoreduced CO (26 μmol/g-catalyst/h) and CH_4 (115 μmol/g-catalyst/h) production owing to their enriched surface e^- density (Pt sites). Furthermore, it was found that photoactivity of Pt/TiO_2-V_o (141 μmol/g-catalyst/h) was higher than other synthesized TiO_2-V_o, Pt/TiO_2 photocatalyst. EMSI played a decisive role in preventing not only the gradual loss of Pt^0 as well as V_o but also accelerated the transference of e^- from V_0 to Pt surface. Thereby, it was observed from the above-mentioned results that amended electronic

configuration (V_o) of as-synthesized heterostructure enhanced not only the surface activation for CO_2 moiety but also facilitated the segregation of photoproduced charges.

< Please insert Fig. 9 here >

In another work, Tan and his coworkers prepared a novel dopant free method to fabricate stable as well as visible light active graphene oxide/oxygen-rich TiO_2(GO/O-TiO_2), resulting in surface disorderliness [123]. Oxygen-rich defects were created into bare TiO_2 through the wet chemical impregnation route, which strongly absorbed the CO_2 on its surface owing to the hydrophilic nature of GO, as depicted in Fig. 10a. Here, GO acted as an efficient charge-transporting bridge (e^- sink) and made the TiO_2 surface more super-hydrophilic owing to its hydrophilic nature. The upshift in the potential of VB reduced the bandgap of TiO_2 to 2.95eV (UV- vis DRS spectra) and showed extraordinary efficiency in the visible (400-800 nm) range (Fig. 10b). Owing to the formation of favorable fermi level positions, CB e^- would migrate rapidly across the interface (GO sheet) and move freely. Hence, isolation of excitons efficiently obstructed the charge reassembly process, ultimately accelerated the CH_4 production, as illustrated in Fig 10c. The absorbance of CO_2 as well as visible light, induced e^- and h^+ on the surface of as-synthesized nanoparticles, which on interaction with CO_2 undergoes oxidation as well as reduction reactions. It was observed that optimized surface oxygen defects in GO/O-TiO_2 (5wt.% of GO) exhibited the highest CH_4 formation rate of 1.718 μmol /g_{cat} (6h) and reactivity of 95.8%, i.e., 1.6 and 1.4 times more than O_2-TiO_2 and pristine TiO_2, respectively. Remarkable increment in the reduction of CO_2 to CH_4 was ascribed to the formation of the Schottky barrier at the interface, which not only allowed the rapid separation of photoinduced carriers but also improved the photostability rate of nanohybrids.

< Please insert Fig. 10 here >

Similarly, porous defect rich TiO_2 were prepared by Mustapha *et al.* using a template-free hydrothermal process. Enhanced photocatalytic degradation of MB (90.4%) was observed due to the visible-light assimilation and prolonged e^- - h^+ isolation by ample surface-active OH sites and V_o (ESR peaks) as presented in Fig. 11a [112]. In other reports, analysis of defect rich TiO_2 photocatalyst depicted the highest photodecomposition efficiency due to optimum phase composition and high surface area upon doping the TiO_2 lattice with small radii ions of Al^{3+} and V^{5+} [111]. Similar to TiO_2 and ZnO photocatalytic materials, generated V_o in WO_3 nanomaterials can also prolong the light absorption range even to the NIR region. Defects can alter the electronic properties as reported in WO_3/Bi_2WO_6 using the CTAB-assisted hydrothermal route. The as-fabricated nanocomposite exhibited XPS peak at 531.58 eV owing to the formation of V_o, as depicted in Fig 11b. Stable face to face WO_3/Bi_2WO_6 heterojunction facilitated the faster tunneling of e^- which degraded 76.3% of Ciprofloxacin (Fig. 11c) under visible and NIR irradiations [113].

Conclusively, the synthetic routes adopted to synthesize defect induced ZnO, TiO_2 and many other metal oxide photocatalytic nanohybrids are crucial for controlling their size, shape, surface properties etc. Along with these, concentration, nature, and location of generated point defects (V_o) played a critical role as excessive vacancies (distorted lattice) in the MOs host would also inhibit the migration rate of e^- - h^+ pairs to the surface for their reactions. Moreover, various occurring oxidation and reduction reactions on the surface of MOs, dispense sufficiently higher respective potential for different occurring photocatalytic reactions. For instance, in the case of TiO_2, one V_o, and Ti interstitial in lattice unit, provides two and four excess e^- which in turn boosts (even 20 – 30 times) the output of various surface reduction reactions. It is crucial to consider these parameters for all-encompassing scrutiny and the revelation of the exact

photocatalytic mechanism of as-fabricated various MOs heterostructure. Various defect mediated MOs like TiO_2, ZnO, and others having desired properties are ecologically affable in order to stimulate the redox reactions of the assorted organic moiety or toxic pollutants under visible irradiation. It was observed that in-depth considerate of point defects (role) also helps to study other 1D, 2D, and even 3D defects in MOs. Table. 1 summarize distinct point defect rich MOs as efficient defect drove semiconductor photocatalysts with improved performance for various applications.

< Please insert Fig. 11 here >

5.2 Defect engineering through dislocations

Line defects are mostly 1 D defect, also known as dislocations, which chiefly occur in crystalline nanomaterials to establish their mechanical strength. Dislocations can move if the host atoms from one of the adjoining plane crack their bonds and rebond with the lattice atoms at the terminating edge. Edge dislocation, screw dislocation, and mixed (both) dislocations are the basic three types of dislocations that can be induced in MOs. Edge dislocations in photocatalytic nanomaterials are defined along the end of the extra half-plane of atoms and have been reported for TiO_2, ZnO, WO_3 like MOs. The imperfection may widen in a straight line through the crystal, or it may trail an irregular route [131-133]. Edge dislocation may be petite, extending only a minuscule distance into the host, inducing a slide of one atomic distance along the slither plane. Screw dislocations can be produced by tearing the crystal parallel to the slip direction in the host, for instance, TiO_2, ZnO, Cu_2O, and In_2O_3 [134-137] etc. If a screw dislocation is followed around a complete circuit, it will show a slip pattern similar to that of a screw thread. The slip pattern may be either left or right-handed and necessitates ameliorating of atomic bonds incessantly so that the form of the crystal remains the same. 1D type of defects generally occurs

in a single photocatalytic semiconductor and is also generated very frequently at the interface between two different photocatalytic materials. 1D defect engineering strategy is advantageous to suppress damaging superficial states, accelerating the e^- - h^+ pairs migration rate and also contributes to shifting the band potentials to promote light-harvesting of MOs photocatalyst [132]. Thereby, various examples of different heterostructures with enhanced photo-efficiency by introducing edge and screw-type dislocations are discussed below:

Rare earth metal ions with partially filled 4f orbitals (fully filled 5s and 5p) mainly known to reduce the nucleation rate and the growth of MOs nanocrystals owing to their larger ionic radii along with higher tendency to attract hosts oxygen atom. From the research of Divya and Pradyumnan, it can be found that Er^{3+}/ZnO photosystem showed improved visible light photoresponse owing to the generation of defects like V_o, dislocations, interstitial oxygen defects etc. in the crystal lattice [138]. They synthesized dislocated as well as V_o rich Er^{3+}/ZnO lattice through solid-state route at high temperature (900°C). XRD diffraction peaks showed in Fig. 11a and b depicted no secondary peaks at low (0.6, 0.9 wt%) amount of dopants, whereas at higher concentration (1.2wt%) different plane peak (222, at 29.42˚) appeared which clearly indicated the presence of Er^{3+} in the host. Increased density of various dislocations ($0.264*10^{15}m^{-2}$) resulted in the host lattice strain, which further increased the hardness of photocatalyst. Different elemental (Zn (2p), O (1s), C, Er (4d)) magnified peaks pattern (Fig. 12 c, d and Fig. 13 a, b) were observed separately with the help of XPS, indicating the presence of Zn (1021.6, 1044.6eV), intrinsic oxygen (529.7eV) and Er^{3+} (168.2eV).Er^{3+} acted as a substitution impurity, which decreased the bandgap potential of as-fabricated photocatalytic material. Er^{3+} pair in a lattice required three oxygen atoms, whereas ZnO required only one, due to which the host lattice went through amendment (dislocations) and other V_o like defects. The fluorescence peak

spectrum (maximum at 0.75) of bare and Er^{3+} doped (0.58) nanohybrid (Fig. 13 c and d) illustrated that impurities as well as dislocations played a vital role in lattice redshift (from 325 to 560nm). As-synthesized Er^{3+}/ZnO is highly stable until 5 continuous cycles, and it was observed that photocatalytic output for MB degradation (89.35%, 25min) was increased with increasing the Er^{3+}amount (0.6 wt%) in ZnO. Therefore, lattice distortions, along with impurities (defects) are considered as the main reason for the peaks decomposition and deep band emissions in green wavelength.

< Please insert Fig. 12 and 13 here >

In a similar way, Saravanan *et al*. designed visible active Ce^{3+} mediated Ag/CeO_2/ZnO ternary nanohybrid with vapor-solid conversion mechanism for superior dye and industrial sewage degradation [139]. XRD as well as XPS (Fig. 14 a-e) peak spectrum for Ag (3d), CeO_2($Ce^{3+}$and Ce^{4+}) and ZnO (Zn^{2+}, 2p) (no impurity peaks) confirmed the fabrication of Ag/CeO_2/ZnO nanocomposite. The presence of Ce^{3+}/Ce^{4+} in the host lattice confirmed the presence of defects with newly induced Fermi level (V_o), which easily facilitated the transference of e^- (Surface Plasmon resonance, SPR mechanism) from Ag to CeO_2 followed by ZnO (Fig. 15). These CB, as well as other free e^- finally reacted with oxygen moiety to form reactive •O_2^-which, further react with H_2O to give •OH for effective dye degradation. Line defects in the ternary composite generated V_o, which ultimately increased the absorption, desorption and diffusion of oxygen moiety. TEM images depicted the presence of V_o in the ternary ZnO nanohybrid owing to line defects. These results showed that as-fabricated distorted nanostructure with reduced bandgap (2.66eV), high surface area (39.2m^2/g), and stable nature efficiently degrade phenol (98%, 120 min), MB and MO (100%, 90 min) under visible light illumination. The newly generated

intermediate states reduced the band potentials (CB, VB), indicating the successful, strong interaction between Ag, CeO_2, ZnO nanoparticles.

< Please insert Fig. 14 here >

In order to study the structural, morphological impact on crystal splitting and photocatalytic behavior, Cha *et al*. reported a facile synthetic route for the preparation of TiO_2 rutile nanobelts by using diverse precursors [140]. These nanobelts were prepared with the help of a one-pot hydrothermal method in the presence of concentrated HCl. TiO_2 nanostructures like nanoflowers, nanobelts or nanowires etc. were formed with the replacement of host Ti^{4+}ions with H^+ ions. Consequently, HCl concentration played a vital role in dislocating the TiO_2 lattice atoms during synthesis. PL spectrum was analyzed to compare the bandgap energy of TiO_2 nano-flowers, nanowires, nanobelts, and it was observed that they lie nearly in between 2.1-2.8 eV range. It was analyzed that the reduced bandgap of the photocatalyst was due to the formation of a shallow fermi band (0.27-0.87eV) below the CB of TiO_2. Decreased band gap and applied strain in the host lattice, resulted in surface rich (CB) e^- density and thus ultimately boosted the photoactivity of TiO_2 nanobelts. Dislocations in the TiO_2 host were determined with the help of burgers vector and dislocation line. Edge dislocations in the TiO_2 lattice produced misorientation (6 degrees) between the atoms that influenced its construction by stimulating the formation of TiO_2 nanowires (5nm) from nanobelts. Dislocations thus, along with HCl concentration, played an important role in studying the structural, morphological properties of TiO_2 photocatalyst. Edge dislocations are generally formed during the growth of nanocrystals through imperfect oriented attachments. In another report, Ren *et al*. prepared colored nanostructures of TiO_2 with edge dislocations via one step hydrosolvothermal route. Edge dislocations characterized through HRTEM analysis served as active centers that induced Ti^{3+} defects, tunned electronic properties

and ultimately improved the light response region (UV-vis spectra; 400-900 nm). In summary, the controlled edge dislocations, along with Ti^{3+} defects, were positive for improving photodegrading efficacy up to 1.8 times for MB as compared to defect-free TiO_2 [131]. Similarly, Vo-rich Pt/WO_3 nanosheets displayed 98% toluene conversion and 95% CO_2 reduction ascribed to more host lattice dislocations than bare WO_3 [135]. The effective tunneling of photogenerated e^- - h^+ pairs from CB of WO_3 to Pt was comparatively prolonged due to the presence of V_o, which significantly enhanced the formation of •OH and •O_2^- on the surface of Vo-rich Pt/WO_3.

< Please insert Fig. 15 here >

Afforecited examples of 1D defect epitomized the vital role of dislocations for the outstanding photoactivity under visible light illumination. Thereby, it was observed that screw and edge dislocations within the 1D host photocatalyst boosted the photocatalytic output for various applications by altering their bandgap potentials. In macroscopic crystalline photocatalytic semiconductors, it is sensible to suppose that in the improvement of morphological structures (like TiO_2 nanobelts to nanowires), dislocations played a vital role. Whereas, it is observed that in comparison to point defects, 1D defects have very little influence on electronic properties (band potentials, fermi level) of MOs semiconductors. These defects may act as a source or sink of vacancies and M^{n+} (0D defects) hence, indirectly alter the electronic properties. The most crucial benefit of inducing a 1D defect is to influence the flow of excitons during the redox reaction process. The induced strain brought lattice disorientation in the host lattice, which improved their pollutant absorbance rate, exposed their e^- and h^+ rich surface as well shifted the optical response towards visible range to make it a good photocatalyst.

5.3 Defect engineering through boundaries

Planar defects are also known as boundaries, which basically have two dimensions as well as separate regions of the materials with different crystal structural morphology or crystallographic orientations. The planar defect arises across a plane and thus are of further two types: grain boundaries and twin boundaries. The grain boundary is the outside area of a grain that separates it from the other grains. Grains with different sizes usually rotated with respect to the neighboring grains, i.e., when one grain stops, another begins. Similarly, twin boundaries are with different nonrandom crystal orientations on either side of a plane. Twins are either grown-in during the crystallization or the result of mechanical or thermal work [141-145]. Grown twins are the consequence of disruption or change in the host lattice during growth attributable to a possible deformation from a more abundant substituting ion. Defects generally boost up the light absorption as well as excited charge carriers transport by enhancing effective active surface. Decreased charge reassembly is mainly due to the increased charge transfer rate as well as generated grain boundaries in MOs. Several examples of 2D defect rich MOs photocatalytic nanohybrids are as follows:

Zhu *et al.* reported the novel synthesis of grain boundary engineered metal (Rh and Pd) nanowire on the 2D TiO_2 (nanosheets) through a solvothermal route followed by heat treatment (160℃) [146]. Inter band transition due to non-plasmonic Rh or Pd resulted in the absorption of solar radiation with λ>400nm, otherwise pristine TiO_2, TiO_2-Rh/Pd nanoparticles, TiO_2-Rh short nanowires (SWs) as well as TiO_2-Rh Long nanowires (LWs) absorbed only the UV light

radiations (λ<400nm). It was observed from the above UV-vis-NIR diffuse reflectance spectrum analysis (Fig. 16 a and b) that Rh and Pd (cocatalyst) effectively encouraged the segregation of photoexcited charge carriers in the TiO_2 nanosheets. The highest yield in TiO_2-Rh LWs for CO, CH_4, C_2H_5OH (reduced CO_2 products) were calculated to be 13.5 μmol/g/h, 4.5 μmol/g/h, 12.1 μmol/g/h, respectively. Boosted CO_2 reduction rates were owing to deprived recombination rate (charge carriers) and effective e^- transmit from the surface of TiO_2 (CB) to Rh or Pd but also due to the formation of highly active (grain boundaries) as well as stable TiO_2-Rh photocatalyst. Increased temperature conditions (280℃) significantly reduced the density of grain boundaries (from 0.42n/m to 0.11n/m) from the surface of Rh or Pd (from 0.32 to 0.07n/m) cocatalyst indicating the improved interfacial contact between the two. Increased or decreased photocatalytic output of various reduced CO_2 products with temperature depicted the importance of grain boundaries on the surface of TiO_2-Rh and TiO_2-Pd for sufficient CO_2 selectivity and reduced photocatalytic H_2 activity. High-temperature conditions during fabrication and the formed grain boundaries in the host had not altered the surface morphology of the formed TiO_2-Rh nanowires. On the other hand, with increasing temperature, TiO_2-Pd nanostructures were showing altered surface morphology from nanoparticles to nanowires. Thereby, ingenious surface engineering of TiO_2-Pd depicted their less stable properties than another TiO_2-Rh (Fig. 16 c and d).

< Please insert Fig. 16 here >

Similarly, Senthamizhan *et al*. found the enhanced photodegradation capacity of as-synthesized grain boundaries rich electrospun ZnO nanohybrids via electrospinning technique [147]. Grain boundaries are known as an effective sink for the defects, which facilitates the chemical absorption of various oxygen-related moieties (pollutants). With an increase in the temperature

conditions, the sharp XRD diffraction peaks depicting the enhanced crystallinity as well as increased grain size of the ZnO host lattice. Electrospun ZnO nanofibers photocatalyst showed higher photoactivity due to their large surface area, more number of reactive oxygen moieties as well as other dominant properties. Photoactivity with respect to time, temperature for various pollutants like MB, RhB, and 4-Nitrophenol with diverse ZnO morphologies (ZNF-1, ZNF-2, ZHT, ZBF, ZSF, and ZNP) depicted the correlation between the grain boundaries and their respective output. Photodegradation activity of ZNF-2 with a higher rate constant (0.0419 min^{-1}) was observed for MB (100 %), RhB (91%), and 4-Nitrophenol (92%), respectively. It was confirmed from the above-mentioned results that with surface area, grain boundaries in the host also played an essential role in studying various physical as well as chemical characteristics of the ZnO nanofibers photocatalyst.

In order to boost the photodegradation rate of TiO_2 semiconductor for MB dye, Jaimy *et al*. constructed Fe^{3+} as well as Ce^{4+} codoped visible, active TiO_2 with the help of an aqueous sol-gel route [148]. These rare earth metal (Fe^{3+}) and lanthanide ions (Ce^{4+}) improved the charge carriers segregation rate owing to rapid e^--h^+ pairs trapping and transferring as well as stable electronic arrangement. Ce^{4+} (at grain boundaries) mainly responsible for the bending of VB as well as CB levels, which ultimately resulted in TiO_2 dislocations with reduced crystal growth. It was demonstrated with the help of XRD peaks that oxygen vacancies/M^{n+} defects were created with Fe^{3+} dopant owing to its similar size (0.64 Å) as that of Ti^{4+} (0.68). However, significant lattice distortion (strain or defects) were analyzed in the case of lanthanide ion (Ce^{3+}/Ce^{4+}, 0.97/1.143Å) due to its highly incompatible ionic radii. An increased amount of Ce^{3+}/Ce^{4+} dopant in the TiO_2 crystal usually increased the BET surface area (30.6 m^2/g) with decreased crystallinity as compared to pristine TiO_2. Bare TiO_2 lattice was free from any type of crystal defects (i.e., well-

arranged fringes), but codoping in the host illustrated (with Energy dispersive x-ray spectroscopy, EDS) the generation of stress as a result of a line as well as screw dislocations. Continuous overlapping of the d-orbital (Fe^{3+}) with the CB (TiO_2) yielded decreased bandgap, redshift, and high absorption rate of as-fabricated Fe^{3+}/Ce^{4+} doped TiO_2. Monitored photoactivity results illustrated the improved MB photodegradation (100%, at 160 min) rates than undoped TiO_2 (32%). Grain boundaries, as well as dislocations in the crystal lattice, were thus known as active sites to generate labile V_o defects, portable oxygen reactive moieties which facilitated the trapping as well as migration rate of excited e^- and h^+. In another report, Kamei and coworkers investigated the effect of grain boundary induced in crystalline TiO_2 for the photoreduction of Ag ions. The bunched surface of the bicrystal was the main localization centre for photocatalytic reduction, as observed with the help of AFM images. Bending of both CB and VB due to induced grain boundary ultimately suppressed the recombination rate of excited charge carriers and, in turn, enhanced the Ag precipitation [142].

Conclusively, an ample amount of grain and twin boundaries with developed surface areas in 2D nanocrystals suggested more opportunity for the absorption, diffusion, and desorption of reactants and subsequent products. The generation of more than one type of defect in a photocatalyst simultaneously can significantly increase their shoulder or tail absorption, which is known as the root cause for boosted photocatalytic output [33, 68]. Along with these properties, it was also found that formed boundaries help to assist the interfacial charge relocation process owing to the presence of intergranular layers. Various stable defective MOs nanohybrids depicted high pollutant absorption or degradation rate due to the presence of discontinuous lattice fringes, surface terraces, steps, kinks, and vacancies etc. From the photocatalytic results, it was analyzed that the density of the grain and twin boundaries in the nanocrystals continuously

decreased with the increasing temperature conditions. In 2D defect rich MOs photocatalytic material, grain or twin boundary terminations thus played an essential role in catalyzing various photoreactions. Table. 2 summarizes distinct 2D defect rich MOs as efficient defect driven photocatalytic materials with enhanced photoactivity for various environmental and energy applications.

5.4 Surface modifications through voids

These defects are 3D macroscopic defects (larger scale) and hence also known as bulk defects. These are generally introduced into a nanomaterial during refinement from its raw state or during fabrication processes, for instance: cracks, pores, foreign inclusions etc. [157]. These can exist in both crystalline and amorphous nanocrystals and are hence categorized into two types: Voids and disorders. Voids are known as pits small regions where there are no atoms and which can be thought of clusters of vacancies. In parallel, disorders are also typed of volume defects in which atoms are dislocated from their position to form anarchy in the host lattices. Low density, high surface to volume ratio, high shell permeability, excellent optical as well as electronic properties due to 3D defects are mainly responsible for accelerating various surface redox reactions with extended MOs photoresponse. 3D voids were showed in the photocatalytic MOs, which are present either on the surface or on the bulk, e.g., In_2O_3, ZrO_2, CdO, SnO_2, ZnO etc. [158-160].

From various research studies, it is scrutinized that the SPR effect of various Nobel metals boosts the photocatalytic rate of MOs. For instance, Koppala and his team used an environmentally friendly microwave-assisted route to fabricate ZnO/Ag nanostructure in order to study the different phase, structural as well as morphological properties [161]. Ag is known as an ideal

noble metal owing to its various advantages: e^- sink nature, non-noxious, low cost etc. They compared the different photocatalytic results for RhB degradation at different concentrations of Ag in ZnO/Ag nanocomposite. XPS spectrum (Fig.17 a-d) illustrated the triumphant fabrication of ZnO/Ag-2 with corresponding Zn (2p), Ag (3d), O (1s) peaks. At 540, 467, and 378 nm PL spectrum demonstrated the new fermi trap level, improved excitons segregation rate, and deposition of h^+ on the surface of Ag, respectively. Schottky junction formed at the Ag/ZnO interface played a vital role in e^-displacement as well as its scavenging action. O_2 voids in the ZnO host facilitated trapping of photoexcited e^- (CB) and h^+ (VB). Charge carriers (trapped) then reacted with surface absorbed O_2 and H_2O to produce superoxide and •OH radicals, respectively. Ag functionalization on the surface of semiconductor ZnO lessened the work function which significantly, augmented the photocatalytic reaction performance of Ag/ZnO. Therefore, voids and Ag deposition (SPR effect) on ZnO boosted the RhB degradation rate from 45.5% to 99.8%, i.e., approximately 8.5 times more than bare ZnO semiconductor.

< Please insert Fig. 17 here >

In another work, Kwiatkowski *et al*. investigated the effect of voids on photocatalytic yield in the ZnO/TiO_2 core/shell (ZT) photosystem. They fabricated ZnO/TiO_2 core/shell nanohybrid through the sol-gel deposition route, followed by further calcination at a higher temperature (450°C) [162]. Calcination for 1h generated empty spaces (Fig. 18 a) due to the diffusion of Zn^{2+} into TiO_2 at the ZT interface called voids (Kirkendall effect). The preferential outward diffusion of Zn ions into the TiO_2 surface would lead to the creation of voids at the ZnO/TiO_2 interface, as depicted with the help of XPS as well as EDX analysis. Voids (more V_o) in the sample shifted the light-absorbing range (Visible, 420-600nm), reduced the band gap (2.9eV) potential via generating fermi level as well as generated more excited e^- and h^+. ZT interface played a crucial

role in the photodegradation of MB dye, as illustrated in Fig. 18 b, along with different comparative studies. The above-described results suggested the significantly modified region in ZT nanostructure, which in result boosted the overall photodegradation rate.

< Please insert Fig. 18 here >

Based upon the structural composition of bacteria, a gram-negative *Escherichia coli (E.coli)* is of great concern. Thereby, Liu *et al*. demonstrated that the PdO loaded TiO_2 nanocomposite with voids showed high disinfection photoefficiency on *E.coli* [163]. Uniform allocation of PdO inside as well as on the surface of TiO_2 hollow spheres was accomplished through template- free solvothermal route followed by calcination (Fig. 19 a). Elemental peaks of Ti, O, and Pd were depicted with the help of surface analysis based on the XPS characterization technique, which confirmed the synthesis of PdO/TiO_2 heterojunction. UV light absorption (365 nm) spectra, as depicted in Fig.19 b, showed multiple reflections due to photoexcited charges in the hollow spheres (interior voids) of PdO doped TiO_2 photocatalyst. Decreased surface area ($35.0 m^2/g$) with increased pore dimension to 22.2 nm due to the presence of voids acted as charge carrier trapper which facilitated the migration of h^+ and e^- more quickly to the outer surface as well as to PdO, respectively thus, reducing their recombination (Fig. 19 c). As a result, the synergism between extended light absorption and subsequent charge isolation was attained due to the creation of voids. Also, it was observed that PdO doping at 0.4 wt% on TiO_2 host was found to disinfect *E.Coli* cell more efficiently, i.e., 7-log decrease bacterial cell count in 100 min than bare. Therefore, in the as-synthesized sample, both hollow sphere morphology as well as generated voids (trappers), contributed to the primarily improved disinfection cell output.

< Please insert Fig. 19 here >

In a nutshell, with the help of various characterization techniques, it is examined that pits in the lattice usually decreased the surface area of a photocatalyst. But 3D defect rich MOs still exhibit higher photocatalytic output because of their distinctive surface morphology rather than defined decreased surface area. Photoefficacy is affected by the morphological structure of formed void in a photocatalytic material. From the above-cited examples, it is scrutinized that the initial photodegradation rate of toxic pollutants or bacteria increased with an increase in the entire void volume. Both Kirkendall, as well as SPR effects provoked the formation of larger voids at the boundary of heterostructures. Also, relative increasing voids, sagging bonds as well as ledges etc. in the host attributed to the redshift (visible range) as well as lower bandgap potential.

Zhao and his team synthesized visible light active yolk porous shell nanospheres from $Ag/TiO_2/SiO_2$ through oxidative chemical polymerization followed by the sol-gel method (Fig. 20 a). The as-fabricated SiO_2@Ag@Ag/TiO_2 photocatalyst contained three basic units, i.e., Ag/TiO_2, voids from the polypyrrole (PPy) layer, and porous shell-like functional units [164]. Owing to low density and high surface area for the loading of dopant, varied void space like properties contributed to its higher efficiency for the degradation of dye, i.e.,>>99.5%.FTIR spectrum analysis of TiO_2, Ag/TiO_2, PPy-Ag/TiO_2 as well asSiO_2@Ag@Ag/TiO_2photocatalysts were analyzed, which inveterate the fabrication of photocatalyst. It was observed that after calcination, the characteristic peaks (1544cm^{-1}, 1455cm^{-1}, 1192cm^{-1}) for PPy in PPy - Ag/TiO_2disappeared thereby demonstrated the formation of voids in the sample. SiO_2@Ag@Ag/TiO_2 nanohybrid exhibited strong visible light absorption (420nm) and reduced bandgap value (2.96eV), as illustrated in Fig. 20 b. Thus, PPy layers removal in the photocatalyst showed the generation of microreactors called void with large surface area and Ag deposition. Noteworthy, new energy level formation with apt potential and SPR effect due to noble metal

deposition is ascribed as a chief factor for efficient dye removal. In another report, Yoo *et al*. prepared ordered monodispersive Pt/SiO_2-TiO_2 microspheres with high void spaces via core-shell silica microspheres [157]. TEM and EDX analysis depicted the successful void formation in as-synthesized microspheres, which acted as nanoreactors. Pt encased void rich SiO_2-TiO_2 microspheres exhibited multiple reflections of UV light, which in turn enhanced H_2 production rate to 1518 $\mu molh^{-1}g^{-1}$.

< Please insert Fig. 20 here >

Similarly, Zhao *et al*. developed a facile strategy to fabricate Pd decorated N-doped carbon sphere@SnO_2 with 3D defects, prolonging the light absorption range to 425 nm and facilitated the e^- transfer from SnO_2 to Pd NPs (Fig. 21 a). Increased BET surface area (116 $m^{-1}g^{-1}$) showed maximum reactant and active site interactions, resulting in improved reduction efficiency (92%) of 4- nitrophenol [160]. In another report, Saha *et al*. developed novel visible active Au decorated CdS/CdO hollow nanocomposite through the reflux route by use of oleic acid (capping agent), for the efficient remediation of environmental pollution. Ionic diffusion was mainly responsible for the generation of voids inside the nanocomposite. The formation of a central hollow structure was confirmed with the help of TEM images and BET. Increased surface area (36.74 m^2/gm) depicted that voids in the Au@CdS/CdO nano sample shortened the distance of photogenerated e^- - h^+ pairs to reach its surface and effectively reduced the rate of recombination as shown in Fig 21 b. CB potentials of CdO and CdS were appropriate to design Z-scheme heterostructure (Fig. 21 c), endowed the higher H_2 evolution (7.412 mmol g^{-1} h^{-1}), RhB (0.1947 min^{-1}), MB (0.095 min^{-1}) degradation and Cr (0.24 min^{-1}) reduction rate [159].

< Please insert Fig. 21 here >

Recently, Thennarasu *et al.* prepared visible, active $ZnO/ZnCr_2O_4$ nanolayered composite by combustion route to degrade organic pollutants (AO) in slurry photoreactor with unstable intermediates [165]. The decomposition of various precursors with abundant gas emission depicted the creation of voids in the $ZnO/ZnCr_2O_4$ as analyzed with the help of FE-SEM micrographs. As-resulted narrowed bandgap (2.77 eV) further reduced the reassembly rate of e^- (CB of ZnO) as well as h^+ (VB of $ZnCr_2O_4$), which ultimately facilitated the AO photodegradation efficiency. At pH 6.86 (optimal) of the reaction mixture, the highest AO degradation (99%) was analyzed under visible light range due to the presence of more voids. Mechanistic studies revealed that adsorbed dye moiety on the photocatalyst was degraded into H_2O and CO_2 owing to the production of superoxide and •OH radicals on the surface of ZnO as well as $ZnCr_2O_4$, respectively.

Conclusively, hollow spaces in the MOs-core interface are known as a void channel that facilitates the diffusion power of different components across its surface. A large number of pits and disorders in nanohybrids (Kirkendall effect) substantially alter their surface morphological properties. Along with these advantages, they also accelerated the pollutant or metal ions absorption speed, improved the storage power (trapper), tailored the band potentials along with electric as well as redox potentials. Thereby, the above-mentioned parameters thus appeared as a favorable route to increase the induced e^--h^+ isolation rate and to improve photocatalytic techniques for wide sanitization of wastewater. In a nutshell, for comprehensive studies as well as clarification of photocatalytic means, it is very crucial to analyze the above-mentioned structure of void generation in a MOs lattice. Distinct void rich MOs as efficient defect driven photocatalytic materials with improved performance for various photocatalytic applications are summarized in Table. 3. Therefore, defect engineering is known as one of the most common

approaches which proved its significance in accelerating the photocatalytic output of most of the metal oxides.

6. Other applications

As reviewed above, defect modulation in MOs semiconductor materials substantially improve the photocatalytic performance owing to extended visible light absorption, charge-carriers isolation, and boosted surface photo-reaction kinetics. Table. 4 summarize distinct MOs as efficient defect driven photocatalytic materials with improved performance. However, the utilization of defect engineered MOs are not limited to photocatalysis only, but their significant potential is explored in other applications as well. Photoelectrochemical sensors (PEC) have gained much attention owing to its several advantages like; simple equipment, high sensitivity, fast analysis, and low cost etc. For instance, Nayak and his group synthesized $WO_3.H_2O$ nanoplates and $W_{18}O_{49}$ nanowires via precipitation and microwave-assisted route, respectively, to study both photocatalytic and PEC RhB degradation, photocurrent density, and H_2 evolution for water splitting applications. From BET and Raman spectra analysis, it was observed that large surface area and generated V_o defects in $W_{18}O_{49}$ could efficiently improve the charge isolation rate, resulting fostered photocatalytic RhB degradation to 91%, photocurrent density to 4.08 mA/cm^{2,} and higher photocatalytic H_2 production rate than $WO_3.H_2O$ [191]. In another report, Rahman *et al.* fabricated visible-active TiO_2 nanowires with abundant surface V_o using a catalyst-assisted pulsed laser deposition route. Surface V_o defects were identified with the help of XPS spectrum analysis. Prolonged charge carrier tunneling and longer wavelength absorption resulting from V_o exhibited improved current density from 1.6 mA/cm^2 to 2.2 mA/cm^2 i.e. 87% of the overall PEC current [192]. Similarly, to analyse the electrocatalytic properties of $NiCo_2O_4$,

Yang *et al*. fabricated stable NiMn LDH/$NiCo_2O_4$ nanohybrids via a hydrothermal route. Interestingly, incorporated defects investigated through XPS spectra in the $NiCo_2O_4$ provided large surface area and active sites on the exposed edge sites, which indeed reduced the energy barrier for O_2 evolution and thereby increased the electrocatalytic oxygen evolution performance of $NiCo_2O_4$ [193]. In another report, versatile catalysts using TiO_{2-x} nanosheets supported by a CNT were fabricated for Li-S batteries. Wang *et al*. investigated the effect of CNT@TiO_{2-x} defects (through XPS) on the electronic conductivity and chemical adsorption and depicted that the surface rich vacancies accelerated the surface e^- exchange process through bandgap engineering. As-synthesized catalyst showed long cycle stability, high area capacity of 5.4 mAh $cm^{-2}s$, the large surface area of $256.5m^2g^{-1}$ [194]. Similarly, Yu *et al*. exploited defect engineered and highly stable $NiCeO_x$ electrocatalyst via a two-step dip-coating method. XPS and Raman spectral analysis depicted the formation of V_o defects, which leads to stronger electronic interactions between Ni and CeO_2. A large number of active sites and favorable reaction kinetics for O_2 in the as-fabricated NiCeOx sample showed improved O_2 evolution rate, a high current density of 10 mA/cm^2 and a low overpotential of 470 mV [195]. Chen *et al*. developed defect rich MgH_2/Cu_xO composite by three-step ball-milling method contributed to the improved CO_2 hydrogenation. As a result, defect rich hydrogen storage MgH_2/Cu_xO composite exhibited 54.8% olefins formation and 20.7% CO_2 conversion rate [196]. Thereby, from the above-reviewed reports, it is clear that defects in MOs semiconductors could serve as highly active (catalytic) sites, which accelerated e^- - h^+ isolation by tunning band potentials thus, holding promising potential for achieving high catalytic, PEC, and electrocatalytic performances.

7. Conclusive outlook

Modulation in photocatalytic efficacy through defect engineering seems to play as an effective approach to improve numerous solar light-driven environmental restoration and energy conversion applications. In recent years significant attention has been drawn to simultaneously modify the optical, electronic, and photoinduced surface reaction kinetics of semiconductor photocatalysts. Thus, the present study has been devoted to highlighting recent progress in defect-engineered MOs photocatalyst for various applications, with significant advances being made. Potentials and certain inherent bottlenecks of MOs as photocatalyst has been concisely summarized, followed by surface modification through anion/cation vacancy. Furthermore, the influential role of defect engineering in MOs through the generation of point defects, dislocations, boundaries, and voids has been explored with their fabrication, identification, and the subsequent effect on photoactivity. Different possible routes to modify the photocatalytic performance of MOs either by generating point defects, dislocations and boundaries or voids were highlighted. Noteworthy, defect induced MOs exhibit superior photocatalytic activity than bare nanomaterial owing to the substantial impact of defect creation on optoelectronic properties. Thereby, assorted defects involving anionic, cationic and multi vacancies, vacancy associates, distortions, dislocations, voids as well as boundaries are introduced to alter the bandgap, morphological arrangement, coordination number, conductivity etc. in various MOs. Defect mediated MOs are fabricated using different effective strategies (high-temperature conditions, UV radiations, Chemical reduction etc.) and are identified by utilizing valid diverse, and advanced characterization methods (EPR, XPS, Raman, STEM etc.). Defects played a pivotal role in a semiconductor photocatalyst owing to the following reasons: Firstly, defects in MOs can improve the dissociative adsorption of moieties like pollutants, CO_2 as well as H_2O etc. Secondly, they tune the electronic band potentials in order to boost optical absorption efficacy.

Thirdly, they act as charge carrier trappers to enhance the segregation rate by exposing excited e^- on to the surface of MOs. Of note, the applications of defect modified MOs are not only limited to photocatalysis, but they also offer great potential in the field of energy storage devices, photo-electrochemical systems, electrocatalysts, catalysts, and membranes for biological functions.

8. Challenges and perspectives

Despite various positive effects of defect engineering in MOs semiconductors, there still remain certain challenges involving fabrication techniques of defect rich MOs, mechanistic studies for their identification, and the role of defects in improving various photocatalytic applications. The efficient production of defect mediated MOs with unique surface area and morphology will be of crucial concern. Besides, certain disadvantages also tend to associate with defect modified MOs, which need critical attention, as follows: 1. Excessive concentration of any (0, 1, 2, and 3D) bulk defects in MOs will form reassembly centers and thus responsible for the reunion of excited carriers, 2. High-temperature conditions (calcination) sometimes even destroy the primary chemical bonding present in between the host atoms, 3. Some defects like surface anion defects in a semiconductor are not much stable and hence could be easily renovated 4. Fabrication of defects in MOs is random, i.e., one impurity may lead to more than one defects in host semiconductor etc. and 5. The stability of a photocatalyst is an essential key factor while fabricating a photocatalyst. Numerous MOs nanomaterial with varied photocatalytic mechanisms and defects can demonstrate different photocatalytic results towards full range applications. Proper understanding of the correlation between induced defects and the resulted modulation in photocatalytic property can help to overcome the limitations or to resolve the problems like quantitative defect analysis, involvement in e^- - h^+ isolation, in-situ characterization, controlled

generation and concentration at the desired location in MOs. These issues mentioned above can provide new insight for defect induced effective e^- - h^+ pairs segregation and for boosted photocatalytic output.

In order to achieve economic as well as environmental benefits, we have to follow specific directions as i) Understanding the origin of certain defects in MOs, ii) Exploring the photocatalytic mechanism (photodegradation, photoreduction, and disinfection etc.) involving certain defects, iii) Fabricating defect mediated metal oxide photocatalyst showing elevated-performance. Appropriate synergism between controlled defect designing, suitable identification technique, and in-situ characterization for investigating the reaction pathway involved in photocatalysis can effectively help researchers working in the field to explore new insights and attain amended photoactivity. Therefore, in a nutshell, defect engineering is known as an essential objective for synthesizing visible light active MO photocatalyst exhibiting higher stability with superior photocatalytic output for environmental and energy-related applications.

References

[1] P. Raizada, P. Singh, A. Kumar, G. Sharma, B. Pare, S.B. Jonnalagadda, P. Thakur, Solar photocatalytic activity of nano-ZnO supported on activated carbon or brick grain particles: role of adsorption in dye degradation, Appl. Catal A: Gen. 486 (2014), pp. 159-169

[2] C. González-Buch, I. Herraiz-Cardona, E. Ortega, J. García-Antón, V. Pérez-Herranz, Synthesis and characterization of macroporous Ni, Co and Ni–Co electrocatalytic deposits for hydrogen evolution reaction in alkaline media, Int. J. Hydrog. Energy 38 (2013), pp. 10157-10169

[3] B. Priya, P. Raizada, N. Singh, P. Thakur, P. Singh, Adsorptional photocatalytic mineralization of oxytetracycline and ampicillin antibiotics using Bi_2O_3/BiOCl supported on graphene sand composite and chitosan, J. Colloid Interface Sci. 479 (2016), pp. 271-283

[4] I. Ganesh, Electrochemical conversion of carbon dioxide into renewable fuel chemicals–The role of nanomaterials and the commercialization, Renew. Sust. Energ. Rev. 59 (2016), pp. 1269-1297

[5] B. Priya, P. Shandilya, P. Raizada, P. Thakur, N. Singh, P. Singh, Photocatalytic mineralization and degradation kinetics of ampicillin and oxytetracycline antibiotics using graphene sand composite and chitosan supported BiOCl, J. Mol. Catal. A: Chem. 423 (2016), pp. 400-413

[6] G. Zhu, R. Ge, F. Qu, G. Du, A.M. Asiri, Y. Yao, X. Sun, In situ surface derivation of an Fe–Co–Bi layer on an Fe-doped Co_3O_4 nanoarray for efficient water oxidation electrocatalysis under near-neutral conditions, J. Mater. Chem. A 5 (2017), pp. 6388-6392

[7] T.R. Cook, D.K. Dogutan, S.Y. Reece, Y. Surendranath, T.S. Teets, D.G. Nocera, Solar energy supply and storage for the legacy and non-legacy worlds, Chem. Rev. 110 (2010), pp. 6474-6502

[8] M.Z. Jacobson, Review of solutions to global warming, air pollution, and energy security, Energy Environ. Sci. 2 (2009), pp. 148-173

[9] P. Singh, P. Raizada, S. Kumari, A. Kumar, D. Pathania, P. Thakur, Solar-Fenton removal of malachite green with novel FeO-activated carbon nanocomposite, Appl. Catal. A: Gen. 476 (2014), pp. 9-18

[10] P. Raizada, P. Singh, A. Kumar, B. Pare, S.B. Jonnalagadda, Zero valent iron-brick grain nanocomposite for enhanced solar-Fenton removal of malachite green, Sep. Purif. Technol. 133 (2014), pp. 429-437

[11] E. Brillas, E. Mur, R. Sauleda, L. Sanchez, J. Peral, X. Domènech, J. Casado, Aniline mineralization by AOP's: anodic oxidation, photocatalysis, electro-Fenton and photoelectro-Fenton processes, Appl. Catal. B: Environ. 16 (1998), pp. 31-42

[12] W.H. Glaze, J.W. Kang, D.H. Chapin, The chemistry of water treatment processes involving ozone, hydrogen peroxide and ultraviolet radiation, Ozone: Sci. 9 (1987), *pp. 335-352*

[13] H. Dong, X. Zhang, J. Li, P. Zhou, S. Yu, N. Song, C. Liu, G. Che, C. Li. "Construction of morphology-controlled nonmetal 2D/3D homojunction towards enhancing photocatalytic activity and mechanism insight," Appl. Catal. B: Environ. 263 (2020), pp. 118270

[14] P. Raizada, A. Sudhaik, P. Singh, Photocatalytic water decontamination using graphene and ZnO coupled photocatalysts: A review, Mater. Sci. Technol. (2019), https://doi.org/10.1016/j.mset.2019.04.007

[15] P. Raizada, P. Shandilya, P. Singh, P.Thakur, Solar light-facilitated oxytetracycline removal from the aqueous phase utilizing a H_2O_2/$ZnWO_4$/CaO catalytic system, J. Taibah Univ. Sci. 11 (2017), pp. 689-699

[16] G. Liu, C.Y. Jimmy, G.Q.M. Lu, H.M. Cheng, Crystal facet engineering of semiconductor photocatalysts: motivations, advances and unique properties, Chem Comm. 47 (2011), pp. 6763-6783

[17] V. Dutta, P. Singh, P. Shandilya, S. Sharma, P. Raizada, A.K. Saini, V.K. Gupta, A. Hosseini-Bandegharaei, S. Agarwal, A. Rahmani-Sani, Review on advances in photocatalytic water disinfection utilizing graphene and graphene derivatives-based nanocomposites, J. Environ. Chem. Eng. 7 (2019), p. 103132

[18] P. Raizada, S. Sharma, A. Kumar, P. Singh, A.A.P. Khan, A.M. Asiri, Performance improvement strategies of $CuWO_4$ photocatalyst for hydrogen generation and pollutant degradation, J. Environ. Chem. Eng. (2020), p. 104230, https://doi.org/10.1016/j.jece.2020.104230

[19] L. Zhang, J.C. Yu, H.Y. Yip, Q. Li, K.W. Kwong, A.W. Xu, P.K. Wong, Ambient light reduction strategy to synthesize silver nanoparticles and silver-coated TiO_2 with enhanced photocatalytic and bactericidal activities, Langmuir 19 (2003), pp. 10372-10380

[20] S. Sharma, V. Dutta, P. Singh, P. Raizada, A. Rahmani-Sani, A. Hosseini-Bandegharaei, V.K. Thakur, Carbon quantum dot supported semiconductor photocatalysts for efficient degradation of organic pollutants in water: a review, J. Clean. Prod. (2019), https://doi.org/10.1016/j.jclepro.2019.04.292

[21] Y.F. Fang, W.H. Ma, Y.P. Huang, G.W. Cheng, Exploring the reactivity of multicomponent photocatalysts: insight into the complex valence band of BiOBr, Chem. Eur. 19 (2013), pp. 3224-3229

[22] Y. Yang, M. Wu, X. Zhu, H. Xu, S. Ma, Y. Zhi, H. Xia, X. Liu, J. Pan, J.Y. Tang, S.P. Chai, 2020 Roadmap on two-dimensional nanomaterials for environmental catalysis, Chin Chem. Lett. 30 (2019), pp. 2065-2088

[23] C. Li, S. Yu, H. Dong, C. Liu, H. Wu, H. Che, G. Chen, "Z-scheme mesoporous photocatalyst constructed by modification of Sn_3O_4 nanoclusters on g-C_3N_4 nanosheets with improved photocatalytic performance and mechanism insight," Appl. Catal. B: Environ. 238 (2018), pp. 284-293

[24] H. Zhang, Ultrathin two-dimensional nanomaterials, ACS Nano. 9 (2005), pp. 9451-9469

[25] M. Zhou, X.W.D. Lou, Y. Xie, Two-dimensional nanosheets for photoelectrochemical water splitting: Possibilities and opportunities, Nano Today 8 (2013), pp. 598-618

[26] B. Pare, P. Singh, S.B. Jonnalgadda, Artificial light assisted photocatalytic degradation of lissamine fast yellow dye in ZnO suspension in a slurry batch reactor, (2009), http://hdl.handle.net/123456789/6122

[27] Q. Lu, Y. Yu, Q. Ma, B. Chen, H. Zhang, 2D transition metal dichalcogenide nanosheet based composites for photocatalytic and electrocatalytic hydrogen evolution reactions, Adv. Mater. 28 (2016), pp. 1917-1933

[28] F. Ma, Y. Wu, Y. Shao, Y. Zhong, J. Lv, X. Hao, 0D/2D nanocomposite visible light photocatalyst for highly stable and efficient hydrogen generation via recrystallization of CdS on MoS_2 nanosheets, Nano Energy 27 (2016), pp. 466-474

[29] N.E. Grant, J.D. Murphy, Temporary surface passivation for characterization of bulk defects in silicon: a review, Phys. Status Solidi RRL 11 (2017), p. 1700243

[30] Y. Wang, D. Widmann, M. Heenemann, T. Diemant, J. Biskupek, R. Schlögl, R.J. Behm, The role of electronic metal-support interactions and its temperature dependence: CO adsorption and CO oxidation on Au/TiO_2 catalysts in the presence of TiO_2 bulk defects, J. Catal. 354 (2017), pp. 46-60

[31] H.P. Komsa, A.V. Krasheninnikov, Native defects in bulk and monolayer MoS_2 from first principles, Phys. Rev. B 91 (2015), p. 125304

[32] X. Wang, D.S. Miller, E. Bukusoglu, J.J. De Pablo, N.L. Abbott, Topological defects in liquid crystals as templates for molecular self-assembly, Nat. Mater. 15 (2016), pp. 106-112

[33] S. Bai, N. Zhang, C. Gao, Y. Xiong, Defect engineering in photocatalytic materials, Nano Energy 53 (2018), pp. 296-336

[34] Z. Fang, B. Bueken, D.E. De Vos, R.A. Fischer, Defect□engineered metal–organic frameworks, Angew. Chem. Int. Ed. 54 (2015), pp.7234-7254

[35] H. Sun, W. Fan, Y. Li, X. Cheng, P. Li, J. Hao, X. Zhao, Origin of improved visible photocatalytic activity of nitrogen/hydrogen codoped cubic In_2O_3: First-principles calculations, Phys. Chem. Chem. Phys. 13 (2011), pp. 1379-1385

[36] H. Tan, Z. Zhao, W.B. Zhu, E.N. Coker, B. Li, M. Zheng, W. Yu, H. Fan, Z. Sun, Oxygen vacancy enhanced photocatalytic activity of pervoskite $SrTiO_3$. ACS Appl. Mater. Interfaces, 6 (2014), pp. 19184-19190

[37] H. Yu, R. Shi, Y. Zhao, T. Bian, Y. Zhao, C. Zhou, G.I. Waterhouse, L.Z. Wu, C.H. Tung, T. Zhang, 2017 Alkali□assisted synthesis of nitrogen deficient graphitic carbon nitride with tunable band structures for efficient visible□light□driven hydrogen evolution, Adv. Mater. 29 (2017), p. 1605148

[38] G. Wang, B. Huang, Z. Li, Z. Lou, Z. Wang, Y. Dai, M.H. Whangbo, Synthesis and characterization of ZnS with controlled amount of S vacancies for photocatalytic H_2 production under visible light, Sci. Rep. 5 (2015), p. 8544

[39] N. Serpone, A.V. Emeline, V.K. Ryabchuk, V.N. Kuznetsov, Y.M. Artem'ev, S. Horikoshi, Why do hydrogen and oxygen yields from semiconductor-based photocatalyzed water splitting remain disappointingly low? Intrinsic and extrinsic factors impacting surface redox reactions, ACS Energy Lett. 1 (2016), pp. 931-948

[40] X. Pan, M.Q. Yang, X. Fu, N. Zhang, Y.J. Xu, Defective TiO_2 with oxygen vacancies: synthesis, properties and photocatalytic applications, Nanoscale 5 (2013), pp. 3601-3614

[41] V. Hasija, P. Raizada, A. Sudhaik, K. Sharma, A. Kumar, P. Singh, S.B. Jonnalagadda, V.K. Thakur, Recent advances in noble metal free doped graphitic carbon nitride based nanohybrids for photocatalysis of organic contaminants in water: A review, Appl. Mater. Today 15 (2019), pp. 494-524

[42] N. Chandel, K. Sharma, A. Sudhaik, P. Raizada, A. Hosseini-Bandegharaei, V.K. Thakur, P. Singh, Magnetically separable ZnO/$ZnFe_2O_4$ and ZnO/$CoFe_2O_4$ photocatalysts supported onto nitrogen doped graphene for photocatalytic degradation of toxic dyes Arab. J. Chem. 13 (2020), pp. 4324-4340

[43] P. Singh, P. Shandilya, P. Raizada, A. Sudhaik, A. Rahmani-Sani, A. Hosseini-Bandegharaei, Review on various strategies for enhancing photocatalytic activity of graphene based nanocomposites for water purification, Arab. J. Chem. (2018), https://doi.org/10.1016/j.arabjc.2018.12.001

[44] R. Saravanan, F. Gracia, A. Stephen, Basic principles, mechanism, and challenges of photocatalysis. In Nanocomposites for visible light- induced photocatalysis, Springer (2017), pp. 19-40

[45] S. Zhu, D. Wang, 2017. Photocatalysis: basic principles, diverse forms of implementations and emerging scientific opportunities, Adv. Energy Mater. 7 (2017), p. 1700841

[46] D. Robert, S. Malato, Solar photocatalysis: a clean process for water detoxification, Sci. Total Environ. 291 (2002), pp. 85-97

[47] M. Schiavello, Some working principles of heterogeneous photocatalysis by semiconductors, Electrochim. Acta 38 (1993), pp. 11-14

[48] P. Raizada, J. Kumari, P. Shandilya, P. Singh, Kinetics of photocatalytic mineralization of oxytetracycline and ampicillin using activated carbon supported $ZnO/ZnWO_4$, Desalination 79 (2017), pp. 204-213

[49] A. Kumar, P. Raizada, P. Singh, R. Saini, A. Saini, A. Hosseini-Bandegharaei, Perspective and status of polymeric graphitic carbon nitride based Z-scheme photocatalytic systems for sustainable photocatalytic water purification, J. Chem. Eng. (2019), p. 123496, https://doi.org/10.1016/j.cej.2019.123496

[50] H. Dong, S. Hong, P. Zhang, S. Yu, Y. Wang, S. Yuan, H. Li, J. Sun, G. Chen, C. Li, "Metal-free Z-scheme 2D/2D VdW heterojunction for high-efficiency and durable photocatalytic H_2 production," J.Chem. Eng. (2020), pp. 125150

[51] P. Raizada, A. Kumar, P. Singh, Graphitic Carbon Nitride-Based New Advanced Materials for Photocatalytic Applications, Curr. Anal. Chem. 16 (2020), pp. 1-00

[52] B. Liu, X. Zhao, C. Terashima, A. Fujishima, K. Nakata, Thermodynamic and kinetic analysis of heterogeneous photocatalysis for semiconductor systems, Phys. Chem. Chem. Phys. 16 (2014), pp. 8751-8760

[53] V. Hasija, P. Raizada, A. Sudhaik, P. Singh, V.K. Thakur, A.A.P. Khan, Fabrication of $Ag/AgI/WO_3$ heterojunction anchored P and S co-doped graphitic carbon nitride as a dual Z scheme photocatalyst for efficient dye degradation, Solid State Sci. 100 (2020), p. 106095

[54] L. Yuan, C. Han, M.Q. Yang, Y.J. Xu, Photocatalytic water splitting for solar hydrogen generation: fundamentals and recent advancements, Int. Rev. Phys. Chem. 35 (2016), pp.1-36

[55] K. Sharma, V. Dutta, S. Sharma, P. Raizada, A. Hosseini-Bandegharaei, P. Thakur, P. Singh, Recent advances in enhanced photocatalytic activity of bismuth oxyhalides for efficient photocatalysis of organic pollutants in water: A review, J. Ind. Eng. Chem. (2019), https://doi.org/10.1016/j.jiec.2019.06.022

[56] P. Raizada, A. Sudhaik, P. Singh, A. Hosseini-Bandegharaei, P. Thakur, Converting type II AgBr/VO into ternary Z scheme photocatalyst via coupling with phosphorus doped g-C_3N_4 for enhanced photocatalytic activity, Sep. Purif. Technol. 227 (2019), p. 115692

[57] L.V. Bora, R.K. Mewada, Visible/solar light active photocatalysts for organic effluent treatment: Fundamentals, mechanisms and parametric review, Renew. Sust. Energy Rev. 76 (2017), pp. 1393-1421

[58] V.Hasija, A. Sudhaik, P. Raizada, A. Hosseini-Bandegharaei, P. Singh, Carbon quantum dots supported AgI/ZnO/phosphorus doped graphitic carbon nitride as Z-scheme photocatalyst for efficient photodegradation of 2, 4-dinitrophenol, J. Environ. Chem. Eng. 7 (2019), p. 103272

[59] J. Low, S. Cao, J. Yu, S. Wageh, Two-dimensional layered composite photocatalysts, Chem. Comm. 50 (2014), pp. 10768-10777

[60] J.L. Gunjakar, T.W. Kim, H.N. Kim, I.Y. Kim, S.J. Hwang, Mesoporous layer-by-layer ordered nanohybrids of layered double hydroxide and layered metal oxide: highly active visible light photocatalysts with improved chemical stability, J. Am. Chem. Soc. 133 (2011), pp. 14998-15007

[61] M. Xiao, Z. Wang, M. Lyu, B. Luo, S. Wang, G. Liu, H.M. Cheng, L. Wang, Hollow nanostructures for photocatalysis: advantages and challenges, Adv. Mater. 31 (2019), p. 1801369

[62] S. Sun, P. Gao, Y. Yang, P. Yang, Y. Chen, Y. Wang, N-doped TiO_2 nanobelts with co-exposed (001) and (101) facets and their highly efficient visible-light-driven photocatalytic hydrogen production, ACS Appl. Mater. Interfaces 8 (2016), pp. 18126-18131

[63] A.K. Singh, K. Mathew, H.L. Zhuang, R.G. Hennig, Computational screening of 2D materials for photocatalysis, J. Phys. Chem. Lett. 6 (2015), pp. 1087-1098

[64] L.C. Buelens, A.N.V.R. Dharanipragada, H. Poelman, Z. Zhou, G.B. Marin, V.V. Galvita, Exploring the stability of Fe_2O_3-$MgAl_2O_4$ oxygen storage materials for CO production from CO_2, J. CO_2 Util. 29 (2019), pp. 36-45

[65] X. Yuan, H. Ge, X. Liu, X. Wang, W. Chen, W. Dong, F. Huang, Efficient catalyst of defective CeO^{2-x} and few-layer carbon hybrid for oxygen reduction reaction, J. Alloys Compd. 688 (2016), pp. 613-618

[66] J. Di, J. Xiong, H. Li, Z. Liu, Ultrathin 2D photocatalysts: electronic□structure tailoring, hybridization, and applications, Adv. Mater. 30 (2018), pp. 1704548

[67] M.A. Rahman, J.P. Thomas, K.T. Leung, A Delaminated Defect□Rich ZrO_2 Hierarchical Nanowire Photocathode for Efficient Photoelectrochemical Hydrogen Evolution, Adv. Energy Mater. 8 (2018), pp. 1701234

[68] J. Xiong, J. Di, J. Xia, W. Zhu, H. Li, Surface defect engineering in 2D nanomaterials for photocatalysis, Adv. Funct. Mater. 28 (2018), pp. 1801983

[69] A. Naldoni, M. Allieta, S. Santangelo, M. Marelli, F. Fabbri, S. Cappelli, C.L. Bianchi, R. Psaro, V. Dal Santo, Effect of nature and location of defects on bandgap narrowing in black TiO_2 nanoparticles, J. Am. Chem. Soc. 134 (2012), pp. 7600-7603

[70] R. Zhang, W. Chen, Recent advances in graphene-based nanomaterials for fabricating electrochemical hydrogen peroxide sensors, Biosens. Bioelectron. 89 (2017), pp. 249-268

[71] Q. Xiang, J. Yu, Graphene-based photocatalysts for hydrogen generation, J. Phys. Chem. Lett. 4 (2013), pp. 753-759

[72] J. Yu, J. Jin, B. Cheng, M. Jaroniec, A noble metal-free reduced graphene oxide–CdS nanorod composite for the enhanced visible-light photocatalytic reduction of CO_2 to solar fuel, J. Mater. Chem. A (2014), pp. 3407-3416

[73] M.V. Ganduglia-Pirovano, J.L. Da Silva, J. Sauer, Density-functional calculations of the structure of near-surface oxygen vacancies and electron localization on CeO_2 (111), Phys. Rev. Lett. 102 (2009), pp. 026101

[74] A. Bouzoubaa, A. Markovits, M. Calatayud, C. Minot, Comparison of the reduction of metal oxide surfaces: TiO_2-anatase, TiO_2-rutile and SnO_2-rutile, Surf. Sci. 583 (2005), pp. 107-117

[75] Z. Pei, L. Ding, H. Lin, S. Weng, Z. Zheng, Y. Hou, P. Liu, Facile synthesis of defect-mediated TiO_{2-x} with enhanced visible light photocatalytic activity, J. Mater. Chem. 1 (2013), pp. 10099-10102

[76] J. Hou, S. Cao, Y. Wu, F. Liang, Y. Sun, Z. Lin, L. Sun, Simultaneously efficient light absorption and charge transport of phosphate and oxygen-vacancy confined in bismuth tungstate atomic layers triggering robust solar CO_2 reduction, Nano Energy 32 (2017), pp. 359-366

[77] H. Chen, F. Zhang, W. Zhang, Y. Du, G. Li, Negative impact of surface Ti^{3+} defects on the photocatalytic hydrogen evolution activity of $SrTiO_3$, Appl. Phys. Lett. 112 (2018), p. 013901

[78] Z. Pei, S. Weng, P. Liu, Enhanced photocatalytic activity by bulk trapping and spatial separation of charge carriers: A case study of defect and facet mediated TiO_2, Appl. Catal. B: Environ. 180 (2016), pp. 463-470

[79] M.J. Zheng, L.D. Zhang, G.H. Li, W.Z. Shen, Fabrication and optical properties of large-scale uniform zinc oxide nanowire arrays by one-step electrochemical deposition technique, Chem. Phys. Lett. 363 (2002), pp. 123-128

[80] H. Osgood, S.V. Devaguptapu, H. Xu, J. Cho, G. Wu, Transition metal (Fe, Co, Ni, and Mn) oxides for oxygen reduction and evolution bifunctional catalysts in alkaline media, Nano. Today 11 (2016), pp. 601-625

[81] A.S. Ahmed, M.L. Singla, S. Tabassum, A.H. Naqvi, A. Azam, Band gap narrowing and fluorescence properties of nickel doped SnO_2 nanoparticles, J. Lumim. 131 (2011), pp. 1-6

[82] M.A. Neouze, U. Schubert, Surface modification and functionalization of metal and metal oxide nanoparticles by organic ligands, Monatsh. Chem. Chem. Mon. 139 (2008), pp. 183-195

[83] G. Grundmeier, M. Brettmann, P. Thiemann, In situ spectroscopic and corrosion studies of ultra-thin gradient plasma polymer layers on zinc, Appl. Surf. Sci. 217 (2003), pp. 223-232

[84] S. Mallakpour, M. Madani, A review of current coupling agents for modification of metal oxide nanoparticles, Prog. Org. Coat. 86 (2015), pp. 194-207

[85] J. Yan, T. Wang, G. Wu, W. Dai, N. Guan, L. Li, J. Gong, Tungsten oxide single crystal nanosheets for enhanced multichannel solar light harvesting, Adv. Mater. 27 (2015), pp. 1580-1586

[86] R. Ren, Z. Wen, S. Cui, Y. Hou, X. Guo, J. Chen, Controllable synthesis and tunable photocatalytic properties of Ti^{3+}- doped TiO_2, Sci. Rep. 5 (2015), pp. 1-11

[87] M. Xing, J. Zhang, F. Chen, B. Tian, An economic method to prepare vacuum activated photocatalysts with high photo-activities and photo sensitivities, Chem. Comm. 47 (2011), pp. 4947-4949

[88] Y. Zhang, H. Zhang, Y. Xu, Y. Wang, Europium doped nanocrystalline titanium dioxide: preparation, phase transformation and photocatalytic properties, J. Mater. Chem. 13 (2003), pp. 2261-2265

[89] C.M. Magdalane, K. Kaviyarasu, J.J. Vijaya, B. Siddhardha, B. Jeyaraj, Photocatalytic activity of binary metal oxide nanocomposites of CeO_2/CdO nanospheres: investigation

of optical and antimicrobial activity, J. Photochem. Photobio. B: Bio. 163 (2016), pp. 77-86

[90] M. Miyauchi, A. Nakajima, T. Watanabe, K. Hashimoto, Photocatalysis and photoinduced hydrophilicity of various metal oxide thin films, Chem. Mater. 14 (2002), pp. 2812-2816

[91] Y. Sun, Q. Liu, S. Gao, H. Cheng, F. Lei, Z. Sun, Y. Jiang, H. Su, S. Wei, Y. Xie, Pits confined in ultrathin cerium (IV) oxide for studying catalytic centers in carbon monoxide oxidation, Nat. Commun. 4 (2013), pp. 1-8

[92] H. Wang, H.W. Lee, Y. Deng, Z. Lu, P.C. Hsu, Y. Liu, D. Lin, Y. Cui, Bifunctional non-noble metal oxide nanoparticle electrocatalysts through lithium-induced conversion for overall water splitting, Nat. Comm. 6 (2015), pp. 1-8

[93] D. Liu, Y. Liu, A. Pan, K.P. Nagle, G.T. Seidler, Y.H. Jeong, G. Cao, Enhanced lithium-ion intercalation properties of V_2O_5 xerogel electrodes with surface defects, J. Phys. Chem. 115 (2011), pp. 4959-4965

[94] W. Liu, P. Oh, X. Liu, M.J. Lee, W. Cho, S. Chae, Y. Kim, J. Cho, Nickel□rich layered lithium transition□metal oxide for high□energy lithium□ion batteries, Angew. Chem. Int. Ed. 54 (2015), pp. 4440-4457

[95] T. Berger, J. Schuh, M. Sterrer, O. Diwald, E. Knözinger, Lithium ion induced surface reactivity changes on MgO nanoparticles, J. Catal. 247 (2007), pp. 61-67

[96] C.M. Magdalane, K. Kaviyarasu, J.J. Vijaya, B. Siddhardha, B. Jeyaraj, J. Kennedy, M. Maaza, Evaluation on the heterostructured CeO_2/Y_2O_3 binary metal oxide nanocomposites for UV/Vis light induced photocatalytic degradation of Rhodamine-B dye for textile engineering application, J. Alloys Compd. 727 (2017), pp. 1324-1337

[97] R.K. Upadhyay, N. Soin, S.S. Roy, Role of graphene/metal oxide composites as photocatalysts, adsorbents and disinfectants in water treatment: a review, RSC Adv. 4 (2014), pp. 3823-3851.

[98] J. Su, X. Zou, J.S. Chen, Self-modification of titanium dioxide materials by Ti^{3+} and/or oxygen vacancies: new insights into defect chemistry of metal oxides, Rsc Adv. 4 (2014), pp. 13979-13988

[99] a) B. Sun, Y. Qian, Z. Liang, Y. Guo, Y. Xue, J. Tian, H. Cui, Oxygen vacancy-rich BiO_{2-x} ultra-thin nanosheet for efficient full-spectrum responsive photocatalytic oxygen evolution from water splitting, Sol. Energy Mater. Sol. 195 (2019), pp. 309-317; b) D. Wu, W. Wang, F. Tan, F. Sun, H. Lu, X. Qiao, Fabrication of pit-structured ZnO nanorods and their enhanced photocatalytic performance, RSC Adv. (2013), pp. 20054-20059

[100] G. Grancini, R.S. Santosh Kumar, A. Abrusci, H.L. Yip, C.Z. Li, A.K. Jen, G. Lanzani, H.J. Snaith, Boosting infrared light harvesting by molecular functionalization of metal oxide/polymer interfaces in efficient hybrid solar cells, Adv. Funct. Mater. 22 (2012), pp. 2160-2166

[101] A. Folger, P. Ebbinghaus, A. Erbe, C. Scheu, Role of vacancy condensation in the formation of voids in rutile TiO_2 nanowires, ACS Appl. Mater. Inter. 9 (2017), pp. 13471-13479

[102] S. Tan, H. Feng, Y. Ji, Y. Wang, J. Zhao, A. Zhao, B. Wang, Y. Luo, J. Yang, J.G. Hou Observation of photocatalytic dissociation of water on terminal Ti sites of TiO_2 (110)-1× 1 surface, J. Am Chem. Soc. 134 (2012), pp. 9978-9985

[103] Y. Jiang, H. Ning, C. Tian, B. Jiang, Q. Li, H. Yan, X. Zhang, J. Wang, L. Jing, H. Fu, Single-crystal TiO_2 nanorods assembly for efficient and stable cocatalyst-free photocatalytic hydrogen evolution, Appl. Catal. B: Environ. 229 (2018) pp. 1-7

[104] J. Xue, X. Zhu, Y. Zhang, W. Wang, W. Xie, J. Zhou, J. Bao, Y. Luo, X. Gao, Y. Wang, L.Y. Jang, Nature of conduction band tailing in hydrogenated titanium dioxide for photocatalytic hydrogen evolution, Chem Cat Chem 8 (2016), pp. 2010-2014

[105] J. Li, X. Wu, W. Pan, G. Zhang, H. Chen, Vacancy□Rich Monolayer BiO_{2-x} as a Highly efficient UV, Visible, and Near□Infrared responsive photocatalyst, Agnew. Chem. Int. 57 (2018), pp. 491-495

[106] D.M. Duffy, J.H. Harding, A.M. Stoneham, The energies of point defects near metal/oxide interfaces, J. Appl. Phys. 76 (1994), pp. 2791-2798

[107] D.C. Sayle, G.W. Watson, Dislocations, lattice slip, defects and rotated domains: The effect of a lattice misfit on supported thin-film metal oxides, Phys. Chem. Chem. Phys. 2 (2000), pp. 5491-5499

[108] A. Dey, Semiconductor metal oxide gas sensors: A review, Mater. Sci. Eng. B 229 (2018), pp. 206-217

[109] R.L. Smith, G.S. Rohrer, An atomic force microscopy study of the morphological evolution of the MoO_3 (010) surface during reduction reactions, J. Catal. 163 (1996), pp. 12-17

[110] D.M. Duffy, J.H. Harding, A.M. Stoneham, A simulation of the NiO/Ag interface with point defects, Acta Metall. Mater. 43 (1995), pp. 1559-1568

[111] Y.-K. Shin, W-S. Chae, Y-W. Song, Y.-M. Sung, Formation of titania photocatalyst films by microarc oxidation of Ti and Ti–6Al–4V alloys, Electrochem. Comm. 8(2006), pp. 465-470

[112] F. H. Mustapha, A. A. Jalil, M. Mohamed, S. Triwahyono, N. S. Hassan, N. F. Khusnun, C. N. C. Hitam, A. F. A. Rahman, L. Firmanshah, A. S. Zolkifli, New insight into self-modified surfaces with defect-rich rutile TiO_2 as a visible-light-driven photocatalyst, J. Clean. Prod., 168 (2017), pp. 1150-1162

[113] M. Zhang, C. Lai, B. Li, D. Huang, S. Liu, L. Qin, H. Yi, Y. Fu, F. Xu, M. Li, L. Li, Ultrathin oxygen-vacancy abundant WO_3 decorated monolayer Bi_2WO_6 nanosheet: A 2D/2D heterojunction for the degradation of Ciprofloxacin under visible and NIR light irradiation, J. colloid interface sci., 556 (2019), pp. 557-567

[114] A.F. Kohan, G. Ceder, D. Morgan, C.G. Van de Walle, First-principles study of native point defects in ZnO, Phys. Rev. B 61(2000), pp. 15019

[115] J. Al-Sabahi, T. Bora, M. Al-Abri, J. Dutta, Controlled defects of zinc oxide nanorods for efficient visible light photocatalytic degradation of phenol, Materials 9 (2016), pp. 238

[116] P.S. Venkatesh, P. Dharmaraj, V. Purushothaman, V. Ramakrishnan, K. Jeganathan, Point defects assisted NH_3 gas sensing properties in ZnO nanostructures, Sensor Actuat. B: Chem. 212 (2015), pp. 10-17

[117] J.N. Heo, J. Kim, J.Y. Do, N.K. Park, M. Kang, Self-assembled electron-rich interface in defected ZnO: rGO-Cu: Cu_2O, and effective visible light-induced carbon dioxide photoreduction, Appl. Catal. B: Environ. (2020), pp. 118648, https://doi.org/10.1016/j.apcatb.2020.118648

[118] P. Li, S. Zhu, H. Hu, L. Guo, T. He, Influence of defects in porous ZnO nanoplates on CO_2 photoreduction, Catal. Today 335 (2019), pp. 300-305

[119] H. Yu, S. Yan, P. Zhou, Z. Zou, CO_2 photoreduction on hydroxyl-group-rich mesoporous single crystal TiO_2, Appl. Surf. Sci. 427 (2018), pp. 603-607

[120] K.K. Mandari, A.K.R. Police, J.Y. Do, M. Kang, C. Byon, Rare earth metal Gd influenced defect sites in N doped TiO_2: defect mediated improved charge transfer for enhanced photocatalytic hydrogen production, Int. J. Hydrog. Energy 43 (2018), pp. 2073-2082

[121] S. Zhu, W. Liao, M. Zhang, S. Liang, Design of spatially separated Au and CoO dual co-catalysts on hollow TiO_2 for enhanced photocatalytic activity towards the reduction of CO_2 to CH_4, J. Chem. Eng. 361 (2019), pp. 461-469

[122] L.Y. Lin, S. Kavadiya, X. He, W.N. Wang, B.B. Karakocak, Y.C. Lin, M.Y. Berezin, P. Biswas, Engineering stable Pt nanoparticles and oxygen vacancies on defective TiO_2 via introducing strong electronic metal-support interaction for efficient CO_2 photoreduction, J. Chem. Eng. 389 (2020), pp. 123450

[123] L.L. Tan, W.J. Ong, S.P. Chai, B.T. Goh, A.R. Mohamed, Visible-light-active oxygen-rich TiO_2 decorated 2D graphene oxide with enhanced photocatalytic activity toward carbon dioxide reduction, Appl. Catal. B: Environ. 179 (2015), pp. 160-170

[124] D. Chen, S. Wu, J. Fang, S. Lu, G. Zhou, W. Feng, F. Yang, Y. Chen, Z. Fang, A nanosheet-like α-Bi_2O_3/g-C_3N_4 heterostructure modified by plasmonic metallic Bi and oxygen vacancies with high photodegradation activity of organic pollutants, Sep. Purif. Technol. 193 (2018), pp. 232-241

[125] A. Hernández-Gordillo, J.C. Medina, M. Bizarro, R. Zanella, B.M. Monroy, S.E. Rodil, Photocatalytic activity of enlarged microrods of α-Bi_2O_3 produced using ethylenediamine-solvent, Ceram. Int. 42 (2016), pp. 11866-11875

[126] L. Liu, N. Chen, Y. Lei, X. Xue, L. Li, J. Wang, S. Komarneni, H. Zhu, D. Yang, Micro-nanostructured δ-Bi_2O_3 with surface oxygen vacancies as superior adsorbents for SeO_x^{2-} ions, J. Hazard. Mater. 360 (2018), pp. 279-287

[127] M. Weber, T. Rüffer, F. Speck, F. Göhler, D.P. Weimann, C.A. Schalley, T. Seyller, H. Lang, M. Mehring, From a Cerium-Doped Polynuclear Bismuth Oxido Cluster to β-Bi_2O_3: Ce, Inorg. Chem. (2020), https://doi.org/10.1021/acs.inorgchem.9b03240

[128] S.P. Vattikuti, A.K.R. Police, J. Shim, C. Byon, In situ fabrication of the Bi_2O_3-V_2O_5 hybrid embedded with graphitic carbon nitride nanosheets: Oxygen vacancies mediated enhanced visible-light–driven photocatalytic degradation of organic pollutants and hydrogen evolution, Appl. Surf. Sci. 447 (2018), pp. 740-756

[129] Y.X. Pan, Z.Q. Sun, H.P. Cong, Y.L. Men, S. Xin, J. Song, S.H. Yu, Photocatalytic CO_2 reduction highly enhanced by oxygen vacancies on Pt-nanoparticle-dispersed gallium oxide, Nano. Res. 9 (2016), pp. 1689-1700

[130] C. Liu, X. Li, Y. Wu, L. Zhang, X. Chang, X. Yuan, X. Wang, R porous structured TiO_2–$ZrTiO_4$–SiO_2 heterostructure towards enhanced photo-degradation activities, Ceram. Int. 46 (2020), pp. 476-486

[131] P. Ren, M. Song, J Lee, J. Zheng, Z. Lu, M. Engelhard, X. Yang, X. Li, D. Kisailus, D. Li, Edge Dislocations Induce Improved Photocatalytic Efficiency of Colored TiO_2, Adv. Mater. Inter. 6 (2019), pp. 1901121

[132] S. Amelinckx, W. Dekeyser, The structure and properties of grain boundaries, J. Solid state Phys. (1959), pp. 325-499, https://doi.org/10.1016/S0081-1947(08)60482-8

[133] F. Spadavecchia, G. Cappelletti, S. Ardizzone, C.L. Bianchi, S. Cappelli, C. Oliva, P. Scardi, M. Leoni, P. Fermo, Solar photoactivity of nano-N-TiO_2 from tertiary amine: role of defects and paramagnetic species, Appl. Catal. B: Environ. 96 (2010), pp. 314-322

[134] T. Mahalingam, J.S.P. Chitra, J.P. Chu, P.J. Sebastian, Preparation and microstructural studies of electrodeposited Cu_2O thin films, Mater. Lett. 58 (2004), pp. 1802-1807

[135] J.J. Li, M. Zhang, B. Weng, X. Chen, J. Chen, H.P. Jia, Oxygen vacancies mediated charge separation and collection in Pt/WO_3 nanosheets for enhanced photocatalytic performance, Appl. Surf. Sci., 507 (2020), p. 145133

[136] P. Srinivasan, J.B.B. Rayappan, Growth of Eshelby twisted ZnO nanowires through nanoflakes & nanoflowers: A room temperature ammonia sensor, Sensor Actuat B-Chem. 277 (2018), pp. 129-143

[137] F. Meng, S.A. Morin, S. Jin, Rational solution growth of α-FeOOH nanowires driven by screw dislocations and their conversion to α-Fe_2O_3 nanowires, J. Am. Chem. Soc. 133 (2011), pp. 8408-8411

[138] N.K. Divya, P.P. Pradyumnan, Solid state synthesis of erbium doped ZnO with excellent photocatalytic activity and enhanced visible light emission, Mater. Sci. Semicon. Proc. 41(2016), pp. 428-435

[139] R. Saravanan, S. Agarwal, V.K. Gupta, M.M. Khan, F. Gracia, E. Mosquera, V. Narayanan, A. Stephen, Line defect Ce^{3+} induced Ag/CeO_2/ZnO nanostructure for visible-light photocatalytic activity, J. Photoch. Photobio. A: Chem. 353 (2018), pp. 499-506

[140] S.I. Cha, K.H. Hwang, Y.H. Kim, M.J. Yun, S.H. Seo, Y.J. Shin, J.H. Moon, D.Y. Lee, Crystal splitting and enhanced photocatalytic behavior of TiO_2 rutile nano-belts induced by dislocations, Nanoscale 5 (2013), pp. 753-758

[141] R.W. Balluffi, P.D. Bristowe, C.P. Sun, Structure of High□Angle Grain Boundaries in Metals and Ceramic Oxides, J. Am. Ceram. Soc. 64 (1981), pp. 23-34

[142] M. Kamei, Localization of the photocatalytic reaction on the grain boundary of bicrystalline TiO_2, Appl. Phys Express 1 (2008), pp. 101201

[143] K.J. Morrissey, C.B. Carter, Faceted grain boundaries in Al_2O_3, J. Am. Ceram. Soc. 67 (1984), pp. 292-301

[144] W.Y. Lee, P.D. Bristowe, Y. Gao, K.L. Merkle, The atomic structure of twin boundaries in rutile, Philos. Mag. Lett. 68 (1993), pp. 309-314

[145] C.R.M. Grovenor, Grain boundaries in semiconductors, J. phys. C: Solid state Phys. 18 (1985), pp. 4079

[146] Y. Zhu, Z. Xu, Q. Lang, W. Jiang, Q. Yin, S. Zhong, S. Bai, Grain boundary engineered metal nanowire co-catalysts for enhanced photocatalytic reduction of carbon dioxide, Appl. Catal. B: Environ. 206 (2017), pp. 282-292

[147] A. Senthamizhan, B. Balusamy, Z. Aytac, T. Uyar, Grain boundary engineering in electrospun ZnO nanostructures as promising photocatalysts, Cryst. Eng. Comm. 18 (2016), pp. 6341-6351

[148] K.B. Jaimy, V.P. Safeena, S. Ghosh, N.Y. Hebalkar, K.G.K. Warrier, Photocatalytic activity enhancement in doped titanium dioxide by crystal defects, Dalton Trans. 41 (2012), pp. 4824-4832

[149] S. Xiao, L. Zhao, J. Lian, Enhanced photocatalytic performance of supported Fe doped ZnO nanorod arrays prepared by wet chemical method, Catal. Lett. 144 (2014), pp. 347-354

[150] P. Ren, M. Song, J. Lee, J. Zheng, Z. Lu, M. Engelhard, X. Yang, X. Li, D. Kisailus, D. Li, Edge Dislocations Induce Improved Photocatalytic Efficiency of Colored TiO_2, Adv. Mater. Interfaces 6 (2019), p. 1901121

[151] H. Choi, E. Stathatos, D.D. Dionysiou, Effect of surfactant in a modified sol on the physicochemical properties and photocatalytic activity of crystalline TiO_2 nanoparticles, Top. Catal. 44 (2007), pp. 513-521

[152] S. Demirci, T. Dikici, M. Yurddaskal, S. Gultekin, M. Toparli, E. Celik, Synthesis and characterization of Ag doped TiO_2 heterojunction films and their photocatalytic performances, Appl. Surf. Sci. 390 (2016), pp. 591-601

[153] X. Hou, ZnO/Ag heterostructured nanoassemblies: Wet-chemical preparation and improved visible-light photocatalytic performance, Mater. Lett. 139 (2015), pp. 201-204

[154] Q.I. Rahman, M. Ahmad, S.K. Misra, M. Lohani, Effective photocatalytic degradation of rhodamine B dye by ZnO nanoparticles, Mater. Lett. 91 (2013), pp. 170-174

[155] J.C. Sin, S.M. Lam, K.T. Lee, A.R. Mohamed, Fabrication of erbium-doped spherical-like ZnO hierarchical nanostructures with enhanced visible light-driven photocatalytic activity, Mater. Lett. 91 (2013), pp. 1-4

[156] M. Umadevi, R. Parimaladevi, M. Sangari, Synthesis, characterization and photocatalytic activity of fluorine doped TiO_2 nanoflakes synthesized using solid state reaction method, Spectrochimacta A: Mol Biomol. Spectrosc. 120 (2014), pp. 365-369

[157] Jung B. Yoo, H. Jin Yoo, B. W. Lim, K. H. Lee, M. Hyun Kim, D. Kang, N. Hwi Hur, Controlled Synthesis of Monodisperse SiO_2@TiO_2 Microspheres with a Yolk–Shell Structure as Effective Photocatalysts, Chem. Sus. Chem 5 (2012), pp. 2334-2340

[158] S.N. Basahel, T.T. Ali, M. Mokhtar, K. Narasimharao, Influence of crystal structure of nanosized ZrO_2 on photocatalytic degradation of methyl orange, Nanoscale Res. Lett. 10 (2015), pp. 73

[159] M. Saha, S. Ghosh, S.K. De, Nanoscale kirkendall effect driven Au decorated CdS/CdO colloidal nanocomposites for efficient hydrogen evolution, photocatalytic dye degradation and Cr (VI) reduction, Catal. Today, 340 (2020), pp. 253-267

[160] X. Zhao, X. Liu, C. Yi, J. Li, Y. Su, M. Guo, Palladium Nanoparticles Embedded in Yolk–Shell N-Doped Carbon Nanosphere@ Void@ SnO_2 Composite Nanoparticles for the Photocatalytic Reduction of 4-Nitrophenol, ACS Appl. Nano Mater., 3 (2020), pp. 6574-6583

[161] S. Koppala, Y. Xia, L. Zhang, J. Peng, Z. Chen, L. Xu, Hierarchical ZnO/Ag nanocomposites for plasmon-enhanced visible-light photocatalytic performance, Ceram. Int. 45 (2019), pp. 15116-15121

[162] M. Kwiatkowski, R. Chassagnon, O. Heintz, N. Geoffroy, M. Skompska, I. Bezverkhyy, Improvement of photocatalytic and photoelectrochemical activity of ZnO/TiO_2 core/shell system through additional calcination: Insight into the mechanism, Appl. Catal. B: Environ. 204 (2017), pp. 200-208

[163] Y. Liu, Q. Li, J. Zhang, W. Sun, S. Gao, J.K. Shang, PdO loaded TiO_2 hollow sphere composite photocatalyst with a high photocatalytic disinfection efficiency on bacteria, J. Chem. Eng. 249 (2014), pp. 63-71

[164] J. Zhao, W. Li, L. Fan, Q. Quan, J. Wang, C. Xiao, Yolk-porous shell nanospheres from silver-decorated titanium dioxide and silicon dioxide as an enhanced visible-light

photocatalyst with guaranteed shielding for organic carrier, J. Colloid Interface Sci. 534 (2019), pp. 480-489

[165] G. Thennarasu, A. Sivasamy, Synthesis and characterization of nanolayered $ZnO/ZnCr_2O_4$ metal oxide composites and its photocatalytic activity under visible light irradiation, J. Chem. Technol. Biotechnol, 90 (2015), pp. 514-524

[166] L. Ren, Y. Li, J. Hou, X. Zhao, C. Pan, Preparation and enhanced photocatalytic activity of TiO_2 nanocrystals with internal pores, ACS Appl. Mater. Inter. 6 (2014), pp. 1608-1615

[167] Y.F. Wang, T.T. Yang, W.L. Liu, D. Zhao, M.M. Ren, F.G. Kong, S.J. Wang, X.Q. Wang, X.L. Duan, Design of double-shelled and dual-cavity structures in Fe_3O_4@Void@PMAA@Void@TiO_2 nanocomposite particles for comprehensive photocatalyst and adsorbent applications, Colloid Polym. Sci. 296 (2018), pp. 1719-1728

[168] D. Wu, W. Wang, F. Tan, F. Sun, H. Lu, X. Qiao, Fabrication of pit-structured ZnO nanorods and their enhanced photocatalytic performance, RSC Adv. 3 (2013), pp. 20054-20059

[169] B. Banerjee, V. Amoli, A. Maurya, A.K. Sinha, A. Bhaumik, Green synthesis of Pt-doped TiO_2 nanocrystals with exposed (001) facets and mesoscopic void space for photo-splitting of water under solar irradiation, Nanoscale 7 (2015), pp. 10504-10512

[170] M. Waqas, S. Iqbal, A. Bahadur, A. Saeed, M. Raheel, M. Javed, Designing of a spatially separated hetero-junction pseudo brookite (Fe_2TiO_5-TiO_2) yolk-shell hollow spheres as efficient photocatalyst for water oxidation reaction, Appl. Catal. B: Environ. 219 (2017), pp. 30-35

[171] G. Fan, W. Sun, H. Wang, F. Li, Visible-light-induced heterostructured Zn–Al–In mixed metal oxide nanocomposite photocatalysts derived from a single precursor, J. Chem. Eng. 174 (2011), pp. 467-474

[172] X. Gao, X. Wang, Z. Yang, Y. Shen, A. Xie, A novel bi-functional SiO_2@ TiO_2/CDs nanocomposite with yolk-shell structure as both efficient SERS substrate and photocatalyst, Appl. Surf. Sci. 475 (2019), pp. 135-142

[173] Y. Lu, Y. Huang, Y. Zhang, J. Cao, H. Li, C. Bian, S. Cheng Lee, Oxygen vacancy engineering of $Bi_2O_3/Bi_2O_2CO_3$ heterojunctions: Implications of the interfacial charge transfer, NO adsorption and removal, Appl. Catal. B: Environ. 231 (2018), pp. 357-367

[174] B. Lei, W. Cui, J. Sheng, H. Wang, P. Chen, J. Li, Y. Sun, F. Dong, Synergistic effects of crystal structure and oxygen vacancy on Bi_2O_3 polymorphs: intermediates activation, photocatalytic reaction efficiency, and conversion pathway, Science Bulletin 65 (2020), pp. 467-476

[175] D. Li, Y. Zhang, Y. Zhang, X. Zhou, S. Guo, Fabrication of bidirectionally doped β-Bi_2O_3/TiO_2-NTs with enhanced photocatalysis under visible light irradiation, J. Hazard. Mater. 258 (2013), pp. 42-49

[176] R. Venkatesan, S. Velumani, K. Ordon, M. Makowska-Janusik, G. Corbel, A. Kassiba, Nanostructured bismuth vanadate ($BiVO_4$) thin films for efficient visible light photocatalysis, Mater. Chem. Phys. 205 (2018), pp. 325-333

[177] L. Jiang, D. Chen, L. Qin, J. Liang, X. Sun, Y. Huang, Enhanced photocatalytic activity of hydrogenated $BiVO_4$ with rich surface-oxygen-vacancies for remarkable degradation of tetracycline hydrochloride, J. Alloys Compd. 783 (2019), pp. 10-18

[178] J.P. Deebasree, V. Maheskumar, B. Vidhya, G. Balaji, Effect of ultrasonication during and after preparation of BiVO4 by chemical coprecipitation technique, Mater. Today, 23 (2020), pp. 131-138

[179] K. Girija, S. Thirumalairajan, A.K. Patra, D. Mangalaraj, N. Ponpandian, C. Viswanathan, Enhanced photocatalytic performance of novel self-assembled floral β-Ga_2O_3 nanorods, Curr. Appl. Phys. 13 (2013), pp. 652-658

[180] Y. Hou, L. Wu, X. Wang, Z. Ding, Z. Li, X Fu, Photocatalytic performance of α-, β-, and γ-Ga_2O_3 for the destruction of volatile aromatic pollutants in air, J. Catal. 250 (2007), pp. 12-18

[181] J. Zhang, Y. Ma, Y. Du, H. Jiang, D. Zhou, S. Dong, Carbon nanodots/WO_3 nanorods Z-scheme composites: remarkably enhanced photocatalytic performance under broad spectrum, Appl. Catal. B: Environ. 209 (2017), pp. 253-264

[182] K. Bao, S. Zhang, P. Ni, Z. Zhang, K. Zhang, L. Wang, L.X. Sun, W. Mao, Q. Zhou, Y. Qian, Convenient fabrication of carbon doped WO_{3-x} ultrathin nanosheets for photocatalytic aerobic oxidation of amines, Catal. Today 340 (2020), pp. 311-317

[183] J. Li, B. Weng, S. Cai, J. Chen, H. Jia, Y. Xu, Efficient promotion of charge transfer and separation in hydrogenated TiO_2/WO_3 with rich surface-oxygen-vacancies for photodecomposition of gaseous toluene, J. Hazard. Mater. 342 (2018), pp. 661-669

[184] L. C. Buelens, A. N. V. R. Dharanipragada, H. Poelman, Z. Zhou, G. B. Marin, V. V. Galvita, Exploring the stability of Fe_2O_3-$MgAl_2O_4$ oxygen storage materials for CO production from CO_2, J. CO_2 Util. 29 (2019), pp. 36-45

[185] S. Demirci, M. Yurddaskal, T. Dikici, C. Sarıoğlu, Fabrication and characterization of novel iodine doped hollow and mesoporous hematite (Fe_2O_3) particles derived from sol-gel method and their photocatalytic performances, J. Hazard. Mater. 345 (2018), pp. 27-37

[186] H. Feng, Y. Wang, C. Wang, F. Diao, W. Zhu, P. Mu, L. Yuan, G. Zhou, F. Rosei, Defect-induced enhanced photocatalytic activities of reduced α-Fe_2O_3 nanoblades, Nanotechnol. 27 (2016), pp. 295703

[187] M. Motola, M. Čaplovičová, M. Krbal, H. Sopha, G. Karthikeyan Thirunavukkarasu, M. Gregor, G. Plesch, J. M. Macak, Ti^{3+} doped anodic single-wall TiO2 nanotubes as highly efficient photocatalyst, Electrochim. Acta 331 (2020), pp. 135374

[188] H. Zhou, T. Fan, J. Ding, D. Zhang, Q. Guo, Bacteria-directed construction of hollow TiO_2 micro/nanostructures with enhanced photocatalytic hydrogen evolution activity, Opt. Express 20 (2012), pp. A340-A350

[189] A. Diallo, K. Kaviyarasu, S. Ndiaye, B. M. Mothudi, A. Ishaq, V. Rajendran,M. Maaza, Structural, optical and photocatalytic applications of biosynthesized NiO nanocrystals, Green Chem. Lett. Rev. 11 (2018), pp. 166-175

[190] C. Hu, H. Teng, Structural features of p-type semiconducting NiO as a co- catalyst for photocatalytic water splitting, J. Catal. 272 (2010), pp. 1-8

[191] Nayak, A. Kumar, D. Pradhan, Microwave-assisted greener synthesis of defect-rich tungsten oxide nanowires with enhanced photocatalytic and photoelectrochemical performance, J. of Phys. Chem. 122 (2018), pp. 3183-3193

[192] M. A. Rahman, S. Bazargan, S. Srivastava, X. Wang, M. Abd-Ellah, J.P. Thomas, N. F. Heinig, D. Pradhan, K. Tong Leung, Defect-rich decorated TiO2 nanowires for super-efficient photoelectrochemical water splitting driven by visible light, Energy Environ. Sci., 8 (2015), pp. 3363-3373

[193] L. Yang, L. Chen, D. Yang, X. Yu, H. Xue, L. Feng, NiMn layered double hydroxide nanosheets/$NiCo_2O_4$ nanowires with surface rich high valence state metal oxide as an efficient electrocatalyst for oxygen evolution reaction, J. Power Sources, 392 (2018), pp. 23-32

[194] Y. Wang, R. Zhang, J. Chen, H. Wu, S. Lu, K. Wang, H. Li, Enhancing catalytic activity of titanium oxide in lithium–sulfur batteries by band engineering, Adv. Energ. Mater. 9(2019), pp. 1900953

[195] J. Yu, Q. Cao, Y. Li, X. Long, S. Yang, J. Kenji Clark, M. Nakabayashi, N. Shibata, J-J. Delaunay, Defect-Rich $NiCeO_x$ Electrocatalyst with Ultrahigh Stability and Low Overpotential for Water Oxidation, ACS Catal. 9 (2019), pp. 1605-1611

[196] H. Chen, P. Liu, J. Li, Y. Wang, C. She, J. Liu, L. Zhang, Q. Yang, S. Zhou, X. Feng, MgH_2/Cu_xO Hydrogen Storage Composite with Defect-Rich Surfaces for Carbon Dioxide Hydrogenation, ACS Appl. Mater. Interf. 11(2019), pp. 31009-31017

Table 1. 0D defect rich metal oxides photocatalytic system

Photocatalyst heterostructure	Modified band gap	Synthetic route	Surface area	Photocatalytic Applications	Characterization techniques	Ref.
Bi/α-Bi_2O_3/g-C_3N_4	2.83eV	Calcination-photoreduction technique		Degradation rate: Tetracycline (90.2%) Rhodamine B (95.6%)	PL and XPS spectrum	[124]
α-Bi_2O_3 (Enlarged Microrods)	In between 2.82-2.85eV	Chemical precipitation method	$1m^2/g$	Indigo carmine dye degradation (6.8 times more than bare)	Diffuse reflectance and UV spectrum	[125]
Micro nanostructured Bi_2O_3 with surface V_o defects	2.85eV	Solvothermal method	~24 m^2/g	Capture hypertoxic SeO_x^{2-} ions specially SeO_3^{2-}anions	XPS spectra	[126]
Beta –Bi_2O_3:Ce	2.3eV	Simple Hydrolysis technique	1 m^2/g	Biocide triclosan decomposition	XPS spectra	[127]
Bi_2O_3/V_2O_5@g-C_3N_4	2.17eV	Co-pyrolysis approach	83.75 m^2/g	Degradation rate was 98.1 % for phenol red (i.e. 1.2 and 1.8 times higher than bare Bi_2O_3 as well asV_2O_5 respectively)	XPS and UV-spectrum	[128]
Vo-rich Pt/Ga_2O_3	4.75eV	Hydrothermal	19.41 m^2/g	CO evolution rate was 21.0μmol/h	EPR and XPS spectrum	[129]
TiO_2-$ZrTiO_4$-SiO_2 heterostructure	2.54eV	Sol-gel method	121.41 m^2/g	RhB degradation (95%, 90 min)	XPS spectra	[130]

Table 2. 1D and 2D defect rich metal oxides photocatalytic system

Photocatalytic material	Band gap and λ-value	Characterization techniques	Mode of fabrication	Surface area	Photocatalytic application	Ref.
Fe doped ZnO nanorod arrays	>3.37eV (480-680nm)	HRTEM and XPS	Wet chemical method		MO degradation	[149]
TiO_2	2.29Ev (UV-visible range)	HRTEM and EELS(e^- energy loss spectroscopy)	One step hydrosolvothermal method	$190m^2/g$	MB degradation (100%, 5h)	[150]
TiO_2 (Surfactant effect)	300-400nm	HRTEM	Simple sol-gel route	$54.3\ m^2/g$	4-Chlorophenol degradation	[151]
Ag/TiO_2	2.93eV (>350nm)	SEM and XPS	Sol-gel spin coating technique		Methylene blue degradation (51.81%)	[152]
ZnO/Ag nanoassemblies	>420 nm	TEM and UV-vis spectrum	One pot nonaqueous method		RhB dye degradation (80%)	[153]
ZnO nanoparticles	3.29eV (370-390nm)	FESEM and TEM	Facile solution method	$7.8703m^2/g$	RhB dye degradation (95%)	[154]
Er/ZnO nanostructures	(430-600nm)	FESEM and TEM	Facile and surfactant-free chemical solution route		Phenol degradation	[155]
F/TiO_2	2.85eV (450nm)	XRD	Solid state		MO degradation	[156]

Table 3. 3D defect rich metal oxides photocatalytic system

Photocatalytic system	Pore size	Mode of fabrication	Calcination temperature	Surface area (m^2/g)	Light absorbed	Photocatalytic application	Ref.
TiO_2 nanocrystals	5-7nm	Novel facile microwave assisted hydrolysis	400℃	73.7	UV	Methyl orange and 4-Chlorophenol degradation	[166]
Fe_3O_4@Void@PMAA@Void@TiO_2	40nm	Dispersion polymerization and hydrothermal strategy	Heating in autoclave at 160℃	61.4	UV	Removal of Pd (II) and Cr (VI)	[167]
ZnO nanorods		Low temperature wet chemical method	300℃	3.52	UV	Methylene blue degradation	[168]
Pt/TiO_2	20	Facile chemical approach using ionic liquid	5℃/min	132	Visible	H_2 evolution (11.2mmol/h/g)	[169]
Fe_2TiO_5 - TiO_2 yolk- shell hollow spheres		Facile sacrificial hard template strategy	1℃/min		UV-visible	High oxygen evolution rate (148µmol/g/h)	[170]
Zn-Al-In metal oxides	5-100nm	Co-precipitation method	450-600℃	65.8	Visible	MB dye degradation	[171]
SiO_2@TiO_2/CDs nanocomposite	8 nm	Facile method	In heating mantle at 60℃	37	Visible	Dinitraphenols dye degradation	[172]

Table 4. Examples of various metal oxides photocatalysts with different band potentials and defects

Photocatalytic materials	CB/VB or bandgap	Types of defects	Synthetic route	Characterization	Photocatalytic application	Ref.
Bi_2O_3						
$Bi_2O_3/Bi_2O_2CO_3$		O vacancies	Hydrothermal	HRTEM, Raman and ESR	Photocatalytic NO removal	[173]
Bi_2O_3 polymorph	Eg = 2.6 eV (β-Bi_2O_3) Eg = 2.1 eV (α-Bi_2O_3)	O vacancies	Solvothermal method followed by calcination	DRIFT spectra And ESR	NO removal rate: β-Bi_2O_3 = 52.0% and α-Bi_2O_3 = 20.1%.	[174]
β-Bi_2O_3 /TiO_2 Nanotubes	(β-Bi_2O_3) Eg = 2.51 eV CB = -0.23 V VB = 2.28 V	Dislocation	Pulse electrodeposition method	UV-vis DRS	Photoelectrocatalytic degradation of carbamazepine = 98%	[175]
$BiVO_4$						
$BiVO_4$ thin films	Eg = 2.4 eV	Surface defects	rf- sputtering method	Raman and UV-Visible absorption	Rh6G dye degradation = 95% in 4 h	[176]
Hydrogenated $BiVO_4$	Eg = 2.31 eV	Surface oxygen vacancies	Hydrogenation treatment	XPS and EPR	degradation rate for tertracycline = 98%	[177]
$BiVO_4$	Eg = 2.4 eV	Dislocations and voids	Coprecipitation method	SEM	90% MB degradation	[178]
Ga_2O_3						
β – Ga_2O_3 nanorods	Eg = 4.59 eV	O and Ga vacancies	Reflux condensation method	Raman and PL	RhB photodegradation rate = 90%	[179]
Ga_2O_3 polymorphs	Eg = 4.2 – 4.9 eV	O and Ga vacancies	Precipitation method	Raman and PL spectra	Maxi. Hydrocarbon removal rate (β-Ga_2O_3) = 0.42 µmol $h^{-1}m^{-2}$ and CO_2 production rate (β- Ga_2O_3) = 2.4 µmol $h^{-1}m^{-2}$	[180]
WO_3						
C-Dots/WO_3	Eg = 2.84 eV (WO_3) CB = 0.20 V VB = 3.07 V	Surface defects and lattice disorders	Oil bath reflux method	Raman spectra	RhB degradation; under UV light = 97.1% under visible light = 97.7% under NIR light = 60.1% .	[181]
Carbon-coated WO_3	Eg = 2.40 eV	Surface defects, O vacancies	Ultra-rapid solution combustion	HRTEM, XPS	Aerobic amines oxidation	[182]

			synthesis method			
TiO_2/WO_3	Eg = 2.50 eV (TiO_2), 3.1 eV (WO_3)	W^{5+},Surface oxygen vacancies	Hydrogen annealing	EPR, XPS	Gaseous toluene conversion rate = 72%	[183]
Fe_2O_3						
Fe_2O_3-$MgAl_2O_4$	-	O vacancies	Co-precipitation method	STEM-EDX	CO yield = 0.6 mol kg_{OSM-1}	[184]
Iodine doped Fe_2O_3	Eg = 2.14 eV	Surface defects and dislocations	Sol-gel method	XPS, FESEM and UV- VIS DRS	MB degradation rate = 97.72%	[185]
α-Fe_2O_3 nanoblades	Eg = 2.2 eV	Oxygen vacancy, dislocation and dense voids	Oxidation and vacuum reduction	TEM, BET and Electron energy loss spectroscopy	RhB degradation = 100%	[186]
TiO_2						
Ti^{3+}/TiO_2	-	Ti^{3+} defects, oxygen vacancies	Electrochemical anodization followed by reduction	XPS	Degradation rate of Mb and RhB = 100% phenol = 99%	[187]
Hollow TiO_2 micro/nanostructures	-	voids	Surface sol-gel process	N_2 adsorption – desorption isotherms	H_2 production rate = 62.55 µmol h^{-1}	[188]
NiO						
Biosynthesized NiO nanocrystals	Eg = 3.4 eV	Grain boundary, voids, Ni^{2+} and Oxygen vacancy	Biosynthetic followed by heating method	XRD, HRTEM, PL	MB degradation rate = 46%	[189]
$NaTaO_3$/NiO	-	voids	Sol-gel and solid – state methods	UV-Visible absorption	H_2 evolution rate = 9000 µmol h^{-1}	[190]

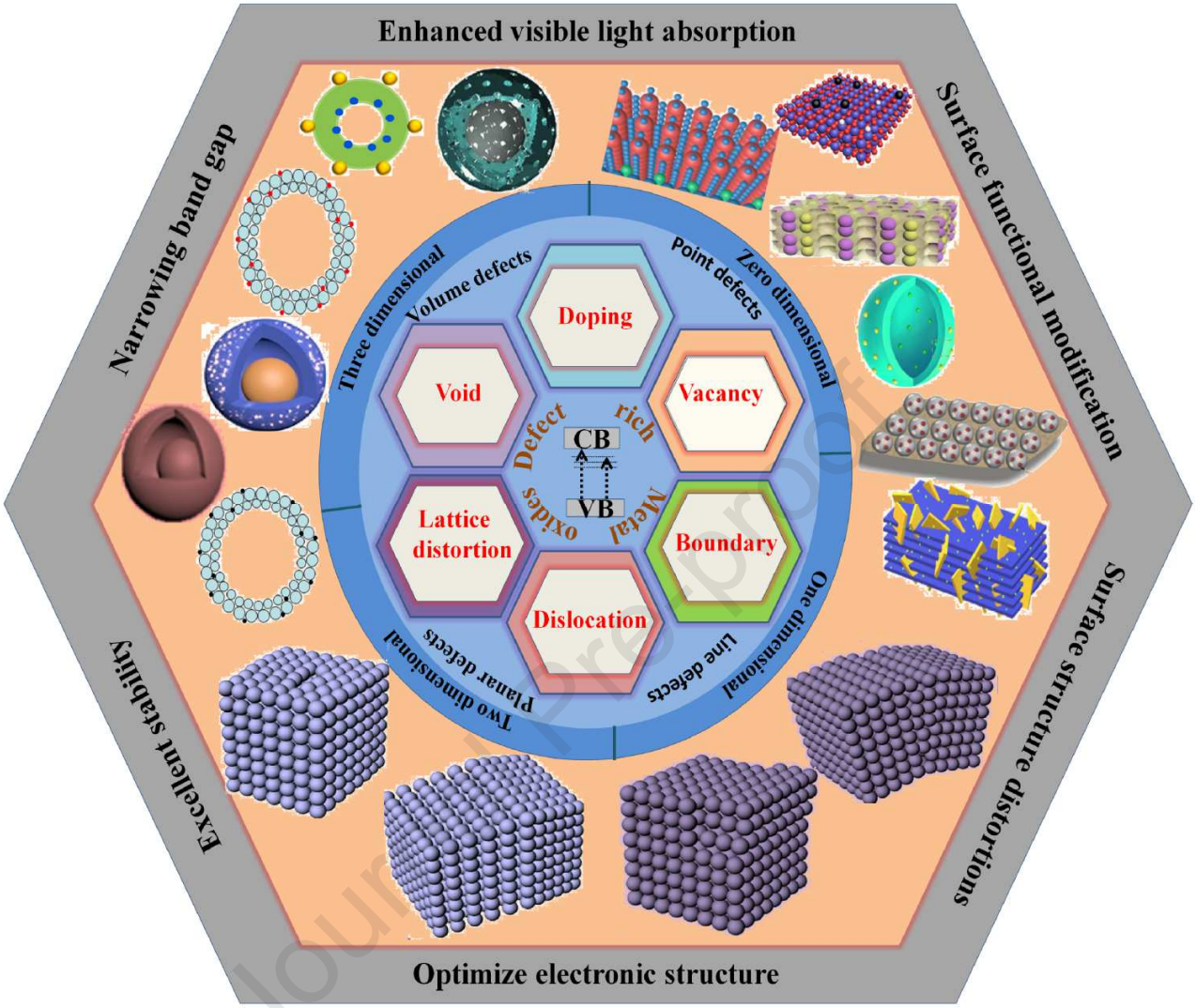

Graphical Abstract: Representation of different dimensionality driven defects in MOs photocatalysts along with strategic modification in photocatalytic activity.

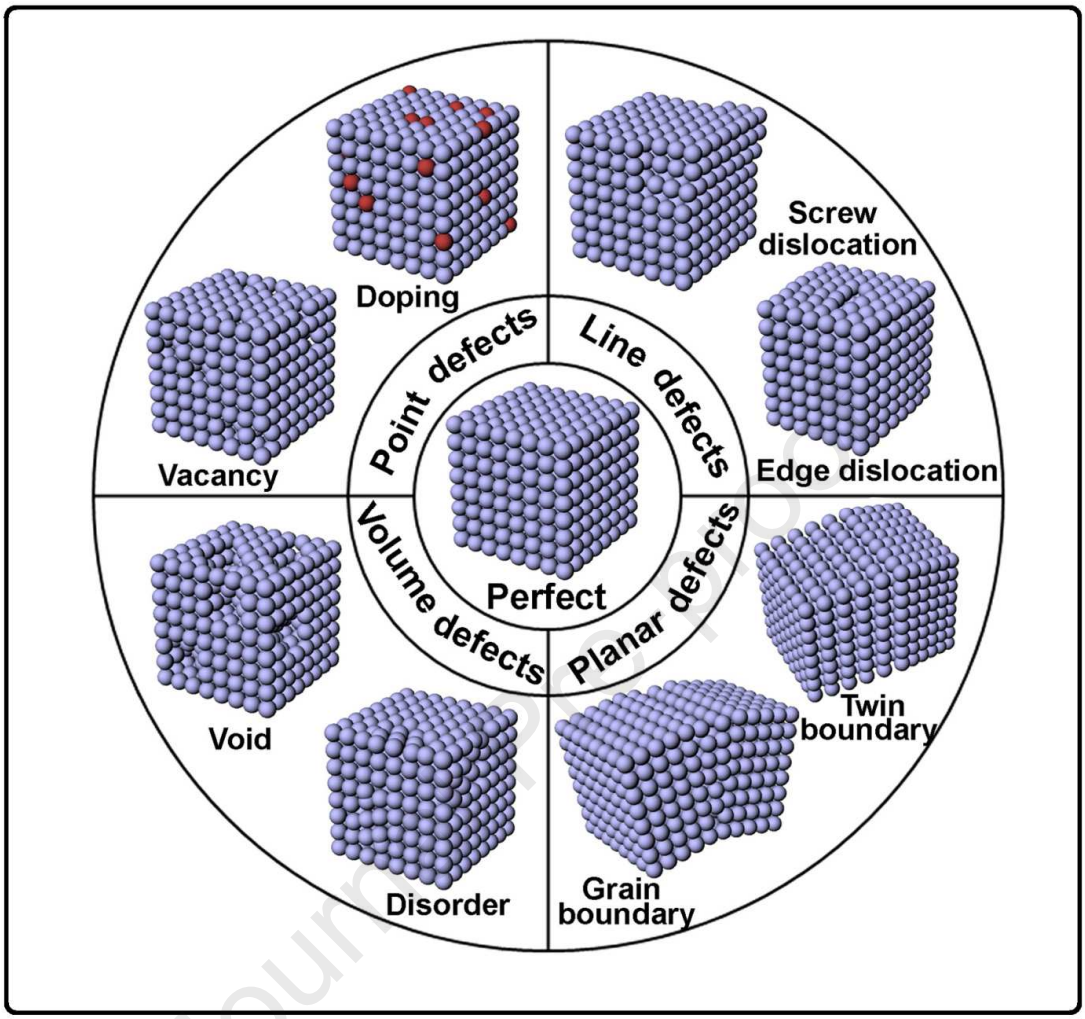

Fig. 1. Schematic illustrating the defects with different atomic arrangement structures in photocatalytic materials, reproduced with permission from Elsevier (license No. 4820611494141) [33].

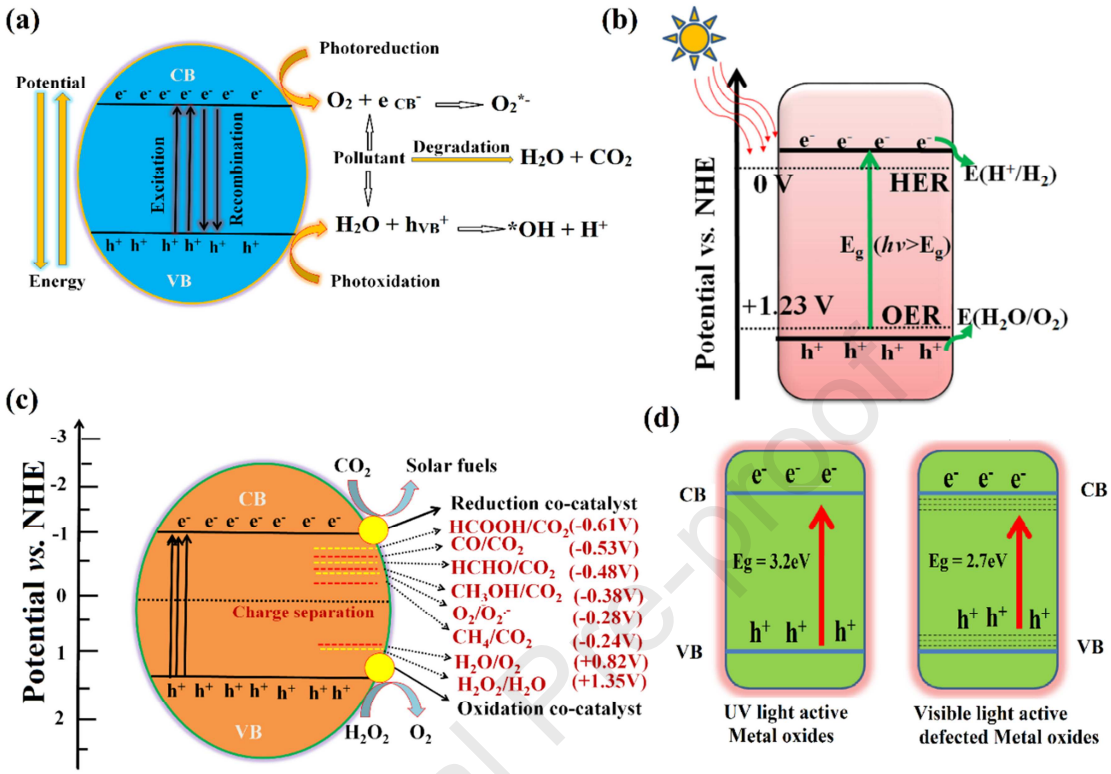

Fig. 2. (a) Basic principle of photocatalysis depicting photo-activation of a photocatalyst and primary surface reactions, (b) Schematic illustration of probable mechanism of various photocatalytic applications mediated by suitable redox cocatalyst, (c) UV light active metal oxides and visible light active metal oxides showing photo excitation.

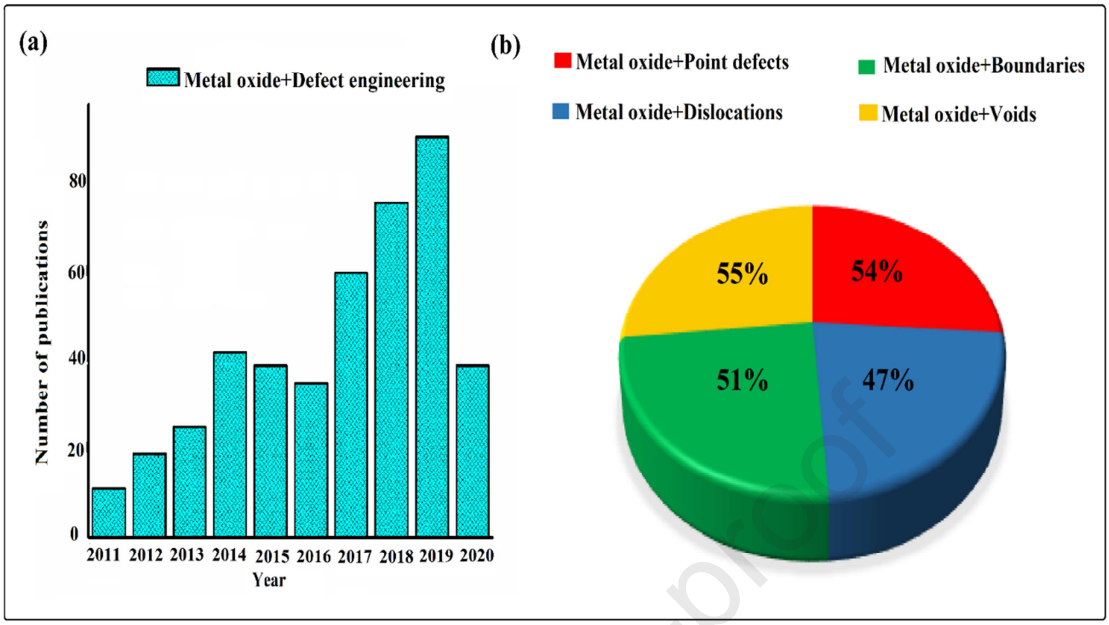

Fig. 3. (a) Bar graph depicting Scopus data interpretation results for number of publications from 2011 to 2020, using keywords "Metal oxide + Defect engineering", (b) pie chart showing the proportion of Metal oxide-based materials using keywords "Metal oxide + Point defects", Metal oxide + Dislocations", "Metal oxide + Boundaries" and Metal oxide +Voids".

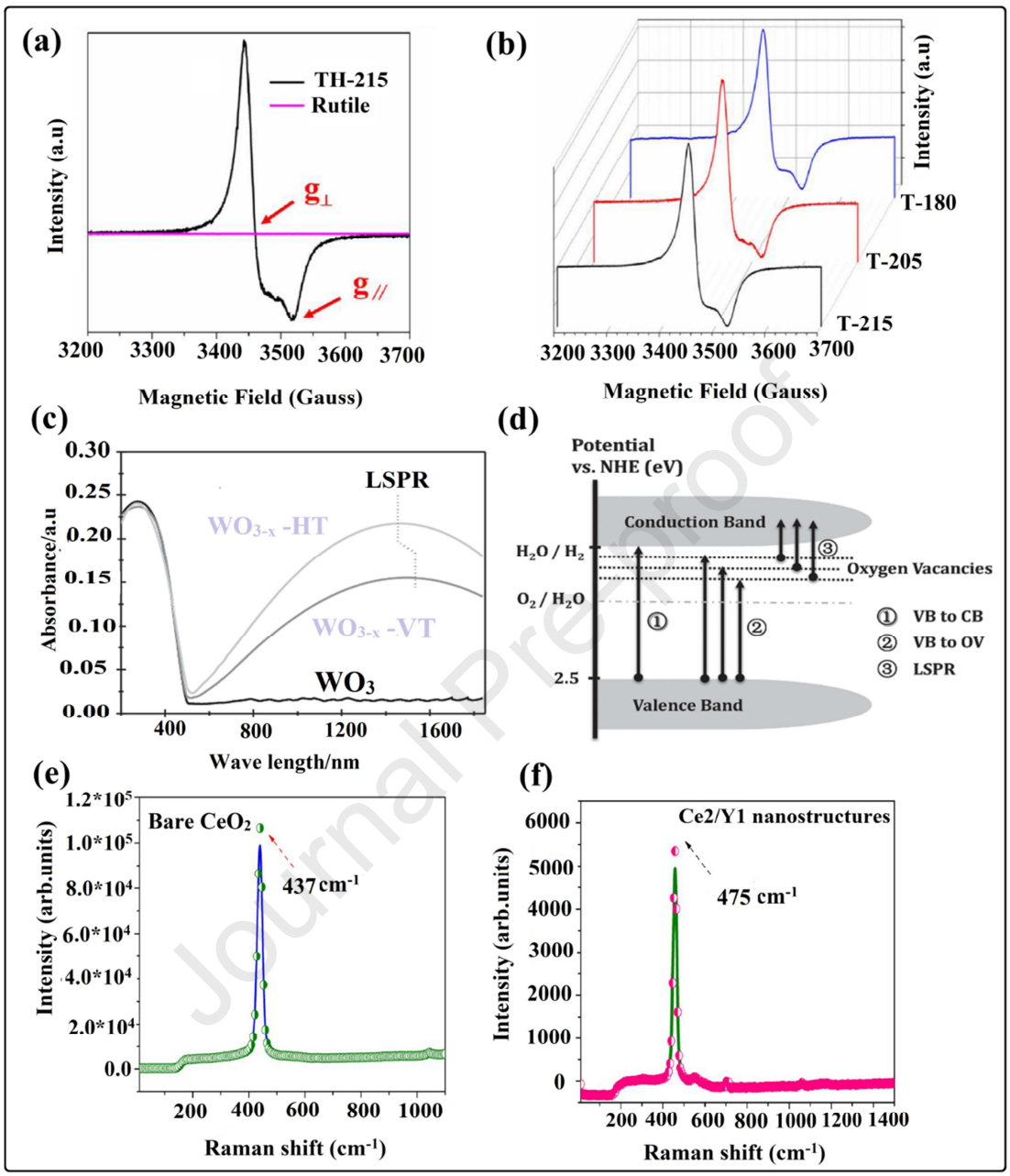

Fig. 4. (a-b) ESR spectra of different as-prepared samples recorded at 77 K in liquid nitrogen, reprinted with permission from Elsevier (license No. 4877150926938) [78], (c-d) UV–vis -NIR spectra, and band level arrangements of tungsten oxide nanosheets with oxygen vacancies, respectively, adapted with permission from Wiley (license No. 4877160450987) [85], (e-f) Raman spectrum of CeO_2/Y_2O_3 nanohybrid (e) pure ceria (f) Ce_2/Y_1 nanomaterials, reprinted with permission from Elsevier (license No. 4877161353660) [96].

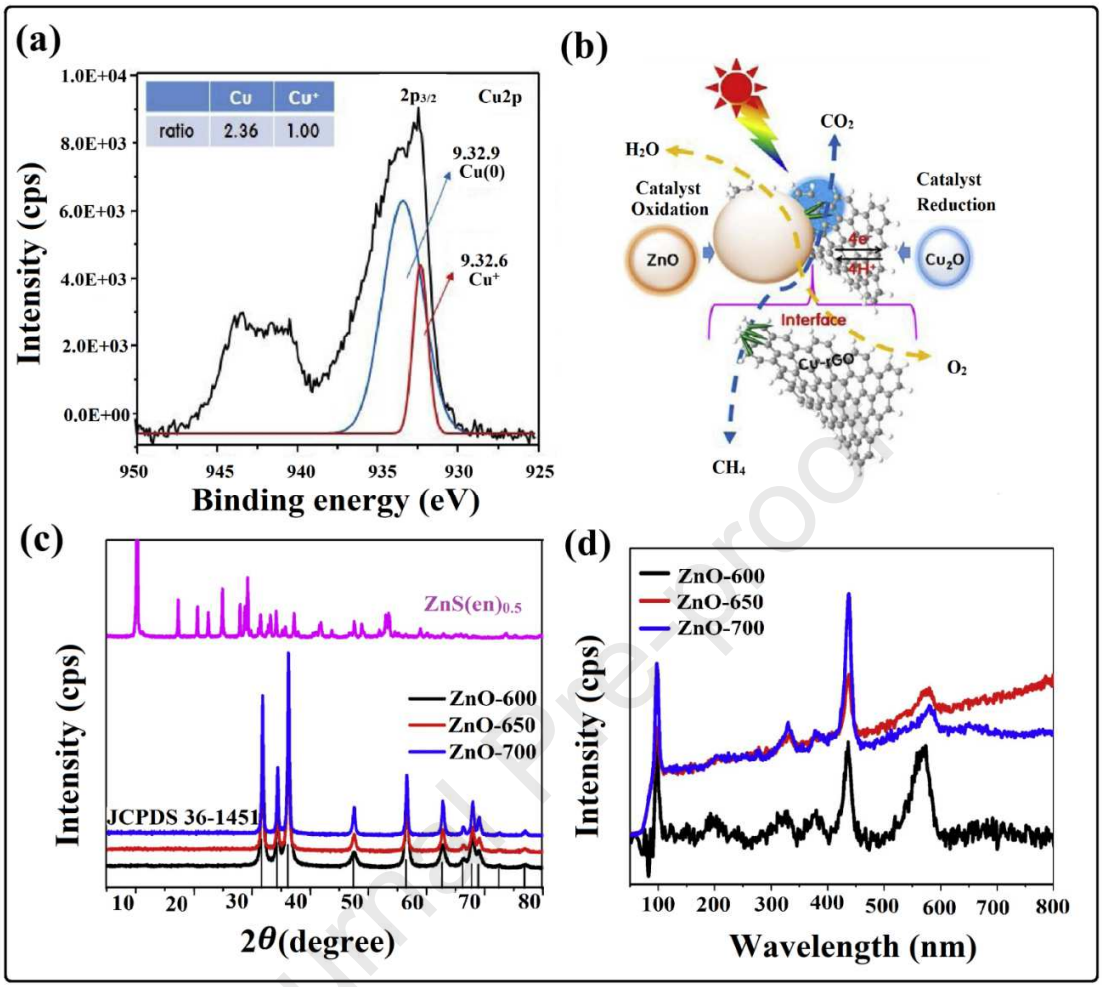

Fig. 5. (a)XPS peaks of Cu 2p in def-ZnO: rGO-Cu:Cu_2O heterostructure, (b) Mechanistic studies of as prepared def ZnO:rGO-Cu:Cu_2O heterostructure, reproduced with permission from Elsevier (license No. 4820630113683) [117], (c) XRD patterns of $ZnS(en)_{0.5}$starting material and the samples by annealing $ZnS(en)_{0.5}$ at different temperature for 2 h, (d)Raman spectra of the as-prepared porous ZnO nanoplates, reprinted with permission from Elsevier (license No. 4820630765968) [118].

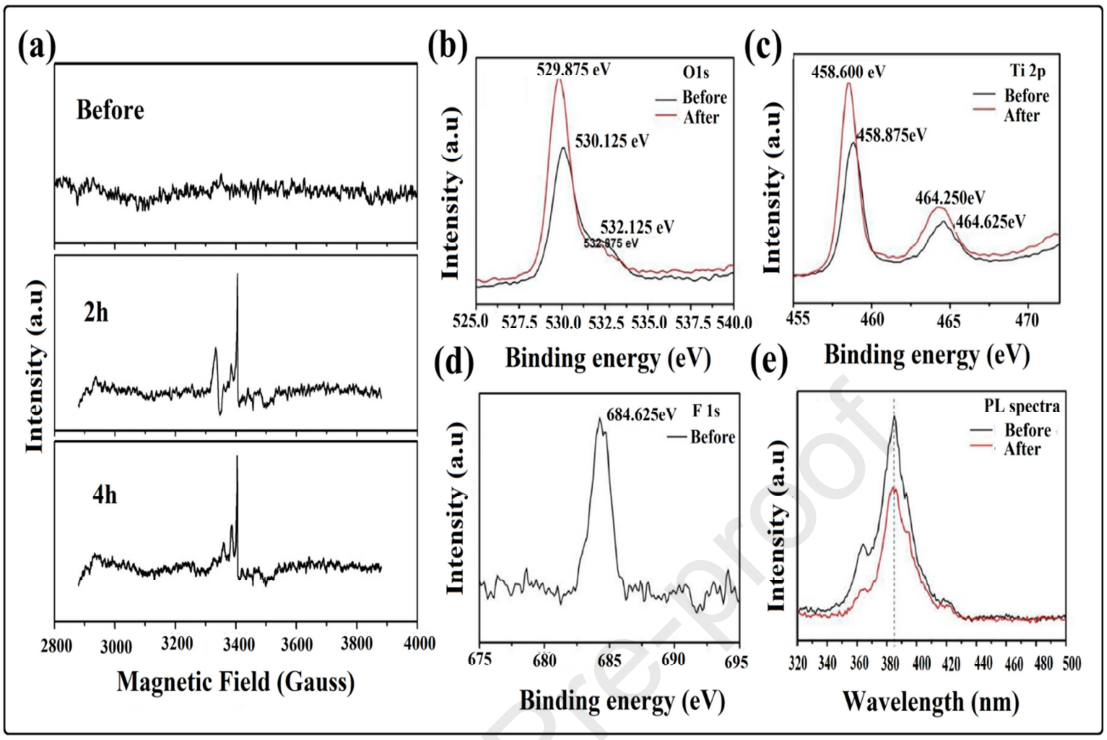

Fig. 6. (a) Quantitative EPR results for TiO_2 samples before calcined and after calcined for 2h and 4 h respectively, (b-d) XPS spectra of TiO_2 before and after calcined (O 1s, Ti 2p and F 1s respectively), (e) PL spectrum of TiO_2 before and after calcined for 2 h, reproduced with permission from Elsevier (license No. 4820631475099) [119].

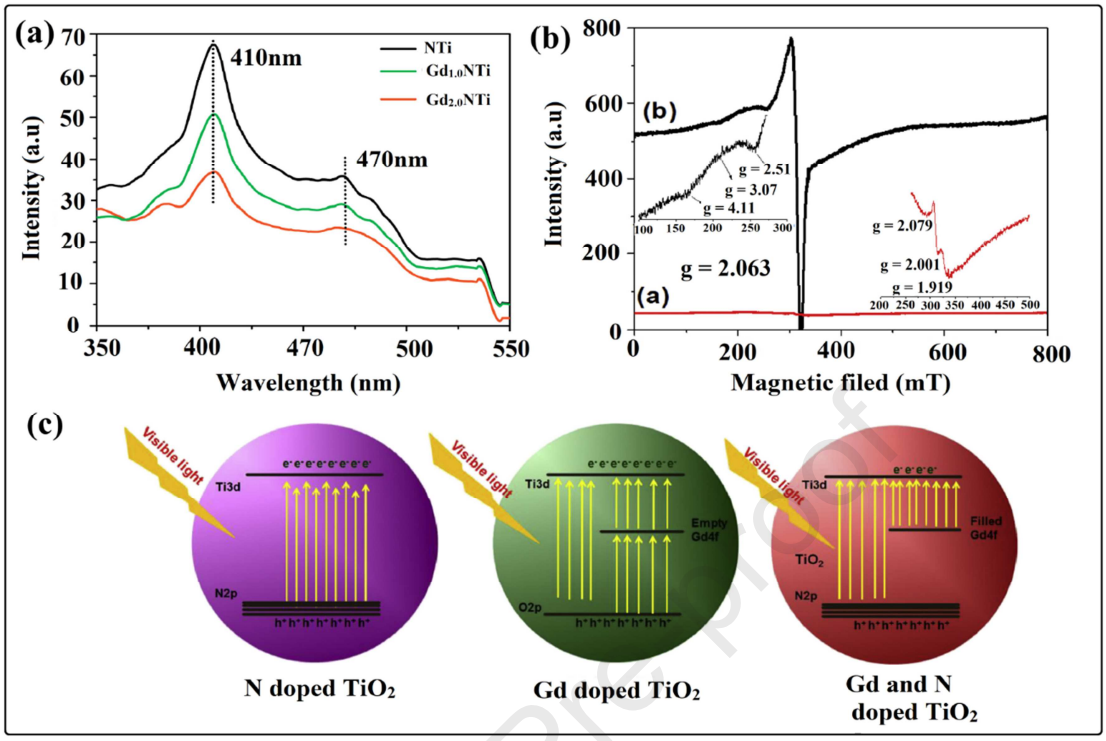

Fig. 7. (a) PL spectra of NTi, $Gd_{1.0}$NTi and $Gd_{2.0}$NTi, (b) EPR spectra of NTi (a), $Gd_{2.0}$NTi (b), (c) Schematic representation of excitations in N-doped TiO_2, Gd-doped TiO_2 and Gd, N co-doped TiO_2, adapted with permission from Elsevier (license No. 4820640600542) [120].

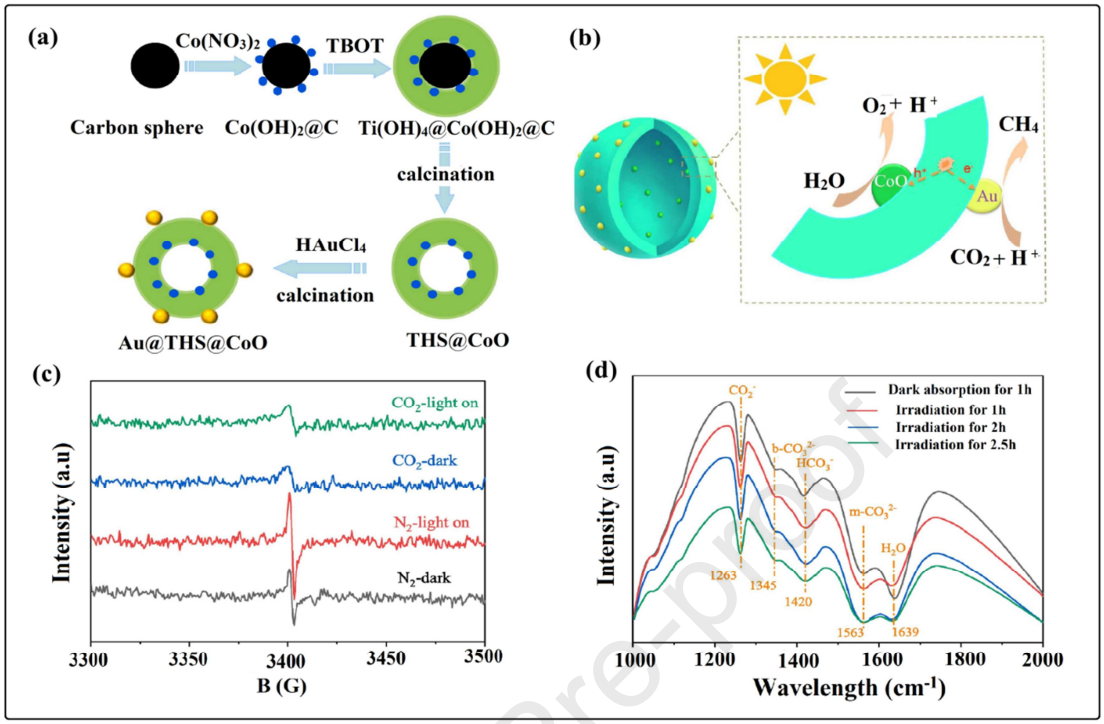

Fig. 8. (a) Illustrations of formation process of Au_x@THS@CoO, (b) The possible mechanism for photoreduction CO_2 over Aux@THS@CoO, (c) EPR spectra of $Au_{2.0}$@THS@CoO in the presence of CO_2 and N_2 before and after the simulated sun light irradiation, (d)In situ FTIR spectrum of CO_2 and H_2O interaction with $Au_{2.0}$@THS@CoO and THS in the dark and light for different times, reproduced with permission from Elsevier (license No. 4820740271566) [121].

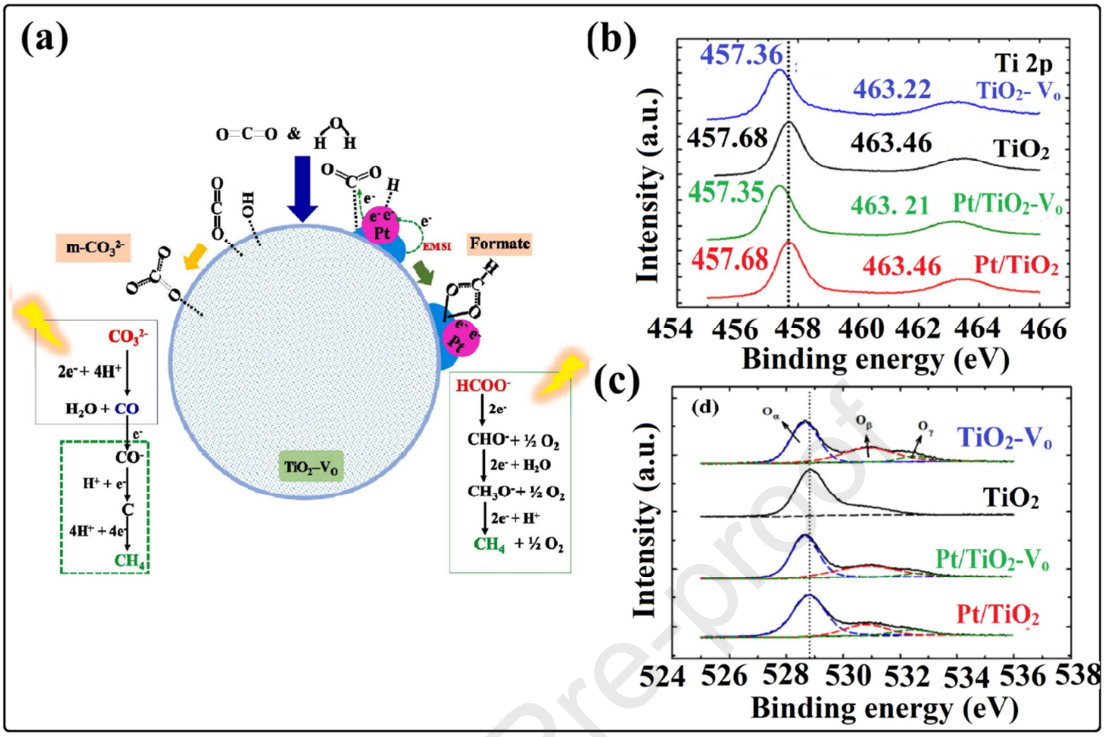

Fig. 9. (a) Proposed mechanism for the formation of CO and CH_4 from CO_2 photoreduction with H_2O on Pt/TiO_2-VO, adapted with permission from Elsevier (license No. 4820780394645), (b-c) XPS spectrum of Ti 2p and O1s of the TiO_2, TiO_2-VO, Pt/TiO_2 and Pt/TiO_2-VO samples, respectively, adapted with permission from Elsevier (license No. 4870171142651) [122].

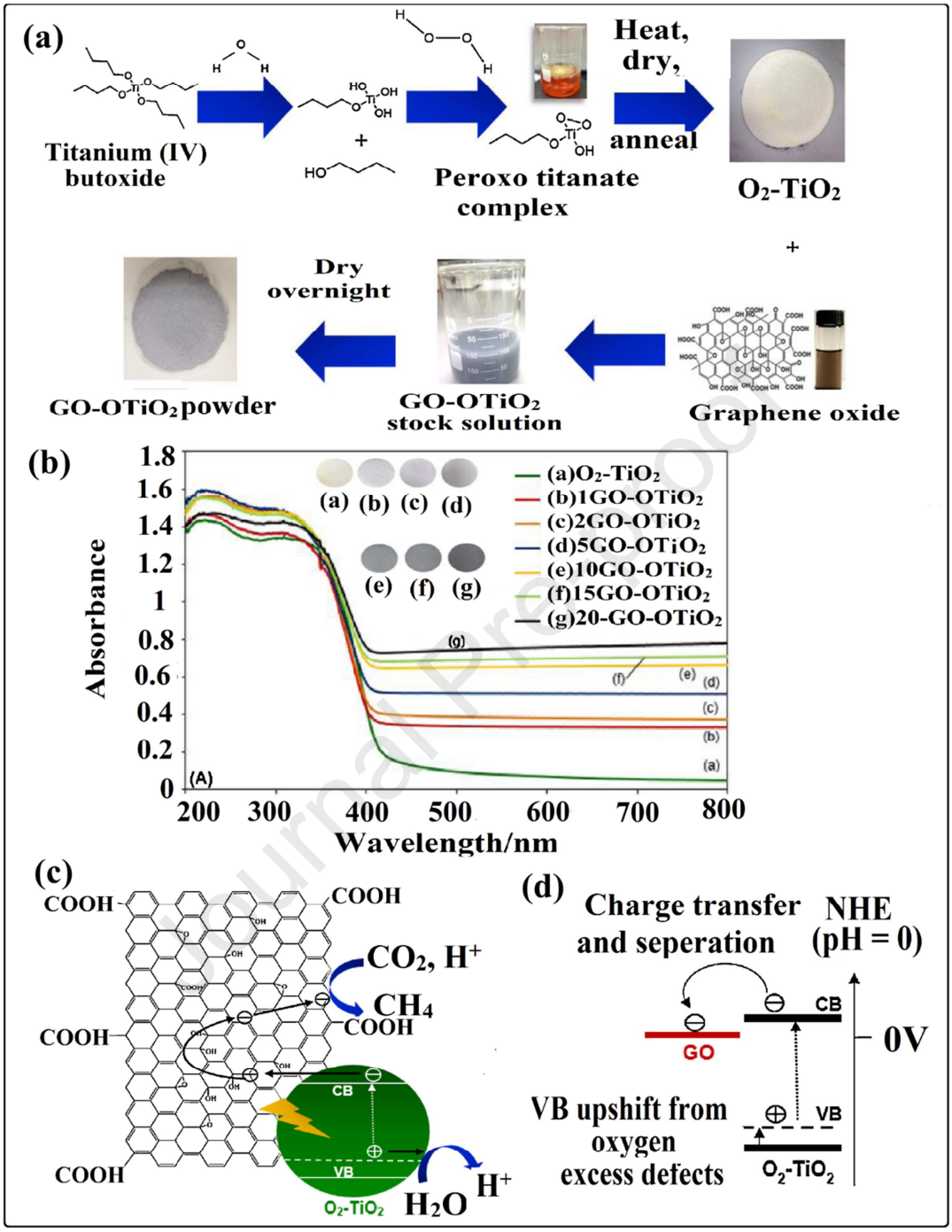

Fig. 10. (a) Synthesis procedure of GO–OTiO$_2$ binary nanocomposites, (b) UV–vis DRS for O$_2$–TiO$_2$ and GO–OTiO$_2$ composites, (c) Schematic illustrating the proposed charge transfer and isolation processes in GO–OTiO$_2$ binary nanocomposite for the photoreduction of CO$_2$ under visible light irradiation, reprinted with permission from Elsevier (license No. 4870630646826) [123].

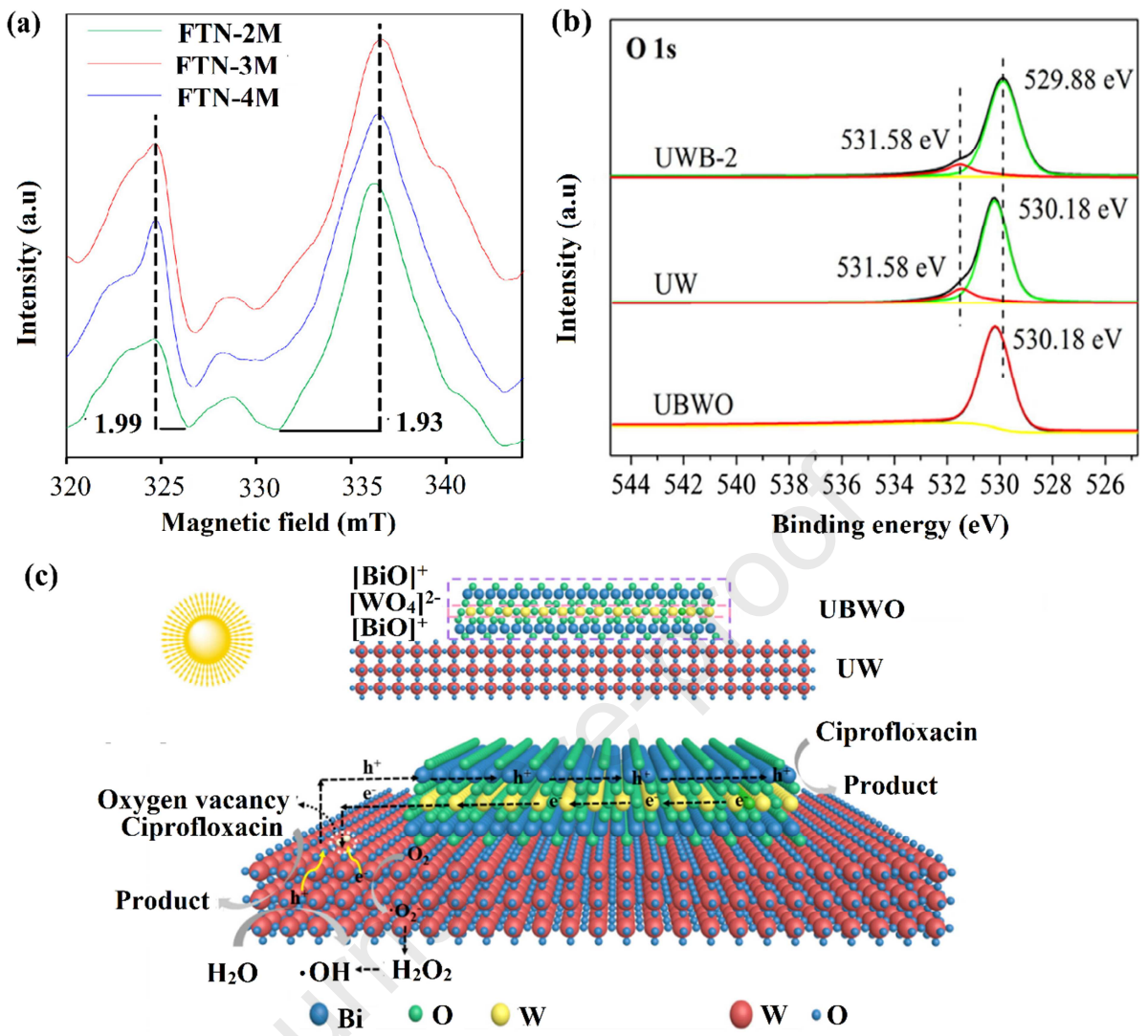

Fig. 11. (a) ESR spectra of FTN photocatalyst depicting different g value, adapted with permission from Elsevier (license No. 4900640102691) [112]; (b) The survey of high resolution XPS spectra of 1Os depicted V_o, (c) Photocatalytic degradation mechanism of UWB photocatalyst under visible light irradiation, Adapted with permission from Elsevier (license No. 4900631140091) [113].

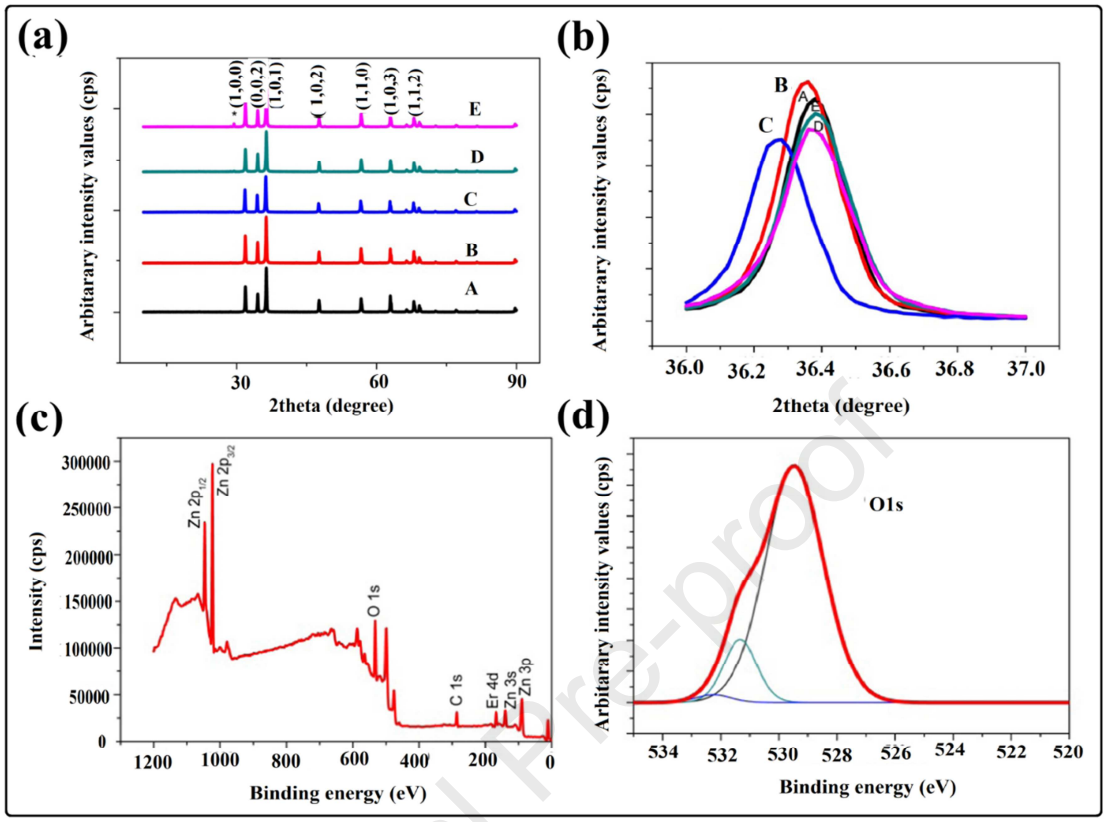

Fig. 12. (a-b) XRD pattern of samples and Shift observed in the pattern for the peak corresponding to (101) plane of ZnO with erbium doping, respectively (A) heat treated pure ZnO, (B) 0.3 wt% Er doped ZnO, (C) 0.6 wt% Er doped ZnO, (D) 0.9 wt% Er doped ZnO and (E) 1.2 wt% Er doped ZnO, XPS spectra of 0.6 wt% Er-doped ZnO particles: (c) full spectrum, (d) O1s, reproduced with permission from Elsevier (license No. 4820780821714) [138].

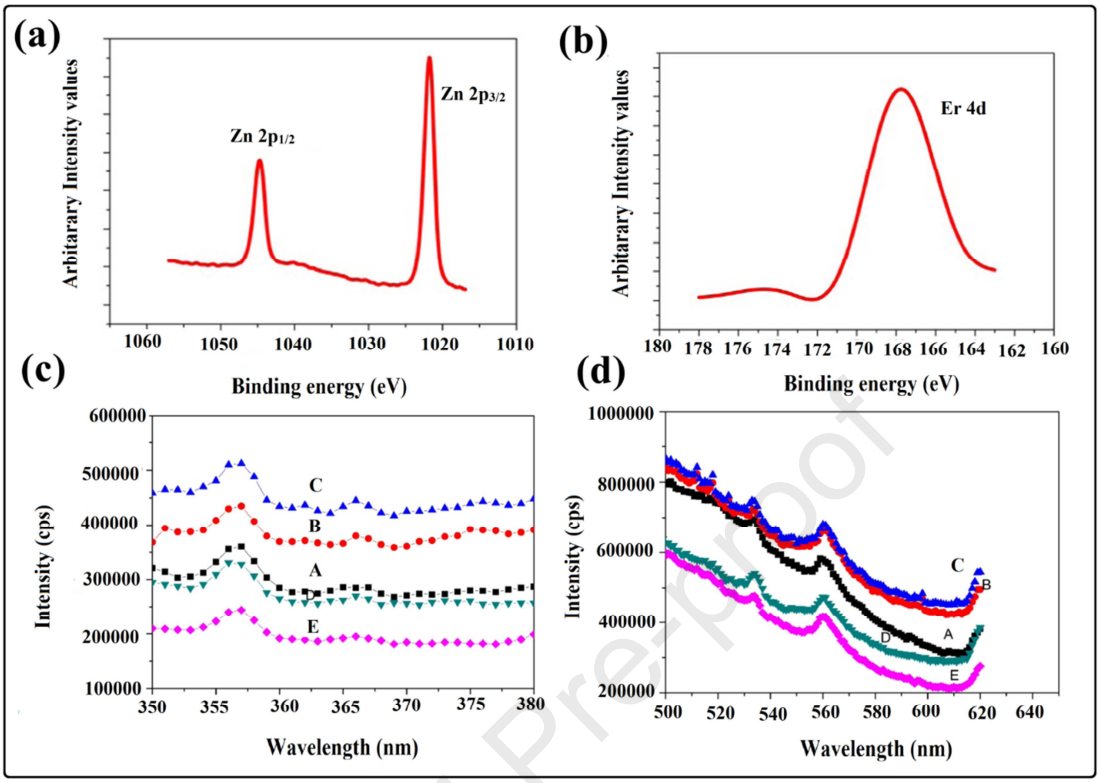

Fig. 13. XPS spectra of 0.6 wt% Er-doped ZnO particles:(a) Zn 2p and (b) Er 4d, reproduced with permission from Elsevier (license No. 4820780821714) [138], (c-d) Fluorescence spectra of the samples in the UV range and Visible range, respectively. (A) pure, (B) 0.3 wt% Er doped ZnO, (C) 0.6 wt% Er doped ZnO, (D) 0.9 wt% Er doped ZnO and (E) 1.2 wt% Er doped ZnO, reprinted with permission from Elsevier (license No. 482079077912) [138].

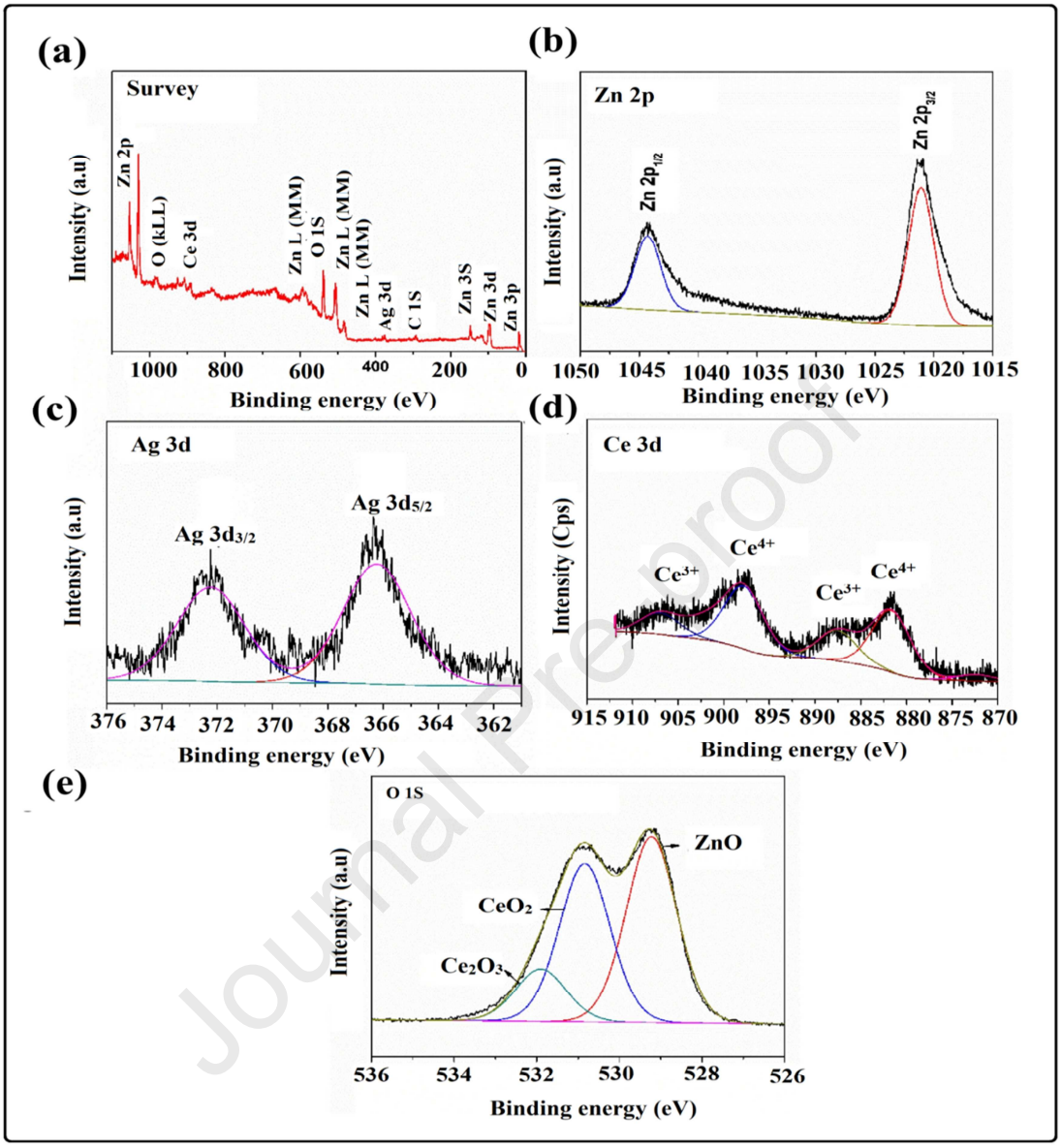

Fig. 14. XPS spectra of ternary Ag/CeO_2/ZnO nanohybrid (a) Survey spectrum, (b) HR-XPS spectrum of Zn 2p, (c) HR-XPS spectrum of Ag 3d, (d) HR-XPS spectrum of Ce 3d, and, (e) HR-XPS spectrum of O 1s, reproduced with permission from Elsevier (license No. 4820791429547) [139].

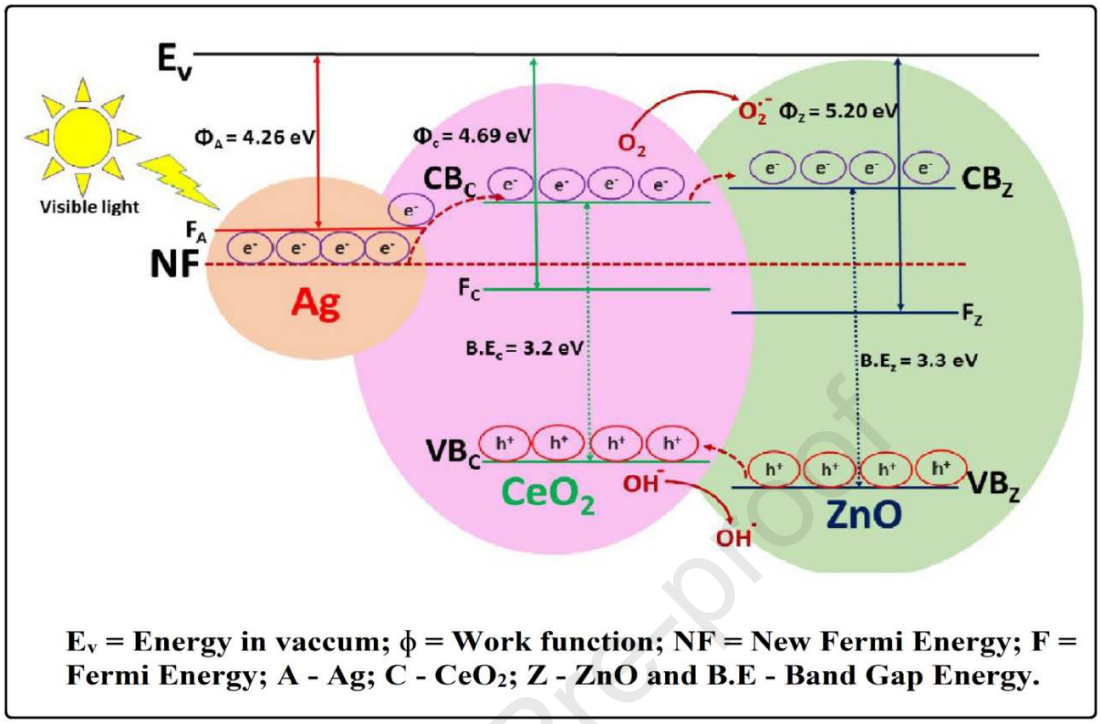

Fig. 15. Schematic diagram depicting the e^- flow and photocatalytic degradation mechanism of pollutants using ternary Ag/CeO_2/ZnO nanohybrid, adapted with permission from Elsevier (license No. 4820791429547) [139].

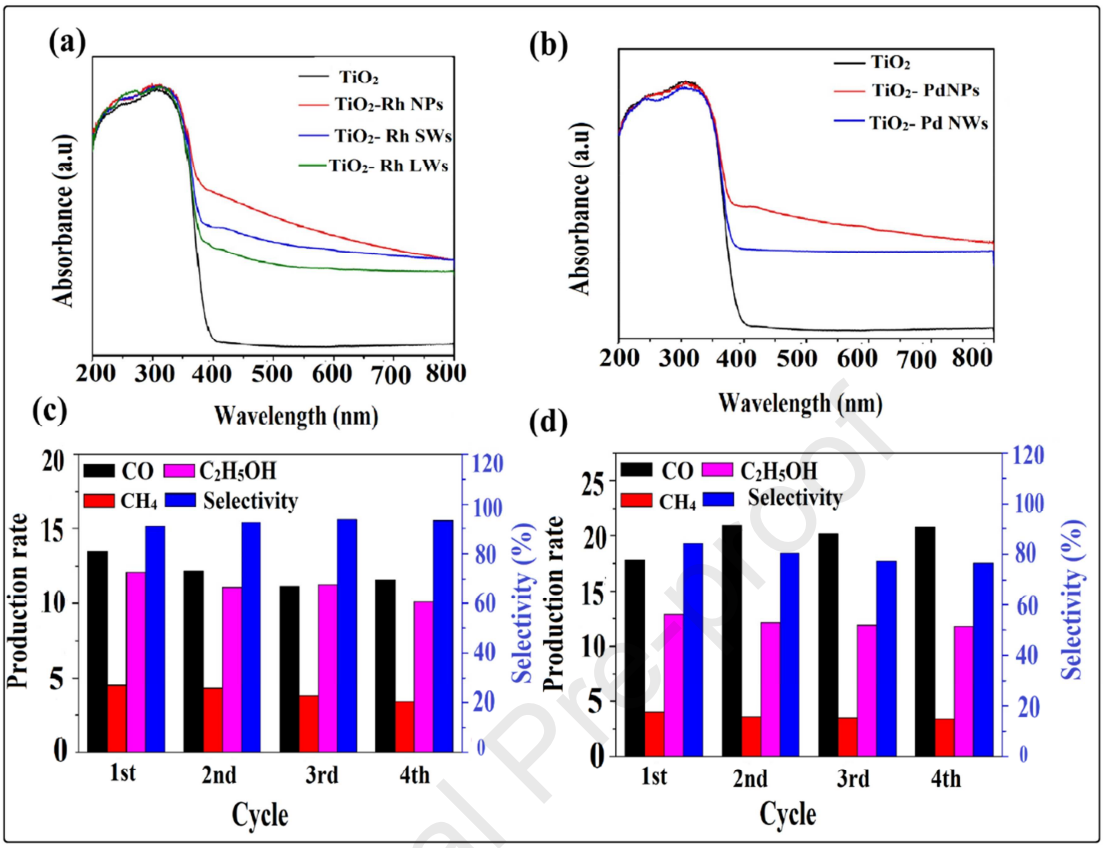

Fig. 16. (a) UV–vis-NIR diffuse reflectance spectra of TiO_2, TiO_2-Rh NPs, TiO_2-Rh SWs and TiO_2-Rh LWs, (b) UV–vis-NIR diffuse reflectance spectra of TiO_2, TiO_2-Pd NPs and TiO_2-Pd NWs, (c) Stability studies of CO, CH_4 and C_2H_5OH evolution rates as well as the selectivity for CO_2 reduction over (a) TiO_2-Rh LWs and (b) TiO_2-Pd NWs in photocatalytic CO_2 reduction reaction, reproduced with permission from Elsevier (license No. 4820800272558) [146].

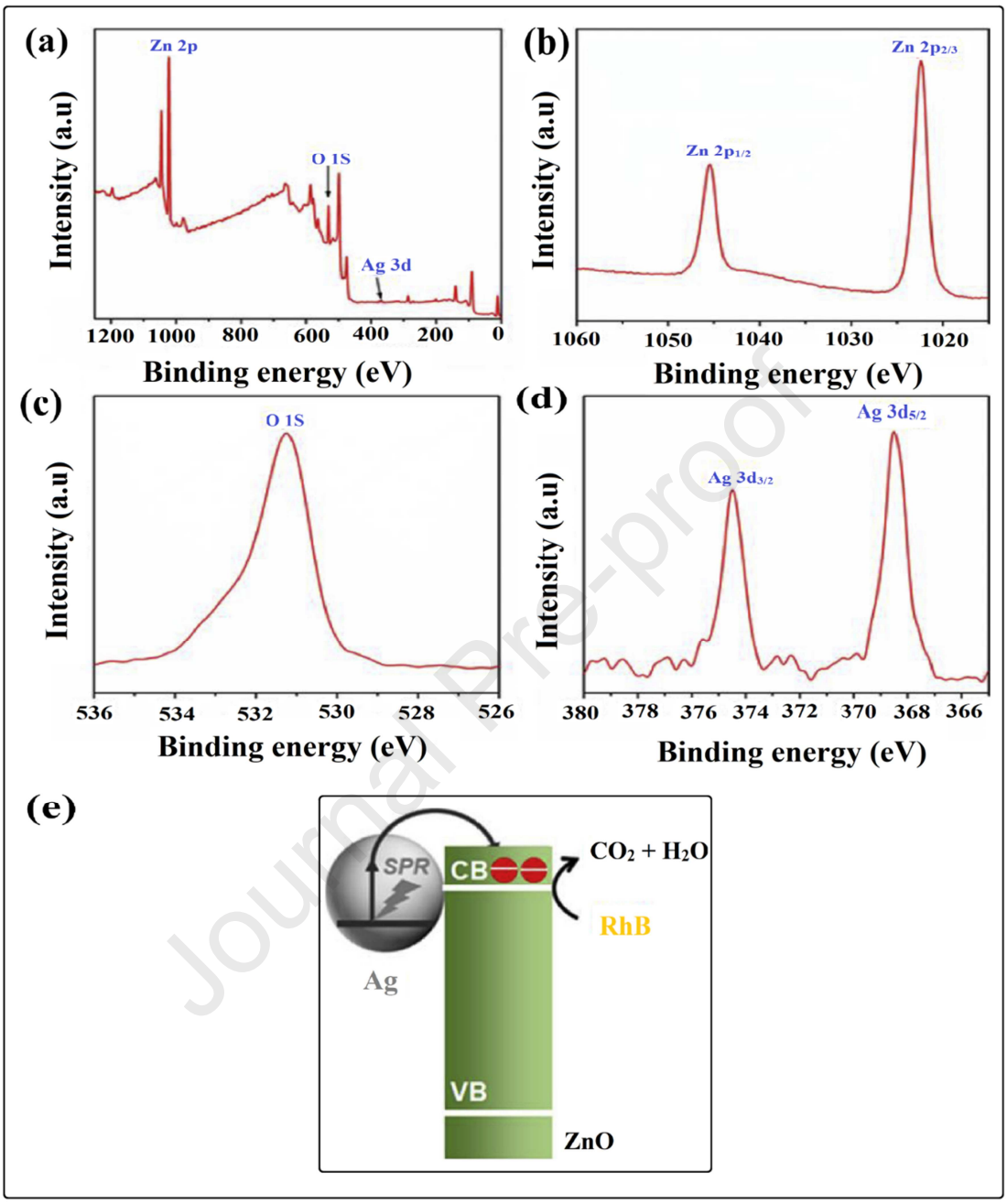

Fig. 17. XPS spectra (a–d) of ZnO/Ag-2 sample, (e) Possible photocatalytic mechanism of ZnO/Ag-2 Sample, reprinted with permission from Elsevier (license No. 4821281041421) [160].

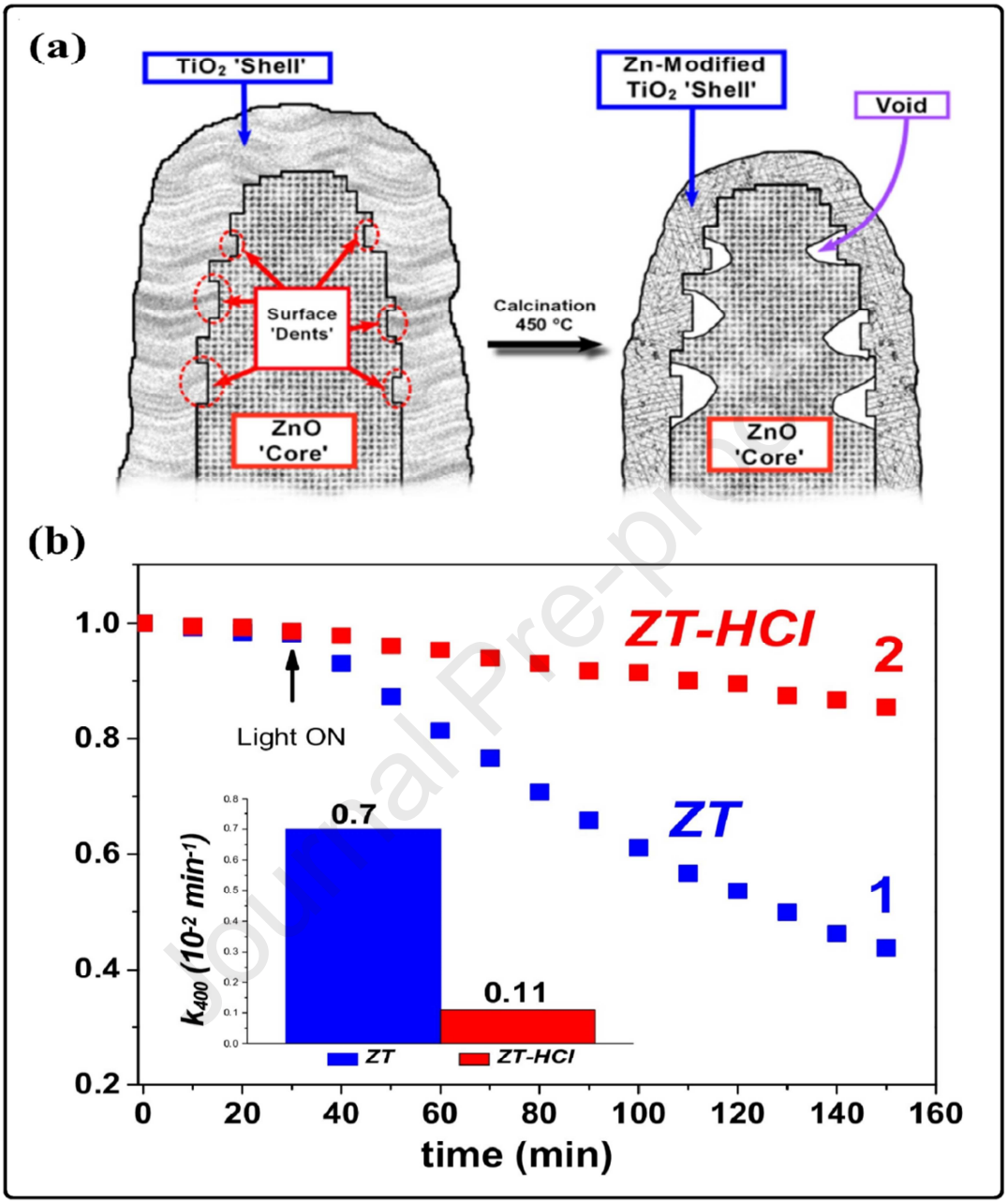

Fig. 18. (a) A schematic illustration resulting presumable thermal diffusion process of Zn ions into TiO_2 at the ZnO/TiO_2 interface at 450°C accompanied with formation of 'voids' in ZnO-core, (b) Photodegradation of MB with the use of the ZnO/TiO_2 composites before (blue scatter 1, ZT) and after dissolution (red scatter 2, ZT-HCl) of ZnO cores in HCl (A). Inset: values of pseudo first-order rate constants (k400) calculated for ZT (blue) and ZT-HCl (red), reproduced with permission from Elsevier (license No. 4821281375028) [161].

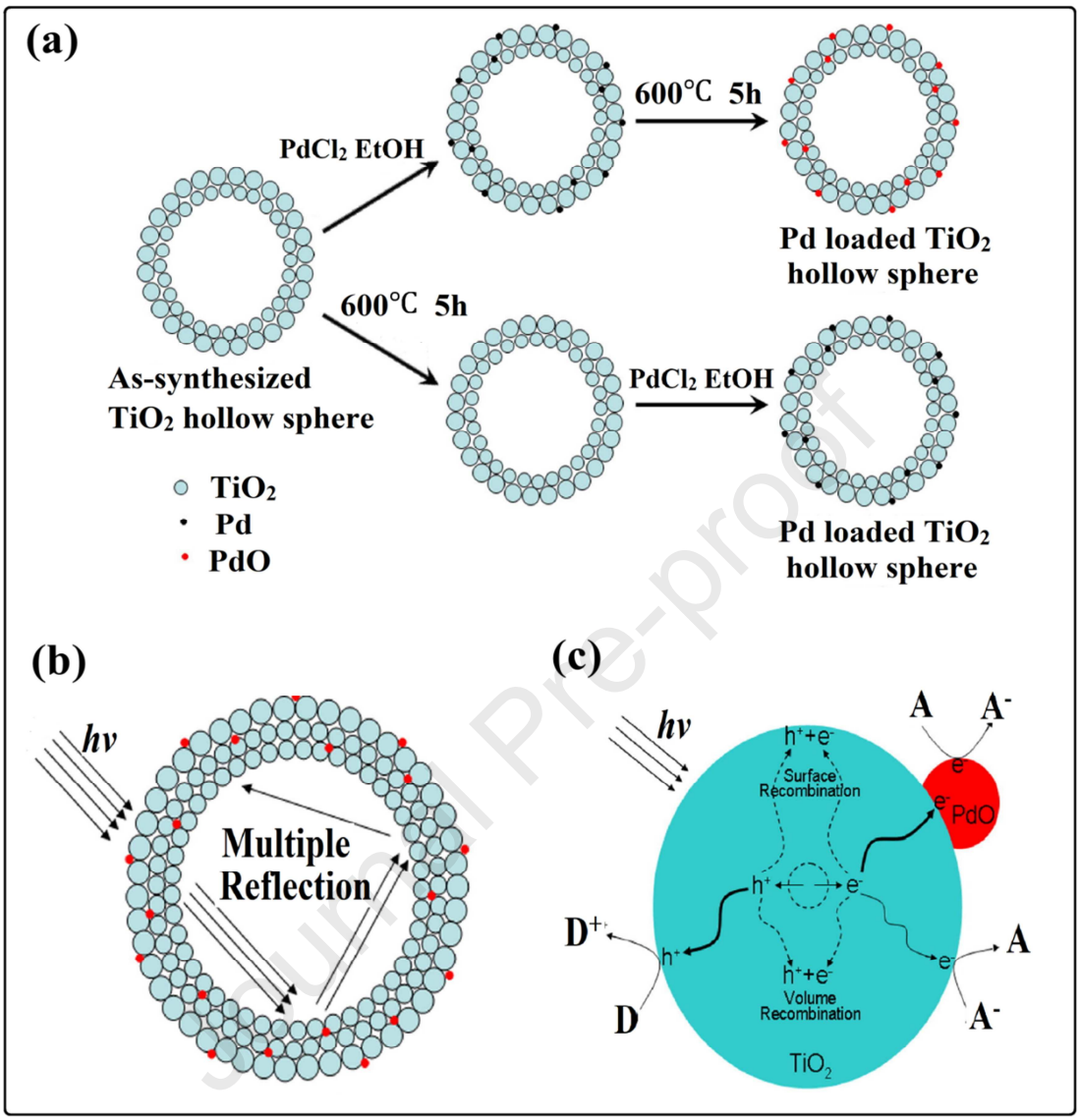

Fig. 19. (a) Schematic illustration of the synthesis processes of PdO and Pd loaded TiO_2hollow spheres, respectively, (b-c) Schematic illustrations for the multiple reflections in the hollow sphere and the e^-/h^+ pair segregation in the composite photocatalyst, respectively, adapted with permission from Elsevier (license No. 4821290102257) [162].

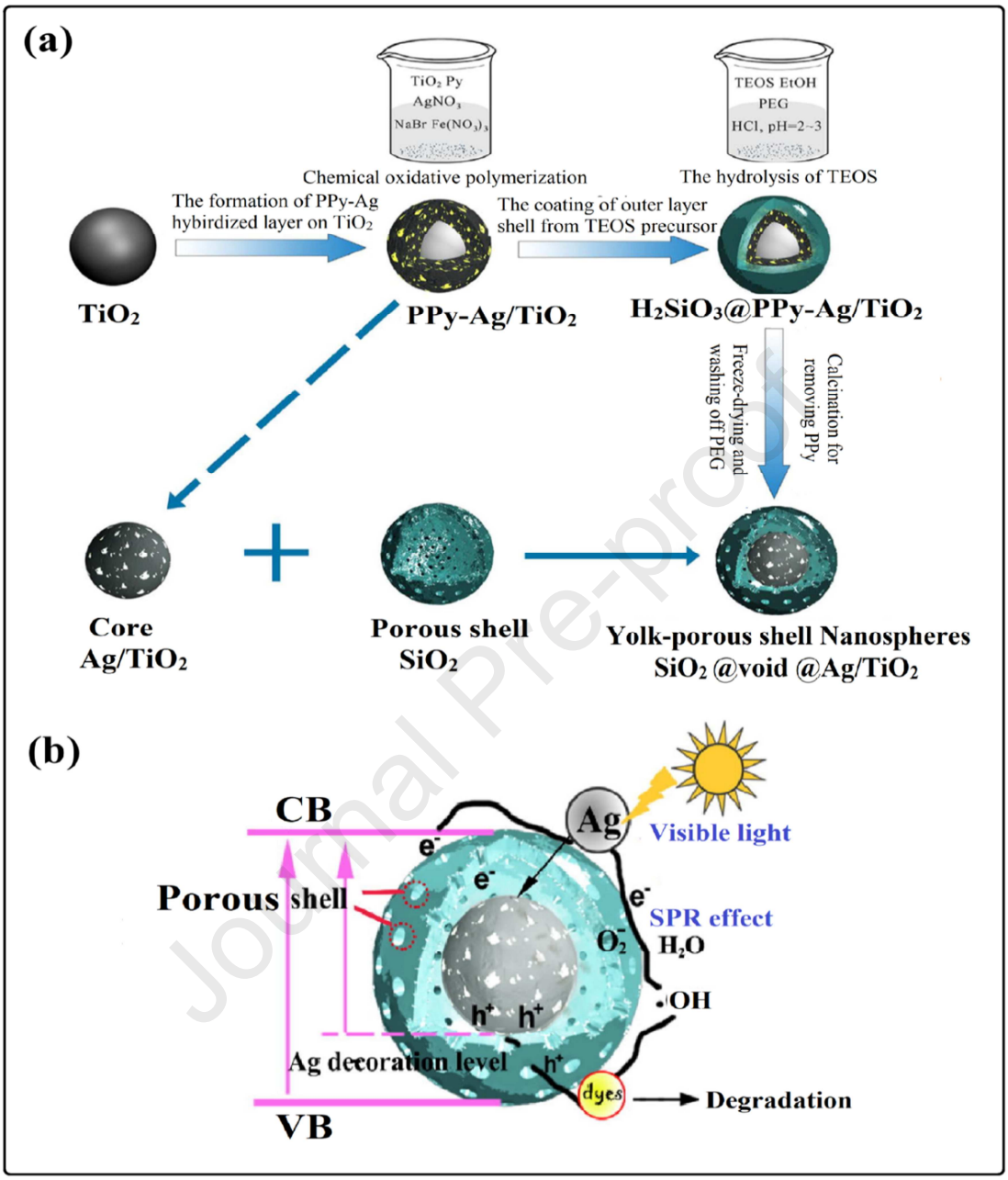

Fig. 20. (a) Schematic representation of SiO_2@void@Ag/TiO_2 yolk-porous shell nanospheres, (b) Possible mechanism for dye removal by as-prepared photocatalyst SiO_2@void@Ag/TiO_2, reproduced with permission from Elsevier (license No. 4821290425051) [163].

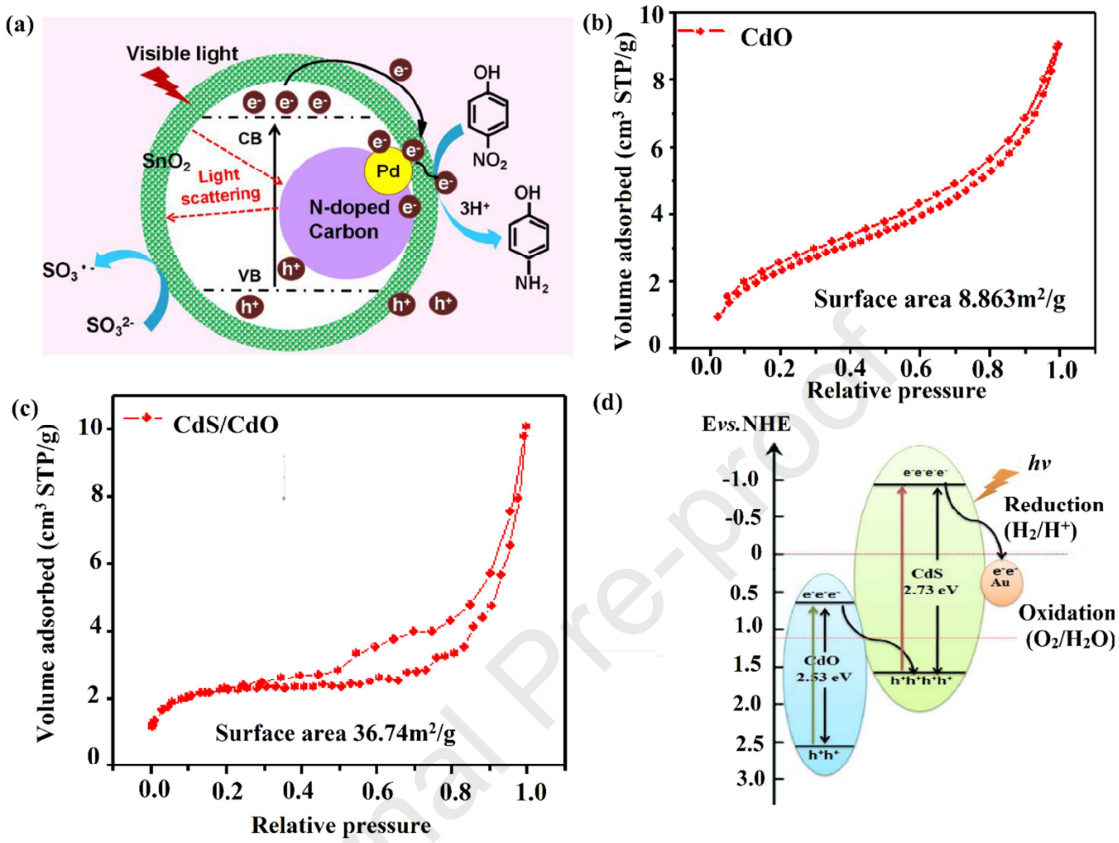

Fig. 21. (a) The proposed synergistic mechanism of yolk-shell Pd/NCs@SnO2 nanoreactor with improved photocatalytic activity, reprinted with permission from ACS [160]. **(**b-c) BET surface area of CdO , CdS/CdO nanocomposite, **(d)** The proposed synergistic mechanism of Au decorated CdO/CdS nanocomposite, adapted with permission from Elsevier, (license No. 400640651325) [159].

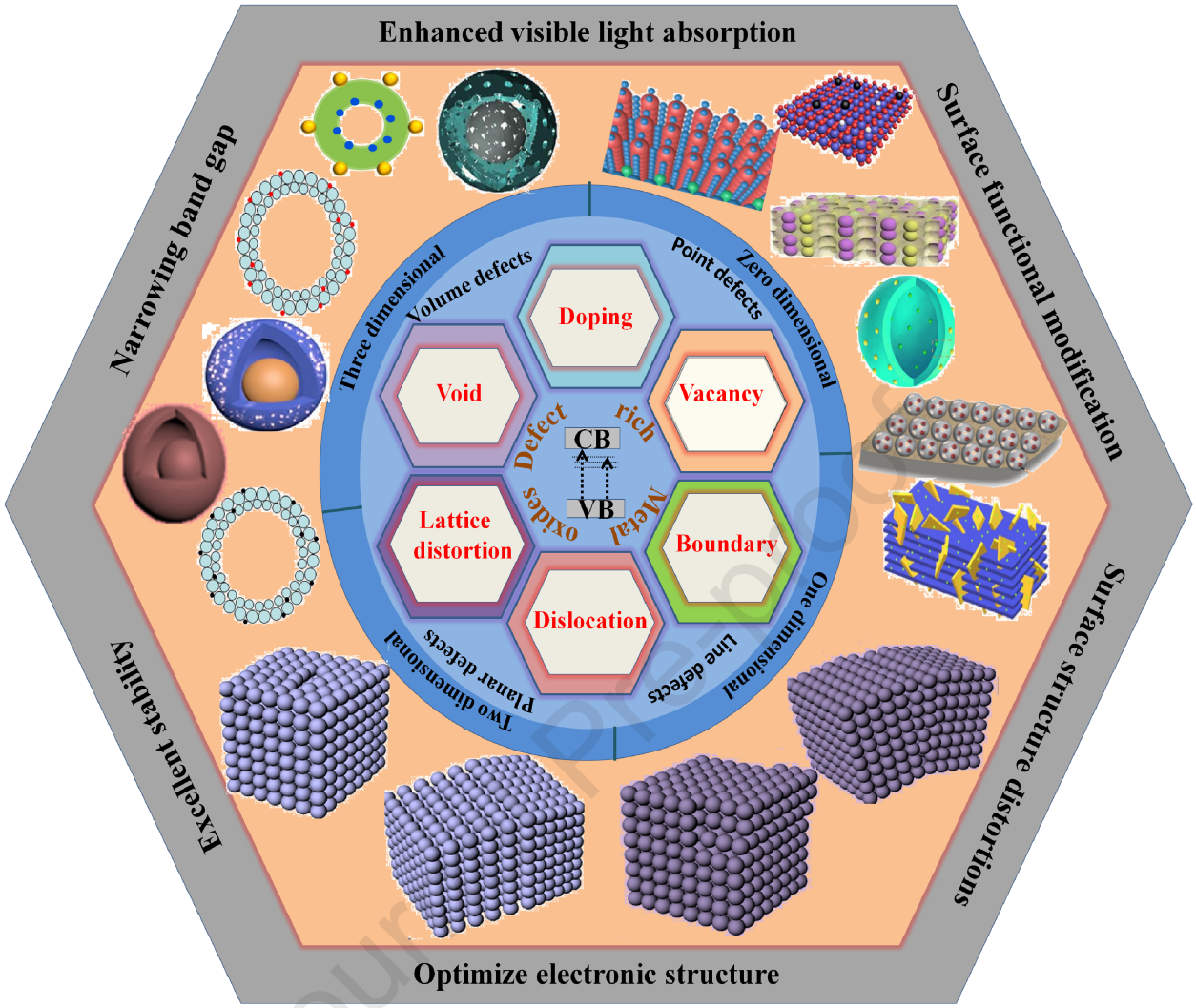

Highlights

- Distinctive surface step defects heighten the photoactivity of porous metal oxides
- Diverse strategies for controlled vacancies, metal defects in metal oxides nanostructure are highlighted
- Spectroscopic techniques were used to reveal the role of dislocations, boundaries, and voids on performance of metal oxides
- Dimensionality driven defects in metal oxide catalysts is explored with systematic modifications in lattice compositions

Biography

Name	Photo
Pankaj Raizada	
Vatika Soni	

Abhinandan Kumar	
Pardeep Singh	

Aftab Aslam Parwaz Khan	
Abdullah M. Asiri	

Vijay Kumar Thakur	
Van-Huy Nguyen	

Declaration of interests

☒ The authors declare that they have no known competing financial interests or personal relationships that could have appeared to influence the work reported in this paper.

☐The authors declare the following financial interests/personal relationships which may be considered as potential competing interests: